UNIVERSITY OF CALIFORNIA

Santa Barbara

Bio and Organo–Oligomeric and Polymeric Approaches to Nanoscale Assemblies

A Dissertation submitted in partial satisfaction of the

requirements for the degree Doctor of Philosophy

in Chemistry

by

Chol Steven Yun

Committee in charge:

Professor Geoffrey F. Strouse, Chair

Professor Curtis B. Anderson

Professor Thomas R. Pettus

December 2004

The dissertation of Chol Steven Yun is approved.

_____
Curtis B. Anderson

_____
Thomas R. Pettus

_____
Geoffrey F. Strouse, Committee Chair

December 2004

Bio and Organo–Oligomeric and Polymeric Approaches to Nanoscale Assemblies

by

Chol Steven Yun

ACKNOWLEDGEMENTS

I would first like to thank Professor Bruce Rickborn for his anecdotes of chemistry that encouraged me through some of the low points of my graduate work. To Professor Curtis Anderson, I would like to thank for being a great instructor and mentor through my graduate school days. I would like to thank Dr. Tom Pettus for keeping me interested in the field of organic chemistry. I wish to extend my most appreciative thanks to Dr. Norbert Reich for his extensive explanations and insights into the enzymatic biochemistry with which I cannot have done this work.

My graduate work cannot have been done without the support of Strouse and Reich research groups. Cheers to all those who helped me with my science and tolerated my caffeine fueled rants.

Most of all I wish to thank Dr. Geoff Strouse, who took a chance with me when I was lost in graduate school. I deeply appreciate the time and patience that he has extended towards me to find the joy in science and research. The mentorship that he has displayed has been beyond any that I have experienced or witnessed in my academic career. He has given me the opportunity to help with the initiation and fruition of scientific ideas.

Finally I wish to thank my wife, Shannon-Nicole, for being there, understanding and her love.

VITA OF Chol Steven Yun
May 2004

EDUCATION

Bachelor of Science in Biochemistry, University of California, Davis, 1996
Doctor of Philosophy in Chemistry, Department of Chemistry and Biochemistry, University of California – Santa Barbara, 2004

PROFESSIONAL EMPLOYMENT

2002-2003 UC Biotek Graduate Fellowship
2001-2003 Center for Polymer Organic Materials
1999-2003 Research Assistant, Strouse Lab

PUBLICATIONS

"Energy Transport in CdSe Nanocrystals Assembled with Molecular Wires." Javier, A.; Yun, C.S.; Sorena, J.; Strouse, G.F. *J. Phys. Chem. B*, submitted, June (2002).

"Effects of Alkylamine Chain Length on the Thermal Behavior of CdSe Quantum Dot Glassy Films." Meulenberg, R.W.; Bryan, S.; Yun, C.S.; Strouse, G.F. *J. Phys. Chem B*, 106, 7774-7780 (2002).

"Enzymatic Modulation of DNA-Nanomaterial Constructs." Yun, C.S.; Khitrov, G.A.; Vergona, D.E.; Reich, N.O.; Strouse, G.F. *J. Amer. Chem. Soc.*, 124, 7644-7645 (2002).

"Inorganic Clusters as Single Source Precursors for Preparation of CdSe, ZnSe, CdSe/ZnS Nanomaterials." Cumberland, S.L.; Hanif, K.M.; Javier, A.; Khitrov, G.A.; Strouse, G.F.; Woessner, S.M.; Yun, C.S. *Chem. Mater.* 14, 1576-1584 (2002).

"Assembly of Nanomaterials Using Bio-Scaffolding." Yun, C.S.; Major, J.L.; Strouse, G.F. Mat. Res. Soc. Symp. Proc., 642, J2.3 (2001).

“Pd(O)-Mediated Mouplings of Aryl Nonaflates and Triflates with Diphenylphosphine-Borane. Preparation of BH3-Stabilized, Unsymmetrical Triarylphosphines.” Lipshutz, B.H.; Buzard D. J.; Yun, C. S. *Tetrahedron Letters*, 40, 201-204, (1999)

FIELDS OF STUDY

Major Field: Assembly of Nanomaterials Utilizing Biological Molecules

ABSTRACT

The Organization and Manipulation of Bio-Inorganic Nanomaterials

by

Chol Steven Yun

The assembly of metallic and semi-conducting nanocrystals into two- and three-dimensional arrays is crucial in the pursuit of nano-electronics. Recently, there has been substantial interest in integrating surface modified nano-scale materials into biologically relevant processes, primarily for imaging, and sensing technologies. However, bio-integrated nano materials may offer an opportunity to build nano-networks for electronic applications by utilizing the highly convergent, native capability for bio-materials to self-assemble. In fact biological scaffolds provide a mechanism for the assembly of nano-molecular arrays possessing the capacity for self-wiring, self-annealing, and self-healing due to the flexibility of DNA, and the strong hydrogen bonding interactions that dominate DNA duplex formation. The design of architectures whose electronic properties are governed by the nano-particle interactions in the 3-D array may allow extrapolation of the bio-assembly strategy above to formation of high-density nano-electronic architectures possessing potentially unique electronic properties governed by the bio-nano-wire interconnects. A major hurdle in the effort is the exhibition of bio-compatibility and

bio-viability of the nano-bio constructs. For biological materials, the contingencies of maintaining tertiary structure and catalytic activity in the presence of nanometer-sized particles are a potential fatal flaw in bio-scaffolded assemblies. In this section we investigate the assembly of bio-scaffolded nanomaterial constructs, specifically polypeptides, while maintaining viability of both components.

TABLE OF CONTENTS

LIST OF FIGURES

Chapter I. Assembly Strategies for Nanomaterials

Materials in the range of 10Å to 100AÅ are considered nanomaterials with those above and below that range to be considered molecular and bulk respectively. Within the last 10 years the area of nanomaterial research has grown exponentially with increasing interest. The definition does not solely depend upon the size of the material but rather the characteristic changes the material has respective to its bulk or molecular counterparts. The characteristics that arise are size dependent optical[1,2,3,4] electronic[5,6,7,8] magnetic[9], and chemical properties.[10,11,12,13,14,15] The promise of these new materials has given rise to possibilities of incorporating and applying them into fields like electronics, bio-detection, memory storage, catalysis and mechanical device engineering. Yet before plans for such integration into these fields can be blueprinted and executed, the challenge of controlling the spatial arrangement and overall topological structure of an ensemble of nanomaterials is crucial.

A. Chemical Methods of Assembling Nanomaterials

Many strategies of assembling nanomaterials have been developed such as self-assembly, electrostatic, and ligand mediated assembly. Most nanomaterials, including nanocrystals, are synthesized with a surfactant capping groups. The organic ligand contains polar head groups that passivate the nanomaterial surface by binding the surface as well as organic tail that impart the solubility in organic

solvents. Self-assembly is the methodology to assemble nanomaterials by means of allowing the nanomaterial to assembly using the Van der Waals interactions of the ligand passivating the nanomaterial surfaces and the ionic attraction between the nanomaterial cores. This strategy allows for the formation of planar sheets of close packed nanocrystals that can be transferred to form three-dimensional monoliths by stacking the planar arrays upon one another.[16,17,18] (Figure 1) However such strategies afford arrangements of nanomaterials whose spatial organization is solely dictated by the polarizabilty of the nanomaterial and the variability of the surface alkyl chains.[17] In addition, this methodology does not allow spatial variations in post assembly. Yet such assemblies have been useful in studying the collective optical behavior of semiconducting nanocrystals[19,20,21] and in metal nanoparticles.[17,22,23]

Electrostatic assembly of nanoparticles is another strategy that has been applied in forming nanoparticles into constructs. In this approach, the electrostatic interactions of positive and negative ligands are used to form the assembly. This requires that one set of nanoparticles is synthesized or ligand exchanged with an organic passivant that bears a functional group at or near the opposite end of the binding head group with a positive or negative group. A second set of nanoparticles is synthesized with a ligand shell possessing the opposite charge of the first. Upon introducing the two species of nanoparticles together in solution the particles assemble to form aggregates held together by electrostatic interactions. (Figure 2)

Figure 1-1. Illustration of ligand induced self-assembly into a planar heaxagonal array; shown by a Tem of 4.5 nm CdSe nanocrystals capped with hexadecylamine.

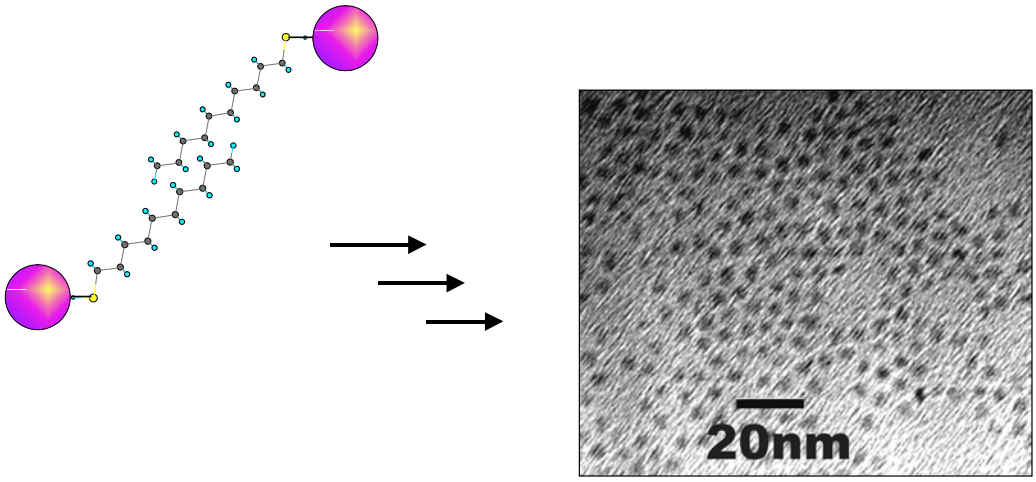

This strategy has been employed to assembly two sizes of gold nanocrystals,[24,25] aggregates of nanocrystals and solid support[26], and gold and cadmium chalcogenide nanocrystals[27]. Though this has meet with success in assembling the nanomaterials of different sizes and varying type of nanomaterials, the assemblies are ill formed and lack both the uniformity of the ensemble. Furthermore, the control of spatial and topological arrangements of the nanomaterials is again fixed and can only be varied by changing the ligand lengths of each nanocrystal. This in itself brings about other issues of difficulty that will be addressed later in this chapter.

The last type of assembly commonly employed is ligand-mediated assembly. In this methodology, to assemble nanomaterials, organic or biological molecules are attached to the surface of the nanomaterial and chemical forces such as metal ligand, electrostatic, or hydrogen bonding form them into cross-linked agglomerates. Varyious types of ligands, from simple bifunctional alkyl systems to complex biological molecules, have been used to assemble nanocrystals. The simplest systems were done with di-thiol alkyl linkers that formed the nanocrystals into aggregates; A. P. Alivisatos used this approach to join together a number of CdSe nanocrystals and observed the optical properties of said assembly.[28] As the first attempt, the strategy proved successful yet this pathway lent little or no control to the size of the assembly or the separation distances of the materials.

Figure 1-2. Illustration of electrostatic assembly of nanomaterials into large irregular aggregates.

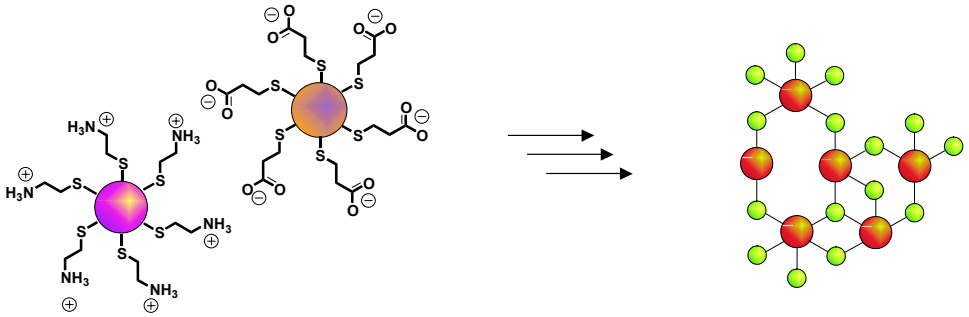

Methodologies in assembling nanocrystals became more complex with the utilization of ligands possessing hydrogen bound pairing moieties. D. Fitzmaurice et al.[29] employed a nucleic acid analog and a complimentary pyridyl moiety appended at the terminal end of alkyl linkers to assembly gold nanocrystals together. Though their attempts meet with nominal success, the assembly once again was limited to the characteristic monolith. The ligands acted as mortar for the assembly but neither imparted any specific control or function to the ensemble of nanocrystals.

In a similar ideology Royce Murray et al.[30,31] produced large multiple constructs that spanned the separation of 1 μm electrodes. These assemblies were done with the use of ion-ligand mediated assembly. The basic strategy was to functionalize the surface of gold nanocrystals with an ω–carboxy alkyl thiol. In addition to imparting water solubility to gold nanocrystals synthesized in the organic phase, the carboxylate functional groups were used to coordinate to Cu^{II} ion. This coordination linked the nanocrystals to form large constructs that were used to test the application of gold nanocrystals in electronic devices. One of the most interesting aspects of this research is that the assembly was reversible with a metal chelator that could out compete and sequester the metal ion from the carboxylates for thus allowing reversibility in the construct. (Figure 3) Similarly to most constructs that use alkyl systems, the ligands add little to no enhancement or advantages to the construct. The ability for the assembly to be a reversible construct adds advancement into the control of nanomaterials.

The uses of bifunctional ligands that have selectivity for different nanomaterial surfaces have been employed to create more ordered assemblies that different sizes and types of nanocrystals. Strouse et al[32] have used a readily available heterofunctional ligand containing a thiol and amine on the terminus of a propyl chain. The ligand exchange of CdSe nanocrystals afforded the thiol end bound to the surface and the amine functionality to provide water solubility. The addition of citrate stabilized gold nanocrystals gave a well-formed dilithic construct with the amines binding the surface of the metal nanoparticle and the thiols binding the surface of CdSe. (Figure 4)

B. Polymeric Methods of Assembly of Nanomnaterials.

The ideas of using ligands that not only organize or control the nanomaterial but enhance or benevolently affect the nanomaterial and its construct lends itself to using conjugated organic oligomers and polymers. For possible uses in nanoelectronics, poly-phenyleneethylenes capped with phenylthiols have been used to organize gold nanocrystals.[33,34] In a demonstration of controlled assembly the oligomer was used to form smaller composites of gold nanocrystal dimers. This was done using dilute concentrations of the oligomer and nanocrystal.[35,36] Additional to the formation of dimers, the same study used more complex systems such as tri- and tetrapodal systems that organized the nanomaterials into composites of three and four gold nanocrystals. The hope was that the organic ligands would facilitate the electron transfer in the nanomaterial construct. Similar organic oligomers have been shown by

Figure 1-3. Illustration of ion mediated assembly of nanomaterials into large irregular aggregates.

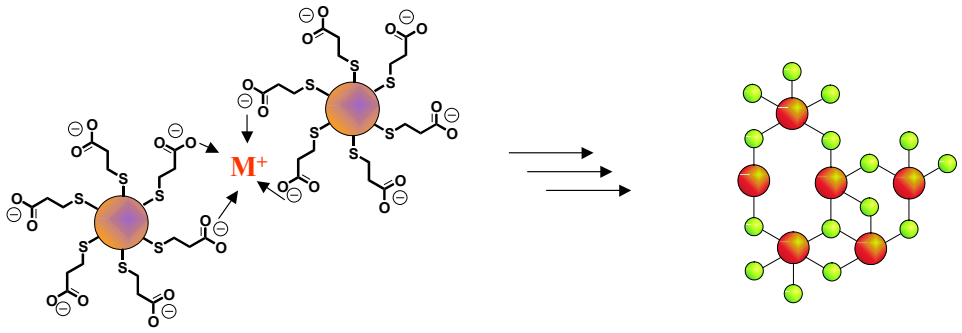

Figure 1-4. Illustration of bi-functional ligand assisted assembly. The current strategy was employed to form dilithic structures of gold and CdSe nanocrystals.

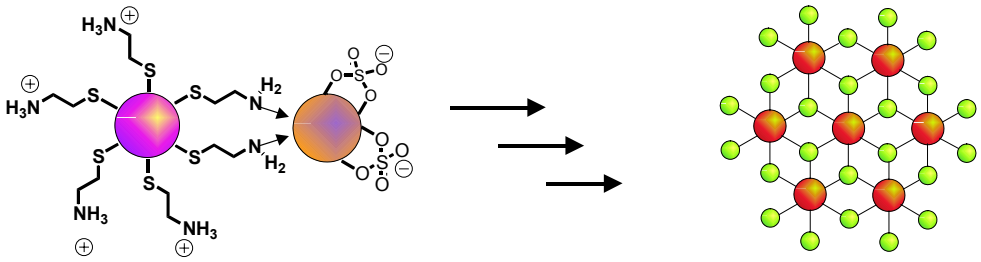

Cumberland, Scott L.; Berrettini, Mia G.; Javier, Artjay; Strouse, Geoffrey F. *Chemistry of Materials*, **2003**, 15, 1047-1056.

James Tour *et al.* notably the oligo-phenyleneethylenes are capable of electron transport and show bias capabilities.[37]

Just recently the Lifshitz et al. used the oligomers functionalized with benzylcarboxylates to coordinate cadmium and lead ions.[38,39] With the addition of hydrogen sulfide into a reaction vessel containing the metal ion ligand complex, an assembly formed of CdS or PbS nanocrystals passivated with the conjugated oligomer. The amorphous constructs shows that the nanocrystals are formed without order and size control. The nanocrystals formed in the matrix are synthesized with a large distribution of size. Preliminary studies on the construct show that the materials show energy transfer from organic ligand to the nanomaterial. The assemblies mentioned above the conjugated ligand systems not only organized the nanomaterials into ensemble but added an enhancement to the whole by allowing the capacity for electron or energy transport.

C. Biological Methods of Assembly of Nanomaterials.

An alternative of organic ligand mediated assembly of nanomaterials is the biomolecular assembly of nanomaterials. The current strategies toward the construction of such matrixes employ both biological and organic molecules as ligands to both pacify and facilitate assembly. Developing non-lithographic techniques for the assembly of nano-scale materials (metals, semiconductors) into high-density nano-arrays fundamentally must incorporate a self-assembly and self-annealing processes. One potential pathway to such constructs lies at the interface

between nano-materials and biology. The tremendous advances in understanding, utilization and control of bio-materials, including DNA and polypeptides, provides an enhanced set of tools for the nanoscale assembly of novel materials with enhanced electronic functions. Materials assembly using biological polymers (DNA, proteins) as scaffolds to direct the assembly of nano-scale components (semiconductors, metals) offers an exciting possibility of blending the inherent self-assembling properties of biological materials and the unique electronic and optical properties of nanomaterials.[40] The concept of using biological molecules and macromolecules to assemble nanomaterials is initiated by the innate ability of biological materials to form topological structures intrinsic to their class. Along and due to the structural morphology, the biological molecules provide a platform for extreme selectivity in binding and catalysis. The ability to harness these capabilities has driven the research of nanomaterial assembly using biological molecules.

The first incidents of nanomaterials and biological molecules were done with simple structural proteins and long plasmid DNA and gold nanocrystals.[41] The application in the case of plasmid DNA was to physio-absorb the macromolecules on to the surface of the nanomaterial and use them as a delivery device for DNA transfection in plants. Though largely neglected by most sciences, the biological community began to use gold nanocrystals as labeling agents for proteins and cellular components. In a simultaneous effort both Alivastos et al[42] and Mirkin et al[43] introduced the aspects of covalently linking synthetic DNA to the surface of gold nanocrystals and assembling, respectively, the nanomaterials into dimeric units

or large monolithic constructs. There are alternative research pursuits that push the designs of these hybrid materials into areas of biological labeling[44] and optical DNA mismatch detection.[45] Further attempts into the utilization nanomaterials with DNA have afforded semiconducting nanocrystals that have been labeled with DNA and used to elucidate complementary strands of DNA.[46] Most of these systems use the specific complexation of the complimentary DNA strands to allow them to function with most of the efforts into attaching nanomaterials with DNA have gone into the development of a reliable optical detection system for biological related problems such as the detection of complimentary DNA and mismatches in DNA sequences.

In addition to the nucleic acids, proteins have been used to assemble nanomaterials. The initial effort was done by Stephen Mann whose initial assembly of gold nanocrystals utilized the water-soluble gold nanocrystals with a mixed surface monolayer passivant containing an alkylthiol with a biotin at the terminus opposite of the surface bound thiol.[47] To assembly the nanomaterials, avidin, a structural protein that finds tightly to biotin, was added. Further efforts have been done this area by Catherine Murphy[48] and Neimeyer[49] with the use of synthetic DNA modified with both a 5' thiol terminus and a complimentary strand of DNA containing a 5' biotin linker. In these experiments the gold nanocrystals were assembled with streptavidin, a homologous protein to avidin. The idea behind these experiments was to allow the use of proteins to assemble the materials.

An application of proteins and nanomaterials is the attachment of peptides or bioactive molecules to the surface of nanocrystals. Similar to the idea behind the

attachment of biotin to the surface of gold nanocrystals, the attachment of other molecules such as serotonin[50] and peptide[51,52] sequences have allowed the binding of nanomaterials to the protein receptors such as sertonin uptake proteins or other proteins that are present that signifiy some malignancy in the cell. In this capacity the nanomaterials has become an optical detection system.

D. Conclusion

In the field of nanomaterial assembly the major focus is controlling how the assembly forms and afterwards controlling the assembly afterwards. The use of functional organic molecules may lend to the development of hybrid materials with applications into electronics, optical materials and memory. The applications of biological and nanomaterial hybrids into the field of biological sensing show a great deal of promise. The ability to load the nanomaterial with either the biological molecule or a bioactive molecule to assemble the nanomaterial into a construct that can selectively interact with another biomolecule lends ground to the use of the nanomaterials intrinsic character, whether it is optical, magnetic or other in the field of sensing. The ability to manipulate the assembly will allow further use in those materials in more diverse fields of application and study.

E. Summary of thesis.

Within this thesis is the research conducted on the appending of organic and biological oligomers and polymers to metallic and semiconducting nanoparticles. In the case of the biological and inorganic nanomaterial hybrids, research is extended

into application of the constructs into optical reporters while the organic-nanomaterial hybrids are an introduction into the assembly of nanomaterials with ligands that either facilitate or enhance the innate qualities of the nanomaterial. In the following chapters; the second chapter entails the covalent appending of the 1.4nm gold nanocrystals with polypeptides, protein domains and duplex strands of DNA. Here the studies were done to examine if the biological molecules can maintain the structural and topological integrity with the attachment of heavy nanomaterials. In addition to the maintenance of the bio-molecule's structure, investigation into the bio-viability of the DNA-gold nanocrystal hybrid to enzymatic manipulation was conducted.

In chapter 3 and 4, the application of the DNA gold nanocrystal hybrid was exploited into a methodology of using the construct with a fluorophore thus providing an optical detection device for the detection of DNA interacting proteins. In Chapter 3, there is a two-fold approach into the study of how the gold nanocrystal-DNA- fluorophore conjugate will be applicable to the detection of the detection of DNA interacting proteins that cause topological changes in the helical structure and to what extent does the gold nanocrystal follow energy transfer mechanisms; this was done by varying sizes of the gold nanocrystals and the length of the DNA strands. In chapter 4, the similar system was used with larger gold nanocrystals. The larger nanomaterials afforded greater quenching of the fluorophore appended to the DNA, thus allowing the aspect of using them as optical beacons for the detection of enzymes that severe the DNA strands.

Chapter 5 will present the assembly and initial energy transfer studies of CdSe by oligophenylethylenes (OPE's). The synthesis of the OPE is presented as well as the conditions of assembly and a mention of the initial energy transfer studies that are being conducted.

Chapter 6 is a synthetic section that gives detailed synthetic procedures on how CdSe and gold nanocrystals are made and their conversion to salt and buffer stable, water-soluble materials. There is a description on the deprotection of functionalized DNA and their appending to colloidal gold nanocrystals and nanogold. A brief mention of how both CdSe and gold nanocrystals and their bio-conjugates are run on electrophoresis gel.

References

1. Heath, J.R. Shianng, J. *J. of Chemical Society Reviews,* **1998**, 27, 68-71
2. Murray, C. B.; Norris, D. J.; Bawendi, M. G. *Journal of the American Chemical Society*, **1993**, 115, 8706-15
3. Nirmal, M. Brus, L. *Accounts of Chemical Research*, **1999**, 32, 407-414
4. Landes, C. F. Link, S. Mohamed, M. B.; Nikoobakht, B. Ei-Sayed, M. A. *Pure and Applied Chemistry*, 2002, 74, 1675-1692
5. Hagfeldt A; Gratzel M. *Accounts of Chemical Research,* **2000**, 33, 269-77
6. Shim, M. Guyot-Sionnest P**.** *Nature*, **2000**, 407, 981-3
7. Wang, C. Shim, M. Guyot-Sionnest, P. *Science*, 2001, 291, 2390-2392
8. Joachim, C. Gimzewski, J. K. Aviram, A. *Nature* **2000**, *408*, 541-548

9. Sun, S. Murray, C. B. *Journal of Applied Physics*, **1999**, 85, 4325-4330

10. Shipway, A. N. Willner, I. *Chemical Communication*, **2001**, 20, 2035-2045

11. Klabunde, K. J. Stark,J. Koper, O. Mohs, C. Park, D. G. Decker, S. Jiang, Y. Lagadic, I. Zhang, D. *Journal of Physical Chemistry*, **1996**, 100, 12142-12153

12. Rao, C. N. R. Kulkarni, G. U. Thomas, P. J. Edwards, P. P. *Chemistry - A European Journal*, **2002**, 8, 28-35

13. Thomas, P. J. Kulkarni, G. U. Rao, C. N. R. *Journal of Physical Chemistry B*, **2000**, 104, 8138-8144

14. Schauermann, S. Hoffmann, J. Johanek, V. Hartmann, J. Libuda, J. Freund, H. *Angewandte Chemie, International Edition*, **2002**, 41, 2532-2535

15. Guczi, L.; Beck, A.; Horvath, A.; Horvath, D. *Topics in Catalysis*, **2002**, 19, 157-163

16. Murray, C. B.; Kagan, C. R.; Bawendi, M. G. *Science*, **1995**, 270, 1335-8

17. Murray, C. B. Kagan, C. R. Bawendi, M. G. *Annual Review of Materials Science,* **2000**, 30, 545-610

18. Markovich, G. Collier, C. P. Henrichs, S. E. Remacle, F. Levine, R. D. Heath, J. R. *Accounts of Chemical Research*, **1999**, 32, 415-423

19. Cordero, S. R. Carson, P. J. Estabrook, R. A. Strouse, G. F. Buratto, S. K. *Journal of Physical Chemistry B,* **2000**, 104, 12137-12142.

20. Torimoto, T. Tsumura, N. Miyake, M. Nishizawa, M. Sakata, T. Mori, H. Yoneyama, H. *Langmuir*, **1999**, 15, 1853-1858

21. Tian, Y.C. Fendler, J.H. *Chemistry of Materials*, **1996**, 8, 969-974

22. Brust, M. Stuhr-Hansen, N. Norgaard, K. Christensen, J. Nielsen, L. Bjornholm, T. *Nano Letters*, **2001**, 1, 189-191

23. Hutchinson, T. O. Liu, Y. Kiely, C. Kiely, C. J. Brust, M. *Advanced Materials*, **2001**, 13, 1800-1803

24. Sadtler B. Wei A. *Chemical Communications*, **2002**, 15, 1604-5

25. Shipway, A. N. Lahav, M. Gabai, R. Willner, I. *Langmuir,* **2000**, 16, 8789-8795

26. Galow, T. H.; Boal, A. K. Rotello, Vincent M. *Advanced Materials*, **2000**, 12, 576-579

27. Kolny, J. Kornowski, A. Weller, H. *Nano Letters*, **2002**, 2, 361-364

28. Colvin, V. L. Goldstein, A. N. Alivisatos, A. P. *Journal of the American Chemical Society,* **1992**, 114, 5221-5230

29. Fullam, S. Rensmo, H. Rao, S.N. Fitzmaurice, D. *Chem. Mater.* **2002,** *14,* 3643-3650

30. Hicks, J. F. Zamborini, F. P. Murray, R. W. *Journal of Physical Chemistry ,* **2002**, 106, 7751-7757

31. Song, Y, Murray, Royce W. *Journal of the American Chemical Society*, **2002**, 124, 7096-7102

32. Cumberland, S. L. Berrettini, M. G. Javier, A. Strouse, G. F. *Chemistry of Materials*, **2003**, 15, 1047-1056.

33. Andres, R. P. Bielefeld, J. D. Henderson, J. I. Janes, D. B. Kolagunta, V. R. Kubiak, C. P. Mahoney, W. J. Osifchin, R. G. Science, **1996**, 273, 1690-1693

34. Henderson, J. I. Feng, S. Bein, T. Kubiak, C. P. *Langmuir*, **2000**, 16, 6183-6187

35. Novak, J. P. Feldheim, D. L. *Journal of the American Chemical Society*, **2000**, 122, 3979-3980

36. Brousseau, L. C. Novak, J. P.; Marinakos, S. M. Feldheim, D. L. *Advanced Materials,* **1999**, 11, 447-449

37. Fan, F. F. Yang, J. Cai, L. Price, D. W. Dirk, S. M. Kosynkin, D. V. Yao, Y. Rawlett, A. M. Tour, J. M.; Bard, A. J. *Journal of the American Chemical Society*, **2002**, 124, 5550-5560

38. Hensel, V. Godt, A. Popovitz-Biro, R. Cohen, H. Jensen, T. R. Kjaer, K. Weissbuch, I. Lifshitz, E. Lahav, M. *Chemistry--A European Journal*, **2002**, 8, 1413-1423

39. Sirota, M. Minkin, E. Lifshitz, E. Hensel, V. Lahav, M. *Journal of Physical Chemistry B,* **2001**, 105, 6792-6797.

40. M. Bruchez Jr., M. Maronne, P. Gin, S. Weiss, A. P. Alivisatos. *Science*, **1998**, 281, 2013-2016, S. J. James, C. A. Mirkin. *Chem. Rev.* **1999** ,99, 1849-1862,**;** W. C. W. Chen, S. Nie. *Science*, **1998**, 281, 2016-2017**;** R. Mahtab, H. H. Harden, C. J. Murphy *J. Am. Chem. Soc*. **2000**, 122*,* 14-7,**;** S.L. Bingham, J.L. Coffer, *J. Phys. Chem*. **1992**, 96, 10581.

41. Hayat, M., Ed. Colloidal Gold. Principles, Methods, and Applications; Academic Press; San Diego, 1989; Vol1

42. Alivisatos, A. P. Johnsson, K. P. Peng, X. Wilson, T. E. Loweth, C. J. Bruchez, M. P., Jr. Schultz, P. G. *Nature*, **1996**, 382, 609-611

43. Mirkin, C. A.; Letsinger, R.t L.; Mucic, R. C.; Storhoff, J. J. *Nature*, **1996**, 382, 607-609

44. Alivisatos, A. P. *Nat. Biotech.*, **2004**, 22, 47-52.

45. Dubertret,B.; Calame, M.; Libchaber, A. J. *Nat. Biotech.* **2001**, 19, 365-70.

46. Gerion, D. Parak, W. J. Williams, S. C. Zanchet, D. Micheel, C. M. Alivisatos, A. P *J. Am. Chem. Soc,* **2002**, *124*, 7070-7074.

47. Li, M.; W., Kim K. W.; Mann, S. *Chem. Mat.* **1999**, 11, 23-26.

48. Gearheart, L.A.; Ploehn, H. J.; Murphy, C. J, *Journal of Physical Chemistry B*, **2001**, 105, 12609-12615.

49. Niemeyer, C.M.; Burger, W.; Peplies, J. *Angewandte Chemie, International Edition,* **1998**, 37, 2265-2268.

50. Rosenthal, S. J. Tomlinson, I. Adkins, E. M. Schroeter, S. Adams, S. Swafford, L. McBride, J. Wang, Y. DeFelice, L. J. Blakely, R. D. *J. Am. Chem. Soc.* **2002**, 124; 4586-4594.

51. Tkachenko, A. G. Xie, H. Coleman, D. Glomm, W. Ryan, J. Anderson, M. F.; Franzen, S. Feldheim, D L. *Journal of the American Chemical Society*, 2003, 125, 4700-4701

Chapter 3. Nanofret (Yun, C. S.; Javier, A.; Peterson, S.; Reich, N. O.; Strouse, G. F. *J. Am. Chem. Soc.* Accepted 2004)

A. 1.4nm Nanogold-DNA-FAM Conjugate

The interrogation of biological systems using ensemble and single molecule Förster resonance energy transfer (FRET) and related resonant energy transfer (RET) processes has provided important mechanistic, as well as highly accurate static and dynamic distance measurements.[1-2] Currently, FRET techniques form an increasingly important component of the biophysicist's tool kit; [3-11] however, typical organic dye FRET pairs work at distances less than 65-100 angstroms due to the R^{-6} distance dependence inherent in a local dipole-dipole exchange process. [11-13] The investigation of a much broader range of macromolecular assemblies with this method is in principle attainable with appropriate reporter moieties; indeed the lack of such reagents has motivated highly creative alternatives.[11] Energy transfer processes involving much longer distances should be accessible using the array of dipoles of a metal nanomaterial surface as an acceptor. This would enable a Chance-Prock-Silbey (CPS) type energy transfer mechanism to dominate the ET process, giving rise to a R^{-4} energy transfer efficiency behavior and distances surpassing a simple local-dipole-dipole type mechanism, which was classically described by Förster. [12-15]

We observe an R^{-4} distance-dependent energy transfer process at distances of 180 angstroms in duplex DNA (60 bp), which we term Nano-FRET. The DNA duplexes are modified at the 5' ends with 1.4 nm Au ($Au_{1.4}$) as the acceptor and fluorescein

Figure 3-1. A) Illustration representing the Au nanocrystal DNA FAM construct and the topological and structural changes induced upon binding by M.*Eco*RI and R.*Eco*RI. B) is the absorption spectra of 1.4nm Au nanocrystals and the emission spectra of Fluorescein.

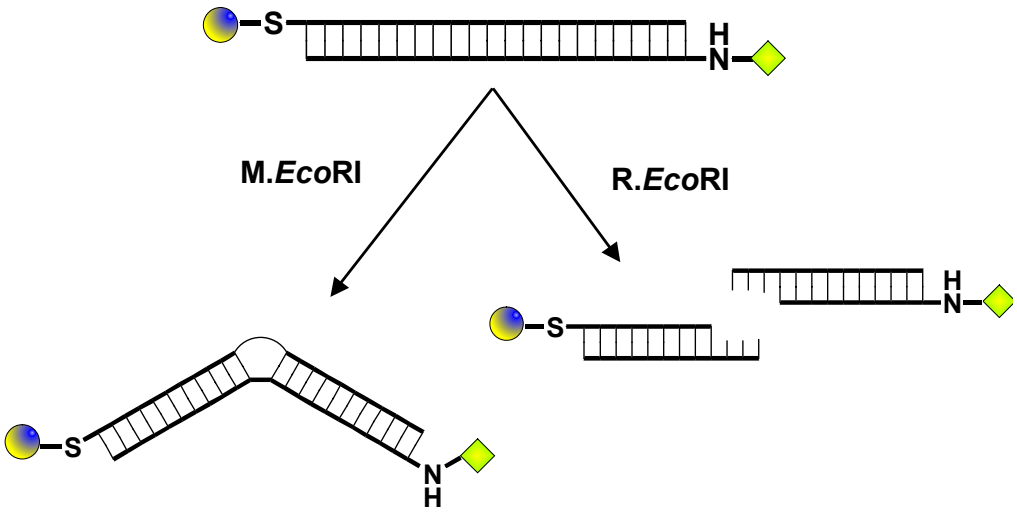

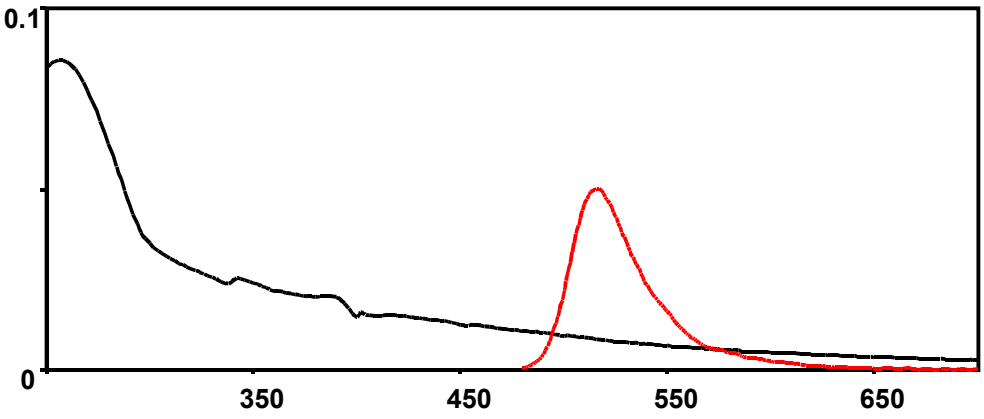

Figure 1. A) Cartoon representing the Au nanocrystal DNA FAM construct and the topological and structural changes induced upon binding by M.*Eco*RI and R.*Eco*RI. B) is the absorption spectra of 1.4nm Au nanocrystals and the emission spectra of Fluorescein.

(FAM) as the donor moiety on the complementary strand (Figure 1). The longer measurable distances arise from a R^{-4} separation dependence on quenching efficiency for the Nano-FRET mechanism, which results in an measurable R_0 value of 92 Å or an experimentally useable distance measurement range between 53 and 160 Å based on a 10-90% quenching efficiency curve for the 1.4 nm Au. The R_o value for Nano-FRET is significantly larger than observed for a Förster energy transfer pair such as TAMRA / FAM donor – acceptor pair with a R_0 of 56 Å.[3-10] The distance dependence of the Au-nanomaterial based Nano-FRET process is described in terms of a CPS type energy transfer mechanism.[15,16] We demonstrate the biological suitability of the Nano-FRET approach with a well-characterized sequence-specific DNA binding protein. In addition, these studies provide critical proof that energy transfer between a molecular donor and a nanoscale metal particle is more appropriately described in terms of an array of dipoles mechanism,[15,16] rather than a simple local dipole interaction, as suggested in earlier studies.[17-19]

The energy transfer behavior for three separation lengths of Au-DNA-FAM structures between 15 and 60 base pairs was analyzed (Figure 2). In all cases the gold nanocrystal-appended DNA exhibited length-dependent photoluminescence quenching. Gold attachment to the DNA via a monomaleimido functional group was carried out according to literature procedures.[20, 21] The 15-mer (6.2nm) displays a 68.2% quenching of the emission of the appended fluorescein relative to the DNA with the fluorophore alone. The 30-mer (10.1nm) and 60-mer (18.1nm) show 16.7%

Figure 3-2. Columns 1-3 present the photoluminescence data (λ_{ex} = 472 nm, 298K) for energy transfer in the Nano-FRET pair FAM – DNA- Au (1.4 nm) at 100 nM, where column 1 is for the 15 bp, column 2 is for the 30 bp and column 3 is for the 60 bp conjugate. The first row of spectra shows the photoluminescence of DNA-FAM without an appended acceptor (–), and with an appended acceptor (–), where Au and TAMRA are the respective acceptors in columns 1-4. The second row of spectra is the FRET conjugate in the presence (–) and absence (–) of 300 nM M.*Eco*RI, a 55-60° DNA bending and methylating enzyme. The third row presents the data for the FRET conjugates without the acceptor (–), with the acceptor (–), and following treatment with R.*Eco*RI endonuclease, a cutting enzyme (–).

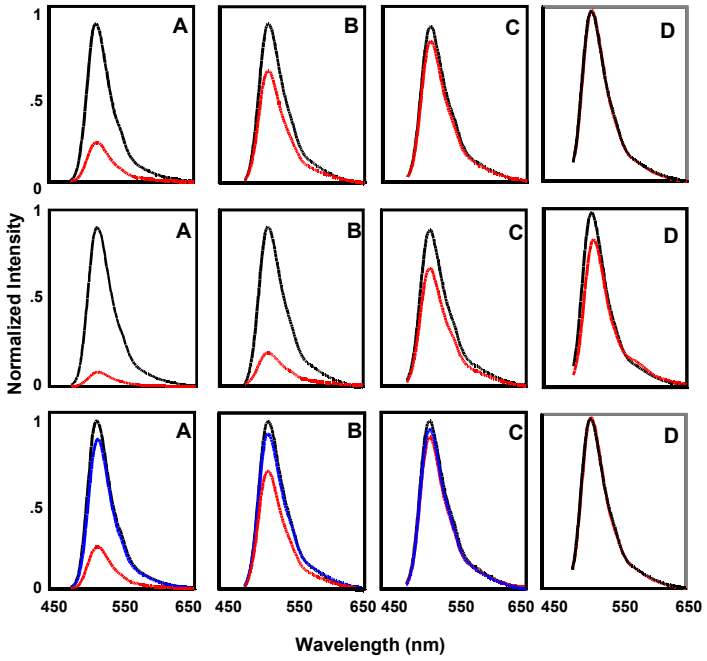

and 2.6% quenching respectively (Figure 2).[22-24] For comparison, energy transfer from FAM to TAMRA in a 30-mer assembly accounts for an energy transfer efficiency of less than 1%, which fits to the normal expected values for this FRET pair (Figure 2). As a control to ensure quenching does not arise from intermolecular interactions, the DNA was cut with R.*EcoR*I endonuclease, thereby releasing the FAM and Au nanocrystal. In analogy to molecular beacons[25-27] the FAM fluorescence intensity is increased, consistent with a characteristic loss of contact distance between the FAM and Au nanoparticle acceptor in the Nano-FRET conjugate structure.

A graphical representation of the distance-dependent behavior for Nano-FRET is shown in Figure 3. The energy transfer efficiency ($\Phi_{eff}=1-I/I_0$) can be calculated from the relative fluorescence intensity of FAM (I/I_0), where I is the intensity of Au-DNA-FAM and I_0 represents the intensity of FAM-DNA without the acceptor attached. Rewriting Φ_{eff} to represent the separation distance of the donor and acceptor (R) allows the Φ_{eff} to be related to the quenching radius R_0, where 50% of the emission intensity is quenched.

$$\Phi eff = \frac{1}{1+\left(R/R_0\right)^n} \qquad (1)$$

The quenching radius R_0, and the distance-scaling factor, *n*, were allowed to float during the fitting. In all replicated experiments, the value of *n* minimized to ~4.0. The minimization of *n*=4 strongly indicates that the distance scaling law is inconsistent with a classical Förster type mechanism typically invoked for a FRET

pair.[2,12] From the quantum efficiency plot, the value of R_0 can be determined when the quenching efficiency is 50%, yielding a surprising value of 92 Å. As a comparison, a theoretical plot indicating the predicted energy transfer efficiency un a purely Förster process between FAM and the 1.4nm Au nanocrystal is shown in Figure 3, which produces a calculated value of R_0 of 59Å in poor agreement with the experimentally observed data for Nano-FRET. From Figure 3, it is obvious that the quenching mechanism cannot be of the Förster-type.

The observation of enhanced long-range energy transfer following a R^{-4} distance dependence for Nano-FRET can be readily understood by inspection of the mathematical relationship for energy transfer from a local donor (FAM) to a nanoscale metallic acceptor ($Au_{1.4}$). The nanoscale metal particle can be described as an array of dipoles arising from the array of electrons with a metallic Fermi gas-like nature at the particle surface.[28] The theory for energy transfer between a molecular local dipole with an array of dipoles on a metallic surface was described by Chance, Prock, and Silbey (CPS) to follow an R^{-4} distance dependence for energy transfer.[15, 16, 29] The change in the scaling law for the distance dependence arises from the nature of the dipole interactions and the selection rules for dipole-dipole coupling. In the classical Förster energy transfer mechanism with a R^{-6} distance dependence, the electrons are assumed to be non-interacting, and therefore the distance-dependence tracks the interaction of two discrete electronic dipoles.[12] In energy transfer by CPS theory, the selection rule for the acceptor is no longer its oscillator strength, as found in Förster's theory, but rather the mean free path of the

Figure 3-3. Energy transfer efficiency plot of experimental quenching data for various DNA lengths of the FAM-DNA-Au conjugate. The red line (—) represents the best fit of the data using CPS theory, while the blue line (—)is the theoretical plot for Förster energy transfer in the FAM-DNA-Au conjugate. Circles (●) represent linear DNA, while triangles (▲) represent DNA treated with the enzyme, M.*Eco*RI. Data for a 30-bp FAM-DNA-TAMRA structure in the absence (○) and presence of M.*Eco*RI (△) are shown for comparison.

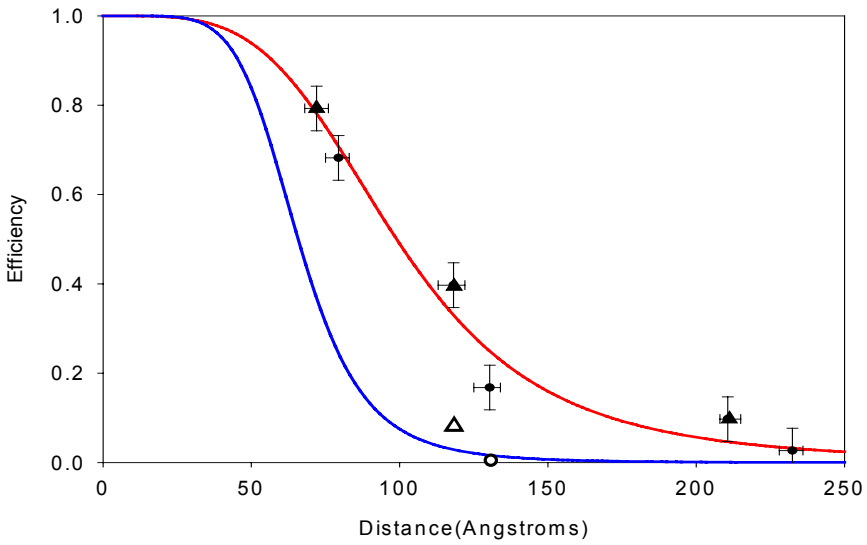

electron (l_e), which is an intrinsic property of the metal.[15,16,29] In the metal nanomaterial – organic dye conjugate the donor dipole oscillations interact with the multiple dipoles on the metal surface, which are parallel with the donor dipole vector. This vectorial selection rule is similar to the single dipole-dipole interaction described in Förster theory by the orientation factor, κ.

The R^{-4} drop in the observed efficiency (Φ_{CPS}) in CPS theory is described mathematically as a product of its rate (k_{CPS}) and the observed lifetime (τ), and depends on the interaction of the electronic transition moment of the electron in the molecule (μ) and the electron array velocities of the metal (l_e). (15)

$$\Phi_{CPS} = k_{CPS}\tau \sim \frac{|\mu|^2}{(l/l_e)}\frac{\tau}{R^4} \qquad (2)$$

This expression can be simplified by expanding the observed lifetime, and incorporating many of the constants, such as the lifetime (τ_0), into the cofactor R_0.

$$\Phi_{CPS} \sim \frac{1}{1+(R/R_o)^4}; \text{ where } R_o \sim \sqrt[4]{\frac{(l/l_e)}{\tau_0|\mu|^2}} \qquad (3)$$

There will also be a dependence on the diameter of the metal, l, such that this effect is enhanced when $l<l_e$; however, this does not suggest that smaller clusters always transfer more efficiently since the number of electrons in the array is correspondingly decreased. Since a "bulk-like" value for the conduction electron

population has been assumed, there will be a global maximum in the efficiency as a function of metal cluster size, as the competing effects of the number of conduction electrons (n_e) and the mean free path of those electrons (l_e) balance out. The experimentally measured distance dependent energy transfer efficiencies and the value of R_0 (Figure 3) in this study is consistent with the values found in CPS previous studies (50-300 Å) on bulk metal surfaces, confirming a metal surface mediated energy transfer mechanism is involved for these Nano-FRET conjugates.[16,29]

Further support for a CPS mechanism in the Nano-FRET process was sought by modulating the separation distance between the molecular donor and nanomaterial acceptor by treatment with a protein that induces a well-known topological change in the DNA structure. M.*Eco*RI, an enzyme known to bind a *GAATTC* sequence in duplex DNA, induces a 50-60^o bend in the DNA, as determined by gel-shifting and AFM methods.[30] This discretely closes the distance between the 5' end of each strand, thereby decreasing the FAM donor and $Au_{1.4}$ quencher separation distance by a predetermined length using a simple geometrical approximation. The DNA bending and subsequent stabilization of the target adenine in an extrahelical position, are critical for the AdoMet-dependent methylation reaction catalyzed by the enzyme.[30] These large-scale conformational transitions occur in the presence of the inactive AdoMet analog, sinefungin.[31,32] Unique to this approach, the enzyme allows discrete distance changes to be induced, thereby providing an internal standard for measurement of the distant-dependent energy transfer in Nano-FRET. Upon combining M.*Eco*RI methyltransferase (300nM), sinefungin 1 μM, and Au-DNA-

fluorescein (100nM), the fluorescein emission is decreased relative to the sample in the absence of protein (Figure 2). The introduction of M.*Eco*RI to the Au-DNA-FAM solutions required the use of protocols to exclude thiol-based reductants. Thiol based reductants were removed from the protein sample by dialysis at 4^0C for 36 h against buffer previously sparged with Argon.

The magnitude of the observed FAM emission quenching upon addition of the site-specific enzyme is increased by 79% for the 15-mer, 40% for the 30-mer, and 10% for the 60-mer (Figure 2) due to the shortened separation distance arising from the induced 55^o bend in the DNA backbone. Comparison to TAMRA and FAM on a 30-mer ds DNA yielded only an 8% change in energy transfer efficiency as predicted for the change in separation distances due to the M.*Eco*RI binding the DNA duplex. The efficiency of energy transfer for these materials follows an R^{-4} distance-dependence, providing further evidence of the participation of a CPS energy transfer mechanism for the Nano-FRET conjugates (Figures 2 and 3).

Measuring the stability of protein-ligand interactions is a hallmark of many bio-assays, and we sought to demonstrate the applicability of the Nano-FRET method to determine the disassociation constant (K_d) for the DNA-M.*Eco*RI complex. The experimentally measured donor fluorescence intensity at a given enzyme concentration (*I(Enz)*) is related to the fractional sum of the intensities without enzyme (*I(0)*) (emitting) and in the presence of a large excess of enzyme (*I(∞)*) (quenched emission). Thus, K_d can be extracted from the signal change of the donor

Figure 3-4: K_d calculations by Nano-FRET analysis of FAM intensity changes for the titration of 5 nM DNA with M.*Eco*RI in the presence of 1*u*M sinefungin for A) 15-mer, B) 30-mer, C) 60-mer.

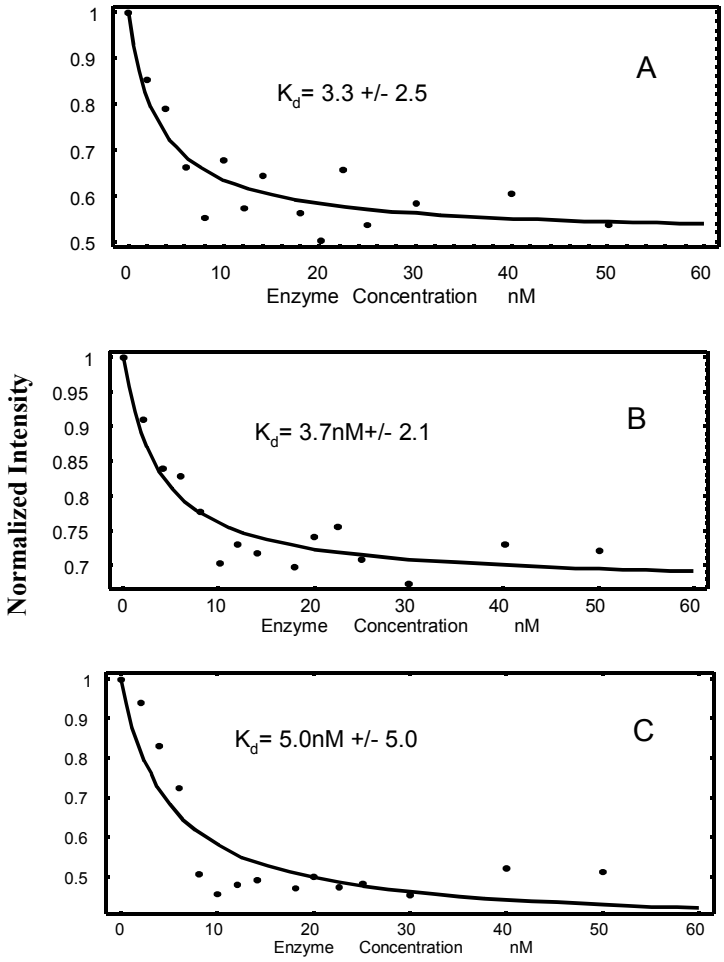

Figure 4: K_d calculations by Nano-FRET analysis of FAM intensity changes for the titration of 5 nM DNA with M.*Eco*RI in the presence of 1*u*M sinefungin for A) 15-mer, B) 30-mer, C) 60-mer.

molecule with increased enzyme concentration. Where E(∞) is the quenching efficiency with excess enzyme, and is a function of the distance-dependent energy transfer efficiencies in both bound ($\Phi_{EnT}(r_b)$) and unbound (Φ^{rb}_{EnT}) species, and

$$E(\infty) = 1 - \frac{I(\infty)}{I(0)} = 1 - \frac{1 - \Phi(r_b)_{EnT}}{1 - \Phi(r_u)_{EnT}} \quad (4)$$

Figure 4 shows the results of fitting Eq. 6, which gives rise to a K_d value between 3.3nM (15 mer) and 5.0nM (60 mer) for the DNA lengths. The measured K_d value is experimentally within the range found in similar experiments of native DNA duplexes (K_d value of 5nM) (32), providing evidence that the Nano-FRET system can be applied in bio-assay applications.

In addition to the studies conducted on the 1.4nm gold nanocrystals, further studies where done in the line of varying sizes of small gold nanocrystals. In this study we add a new dimension by measuring the effect to R_0 by varying the gold nanocrystal sizes in similar energy transfer experiments done with the 1.4nm. The sizes where chosen to flank the 1.4nm; one the smaller side undecagold, a cluster containing 11 gold atoms with a diameter of 0.7nm,[33] and on the larger side the 1.5nm gold nanocrystal[34] that are made up of 101 gold atoms.

B. 0.7nm Gold nanocrystal-DNA-FAM

In the case of the 0.7nm Au (Au_{11} or undecagold), the Au-DNA-FAM conjugates where assembled using the same methodology as that of the 1.4nm nanocrystal hybrids. The treatment of the construct with the M.*Eco*RI enzyme gave a reduction

Figure 3-5. Photoluminescence analysis (λ_{ex}= 472 nm, 298K) of Nano-FRET behavior for the donor-acceptor FRET pair FAM(D) - 0.7 nm Au nanocrystals (A) appended to the 5'-end of A) 10 bp (150nM) , B) 15 bp (150nM), C) 30 bp (150nM) duplex DNA, and D) 60 bp (50nM in buffer, pH = 7). The four spectra in each image represent the photolumonescence of DNA-Fluorescein without appended Au (—), Au-DNA-FAM (—), and Au-DNA-FAM treated with 300nM M.*Eco*RI, a 55° DNA bending and methylating enzyme (—) in the presence of 5*u*M Sinefungin.

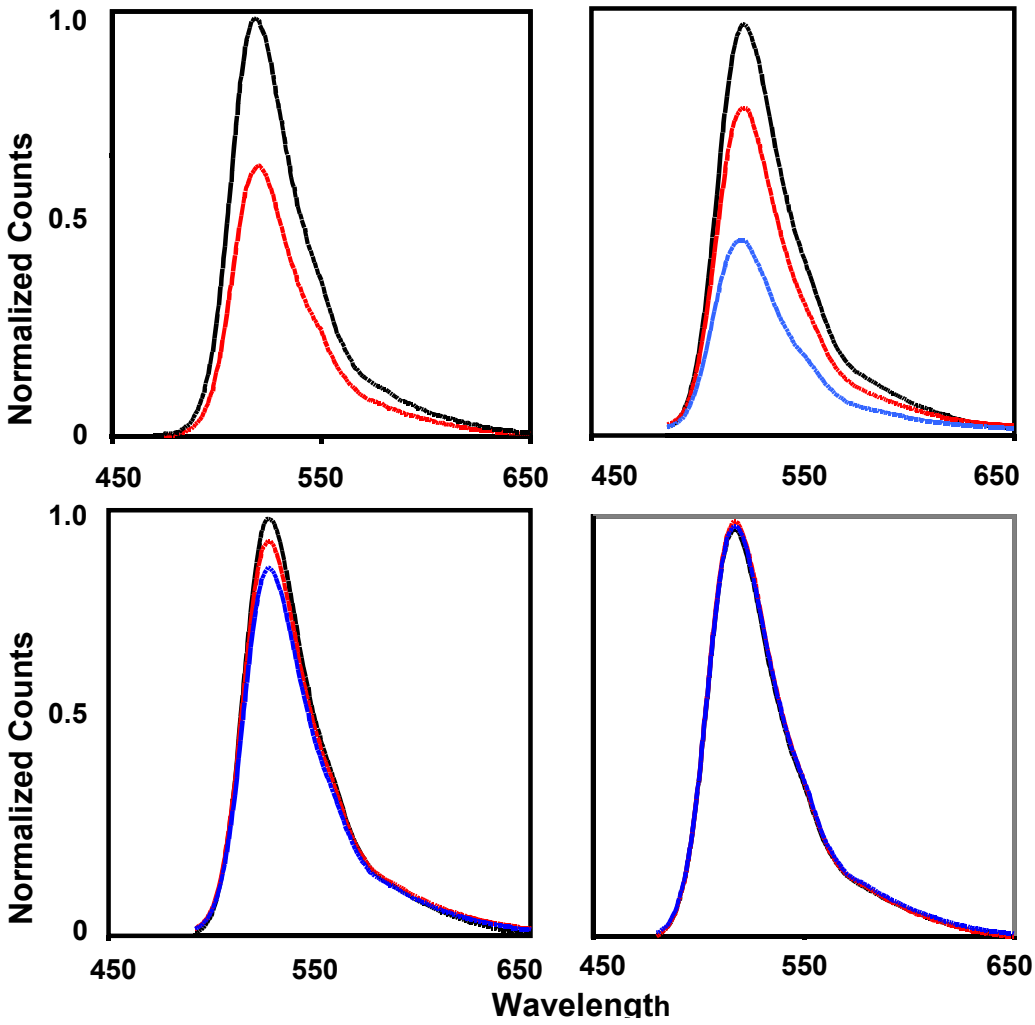

in the photoluminescence of the FAM as the topology of the DNA is bent by 55^{o}. The same experiments where done on the varying lengths of DNA, 15 bp, 30 bp, 60 bp, and an additional length of 10 bp. The results of the quenching experiments of the fluorophore by the nanocrystal are shown in figure 5. Once again there is an exhibition of length dependent quenching in all cases except the 60mer. Here the length of the DNA seems to have reached or exceeded the maxium distance of the nanomaterial to quench the fluorophore. As for the rest of the DNA strands, the gold nanomaterial quenches the FAM with an efficiency of 38%, 21%, and 2% for the 10mer, 15mer, and 30mer. With the treatment of the M.*Eco*RI methyltransferase, the energy transfer from the FAM to the gold nanocrystal is increased. The efficiency of energy transfer increases as the distance decreases between the donor and acceptor. The 15 bp and 30 bp DNA strands showed an increase of energy transfer of 45% and 9% respectively. For reasons of thermal stability the 10 bp DNA oligomer was designed without a recognition site for the methyltransferase thus did not participate in the enzyme bending experiment.

The efficiency of energy transfer between the undecagold and the FAM of various DNA lengths were plotted and fitted to an appropriate energy transfer theory. (Figure 6) The top plot shows the energy transfer efficiencies plotted to an R^{-4} based upon CPS theory while the bottom shows the efficiencies based upon an R^{-6} system. The curve fits are close to both theories, with the CPS theory with an R_0 of 58 Å while the Förster energy transfer yields a value of 62Å. This suggests that the

Figure 3-6. Energy transfer efficiency plot of experimental quenching data for various DNA lengths of the FAM-DNA-Undecagold conjugate. The top graph represents the best fit using CPS theory, while the bottom graph is the theoretical plot for Förster energy transfer in the FAM-DNA-Au conjugate. Circles (●) represent linear DNA, while triangles (▲) represent DNA treated with the enzyme, M.*Eco*RI.

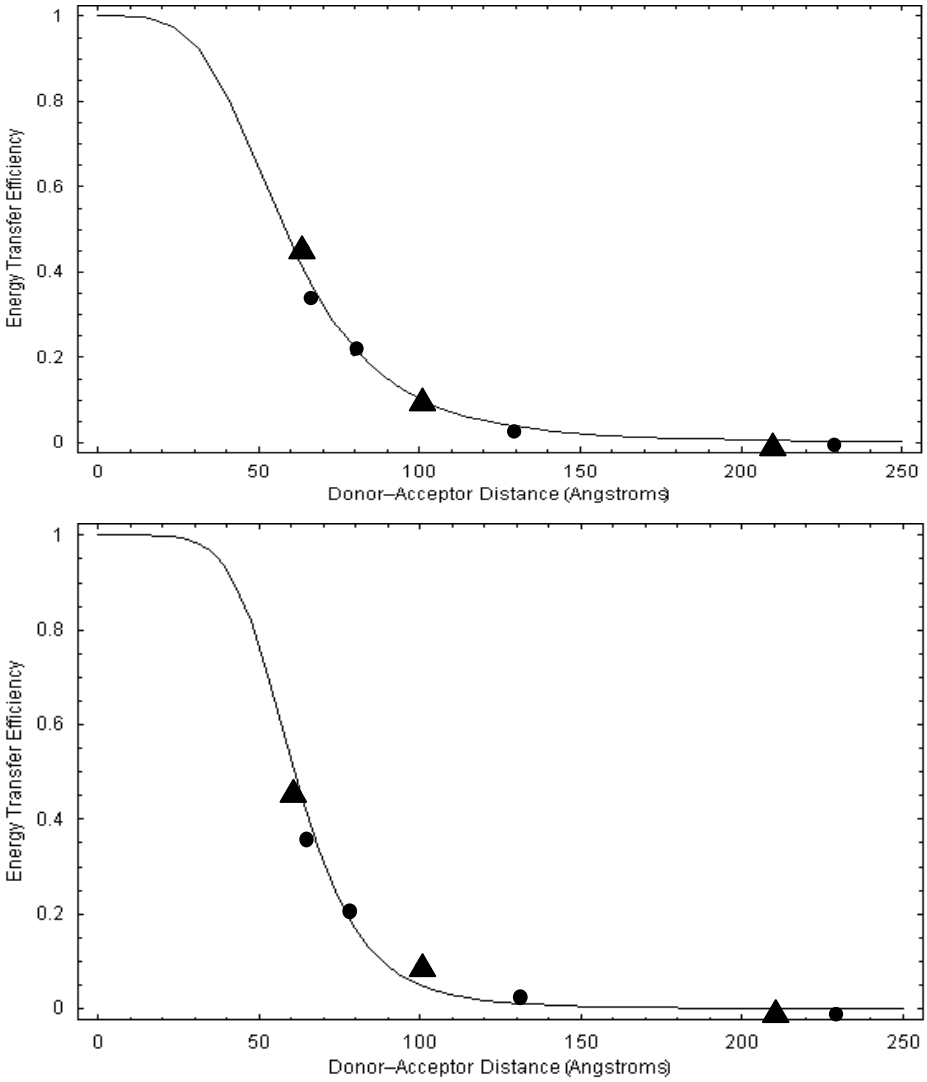

0.7nm gold nanomaterial behaves like a single dipole approximation, suggesting a nanomaterial with 11 gold atoms is molecular like.

C. 1.5nm Gold nanocrystal-DNA-FAM

The 1.5nm Au nanocrystal was used in conjunction with the DNA-FAM conjugate to examine the rates of energy transfer. Unlike the undeacagold and the 1.4nm gold nanocrystal, which bound the DNA through an indirect linkage, a functionalized arylphosphine of the surface that reacted with thiols, the 1.5nm Au nanocrystal was attached to the DNA-FAM complex via a direct linkage from the DNA to the gold surface. The DNA was synthesized with a 5' hexane thiol that can bind to the gold atoms on the surface of the nanomaterial. The attachment of the hexane thiol modified DNA to the nanomaterial is done by ligand exchange of one of the surface ligands.

All four lengths of DNA where employed in the experiment to determine the degree of energy transfer. Under the same conditions the 1.5nm gold nanocrystals appended with duplex DNA with FAM, showed DNA length dependence that is indicative of CPS theory. Figure 7 presents the photoluminescence data for the $Au_{1.5nm}$-DNA-FAM system. When the DNA-FAM system was attached to the surface of the nanomaterial through via the thiol linkage, the fluorphore intensity decreased by 81.6%, 61.1%, 21.7%, and 12% with respect to the 10mer, 15mer, 30mer, and the 60mer. Similarly the introduction of the M.*Eco*RI methyltransferase afforded increase

Figure 3-6. Photoluminescence analysis (λ_{ex}= 472 nm, 298K) of Nano-FRET behavior for the donor-acceptor FRET pair FAM(D) - 1.5 nm Au nanocrystals capped with (A) appended to the 5'-end of 10bp (150nM) B) 15 bp (150nM), C) 30 bp (150nM), and D) 60 bp (150nM) duplex DNA (20nM in buffer, pH = 7). The four spectra in each image represent the photolumonescence of DNA-Fluorescein without appended Au (—), Au-DNA-FAM (—), and Au-DNA-FAM treated with 300nM M.*Eco*RI, a 55 ◦ DNA bending and methylating enzyme (—) in the presence of 5*u*M Sinefungin.

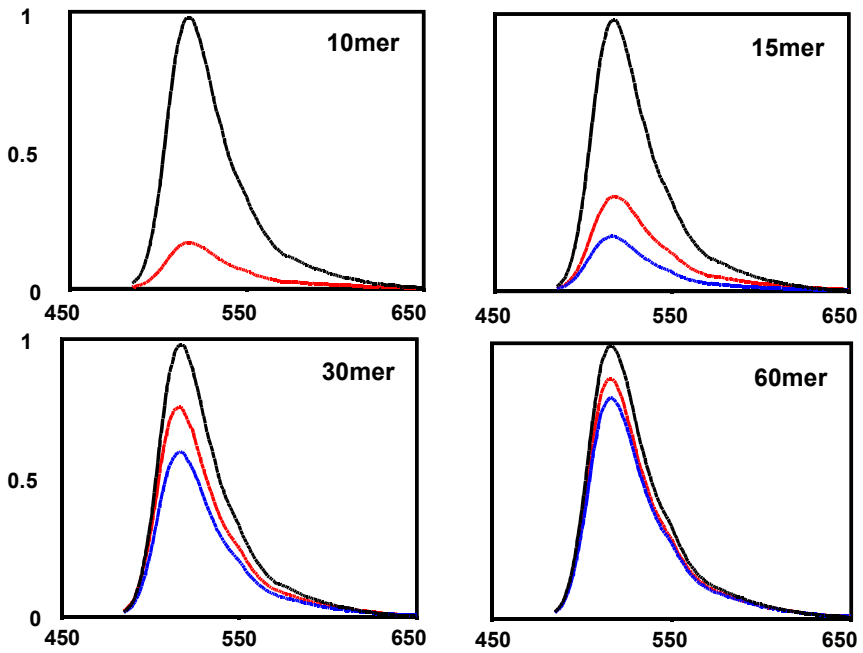

Figure 7. Photoluminescence analysis (λ_{ex}= 472 nm, 298K) of Nano-FRET behavior for the donor-acceptor FRET pair FAM(D) - 1.5 nm Au nanocrystals capped with (A) appended to the 5'-end of 10bp (150nM) B) 15 bp (150nM), C) 30 bp (150nM), and D) 60 bp (150nM) duplex DNA (20nM in buffer, pH = 7). The four spectra in each image represent the photolumonescence of DNA-Fluorescein without appended Au (—), Au-DNA-FAM (—), and Au-DNA-FAM treated with 300nM M.*Eco*RI, a 55 ◦ DNA bending and methylating enzyme (—) in the presence of 5*u*M Sinefungin.

in energy transfer to give a 78%, 31.6%, and 18% with respect to the 15 bp, 30 bp, and 60 bp DNA.

Ploting the energy transfer efficiencies as a function of distance gives a plot that presents a trend that follows the CPS-type of energy transfer. The R_0 that is derived from the plot gives a value of 86Å +/- 9Å compared to the theoretical Förster theory gives an R_0 value of 58Å. (Figure 8) This value is good agreement with the 1.4nm gold nanocrystal suggesting that they are similar materials that the 1.5nm Au nanocrystal follows the same trends as the both the undecagold and the 1.4nm Au nanocrystal. Traditionally the 1.4nm gold nanocrystal were synthesized and classified by Gunther Schmid *et al*. as gold cluster made up of 55 gold atoms and are uniformly monodisperse,[35] though marketed as a similar species of nanomaterial, nanogold is synthesized using a methodology developed by Schlog et al.[36] which has been known to be disperse with an average size at 1.4nm +/- 0.4nm in diameter. The 1.5nm gold nanocrystals are synthesized in a manner that gives them an average core diameter of 1.5nm +/- 0.4nm. It is possible that 1.4nm gold nanocrystals are similar in size to the Hutchison synthesis of gold nanocrystal. This could explain the similarities between the two species of nanomaterials as energy transfer acceptors.

D. Conclusion

Applying CPS-type energy transfer to a biological problem using Nano-FRET methodology allows enhanced energy transfer efficiency over long distances to be realized. Although the efficiency plots are consistent with the participation of a CPS energy transfer process, the absence of a true extended surface in a nanomaterial

Figure 3-7. Energy transfer efficiency plot of experimental quenching data for various DNA lengths of the FAM-DNA-Au 1.5nm conjugate. The plot is a best fit using CPS theory which gives the R_0 of 86Å +/- 9Å while Förster theory gives an R_0 value of 58Å. Circles ( ) represent linear DNA, while triangles ( ) represent DNA treated with the enzyme, M.*Eco*RI.

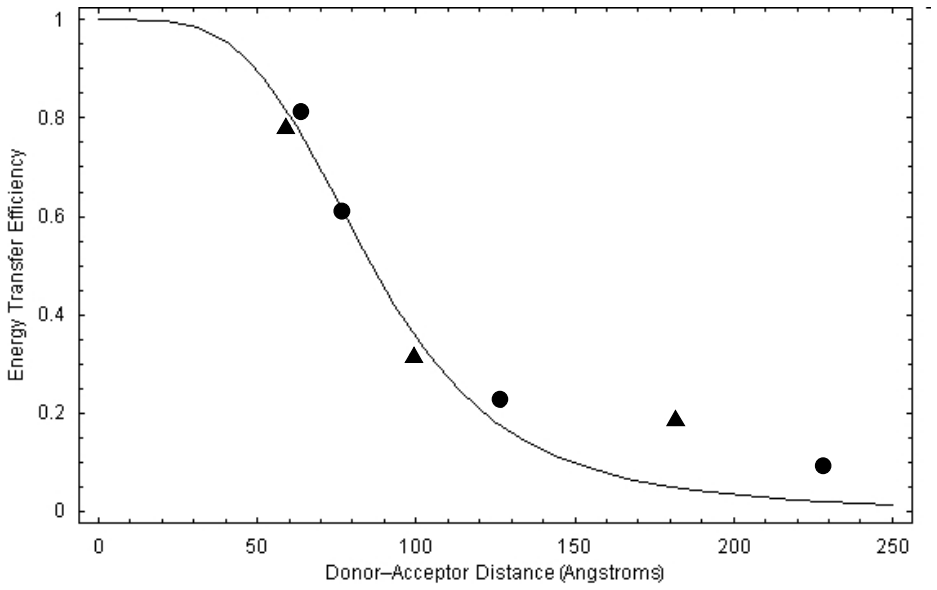

Figure 6. Energy transfer efficiency plot of experimental quenching data for various DNA lengths of the FAM-DNA-Au 1.5nm conjugate. The plot is a best fit using CPS theory which gives the R_0 of 86Å +/- 9Å while Förster theory gives an R_0 value of 58Å . Circles (●) represent linear DNA, while triangles (▲) represent DNA treated with the enzyme, M.*Eco*RI.

cannot be denied. It is therefore not entirely correct to describe this mechanism exclusively as a surface energy transfer process. However, within experimental error the data is consistent with a virtual plane of dipoles, which interact with the donor dipole; thus, although other interactions and mechanisms may be involved, the CPS process is clearly dominant. The Nano-FRET paradigm based on CPS theory extends the experimentally useable distances in biological systems by roughly a factor of two, without influencing the viability of the molecular interactions involved in protein binding on duplex DNA. Preliminary results on larger gold nanomaterials (diameter > 2nm) indicate the distance can be extended by an order of magnitude, consistent with CPS predictions.[14] These results will have a significant impact on the development of long-range optical assay technologies in biochemistry and biosensing.

Reference:

1. D. M.J. Lilly, T. J, Wilson, *Curr. Op. Chem. Bio.* **2000**, 4, 507-517.
2. S. Weiss, *Nat. Struc. Bio.* **2000**, 7, 724.
3. L. Stryer and R. P. Haugland, *Proc. Nat. Acad. Sci. U.S.A.* **1967**, 58, 719.
4. J. Li, R. Geyer. W. Tan, *Nuc. Acid Res.* **2000**, 28 E52.
5. T. Heyduk, E. Heyduk, *Nat. Biotech.* **2000**, 20, 171.
6. M. J. David, W. Lilley, J. Timothy, *Curr. Op. Chem Bio.* **2000**, 4, 507.
7. P. R. Selvin, *Nat. Struc. Bio.* **2000**, 7, 730-734.

8. A. Hillisch, M. Lorenz, S. Diekmann, *Curr. Op. Chem Bio.* **2000**, 11, 201-207.

9. B. Dubertret, M. Calame, A. J. Libchaber, *Nat. Biotech.* **2001**, 19, 365-70.

10. P.G. Shultz, *Proc. Nat. Acad. Sci. U.S.A*. **1999**, 96, 3670.

11. A.N. Kapanidis, Y.W. Ebright, R.D. Ludescher, S. Chan, R.H. Ebright*., J. Mol. Biol.* **312**, 453 (2001).
12. T.H. Förster, *Disc. Faraday Soc*. **1959**, 27.

13. J. R. Lakowicz, *Principles of fluorescence spectroscopy*, (Kluwer Academic/Plenum: New York, ed.2, 1999). [Second edition]

14. C.S. Yun, N.O. Reich, G.F. Strouse, unpublished results.

15. R. R. Chance, A. Prock, R. Silbey, *Adv. Chem. Phys.* **1978**, 37, 1-65.

16. A. P. Alivisatos, D. H. Waldeck, C. B. Harris, *J. Chem. Phys.* **1985**, 82, 541.

17. Artemyev, M. *Nanolett*, **2002**, 2, 1449.

18. Aguila, A.; Murray, R. W. *Langmuir***, 2000,** *16,* 5949.

19. El-Sayed, M. A. *Photochem. and Photobio.*, **2002**, 75, 591–597.

20. C.S. Yun, G.A. Khitrov, D.E. Vegona, N.O. Reich, G.F. Strouse, *J. Am. Chem.* **2002**, 124, 7644.

21. A.P. Alivisatos *et al. Nature,* **1996**, 382, 609.

22. DNA Sequence (15mer): 5'FAM CGA CGA ATT CCG AGC; 5' HS GCT CGG AAT TCG TCG.

23. DNA Sequence (30mer): 5'FAM CGC CTA CTA CCG AAT TCG ATA GTC ATC AGC; 5' HS GCT GAT GAC TAT CGA ATT CGG TAG TAG GCG.

24. DNA Sequence (60mer): 5' FAM CAC TGA TGC TAT ACG GCT GAT GAC TAT CGA ATT CGG TAG TAG GCG AGC TCC TTC ATA GGC; 5' HS GCC TAT GAA GGA GCT CGC CTA CTA CCG AAT TCG ATA GTC ATC AGC CGT ATA GCA TCA GTG.

25. N. E. Broude, *Trends in Biotech.* **2002**, 20, 249.

26. X. Fang, J. J, Li, J. Perlette, W. Tan, K. Wang, *Anal. Chem.* **2000**, 72, 747A.

27. A centered *GAATTC* sequence recognized by M.*Eco*RI methyltransferase[1] and R.*Eco*RI endonuclease was included to enable studies involving protein-DNA interactions.

28. M. Quinten, *Zeitschrift fur Phys. B-Cond. Mat.* **1996**, 101, 211.

29. K. Kuhnke *et al. Phys. Rev. Lett.* **1997**, 79, 3246.

30. R.A. Garcia, C.J. Bustamante, N.O.Reich, *Proc. Natl. Acad. Sci. U.S.A.* 1996, 93, 7618.

31. N. O. Reich, J. Mashhoon, *J. Bio. Chem.* **1990**, 265**,** 8966.

32. N. O. Reich, N. Mashhoon, *Biochem*, **1991**, 30, 2933.

33. Jahn, W. *Journal of Structural Biology* **1999**, 127, 106-112.

34. Weare, W. W.; Reed, S. M.; Warner, M. G.; Hutchison, J. E. J. Am. Chem Soc. **2000**, 122, 12890-12891.

35. Schmid, G.; Pfeil, R.; Boses, R.; Banderman, F.; Meyer, S.; Calis, G. H. M.; van der Velden, J. W. A. Chem Ber. **1981**, 114, 3634.

36. Rapoport, D. H.; Vogel, W.; Colfen, H.; Schlogl, R. *J. Phys. Chem. B.* **1997**, *101*, 4175.

Chapter 3. Nanofret (Yun, C. S.; Javier, A.; Peterson, S.; Reich, N. O.; Strouse, G. F. *J. Am. Chem. Soc.* Accepted 2004)

A. 1.4nm Nanogold-DNA-FAM Conjugate

The interrogation of biological systems using ensemble and single molecule Förster resonance energy transfer (FRET) and related resonant energy transfer (RET) processes has provided important mechanistic, as well as highly accurate static and dynamic distance measurements.[1-2] Currently, FRET techniques form an increasingly important component of the biophysicist's tool kit; [3-11] however, typical organic dye FRET pairs work at distances less than 65-100 angstroms due to the R^{-6} distance dependence inherent in a local dipole-dipole exchange process. [11-13] The investigation of a much broader range of macromolecular assemblies with this method is in principle attainable with appropriate reporter moieties; indeed the lack of such reagents has motivated highly creative alternatives.[11] Energy transfer processes involving much longer distances should be accessible using the array of dipoles of a metal nanomaterial surface as an acceptor. This would enable a Chance-Prock-Silbey (CPS) type energy transfer mechanism to dominate the ET process, giving rise to a R^{-4} energy transfer efficiency behavior and distances surpassing a simple local-dipole-dipole type mechanism, which was classically described by Förster. [12-15]

We observe an R^{-4} distance-dependent energy transfer process at distances of 180 angstroms in duplex DNA (60 bp), which we term Nano-FRET. The DNA duplexes are modified at the 5' ends with 1.4 nm Au ($Au_{1.4}$) as the acceptor and fluorescein

Figure 3-1. A) Illustration representing the Au nanocrystal DNA FAM construct and the topological and structural changes induced upon binding by M.*Eco*RI and R.*Eco*RI. B) is the absorption spectra of 1.4nm Au nanocrystals and the emission spectra of Fluorescein.

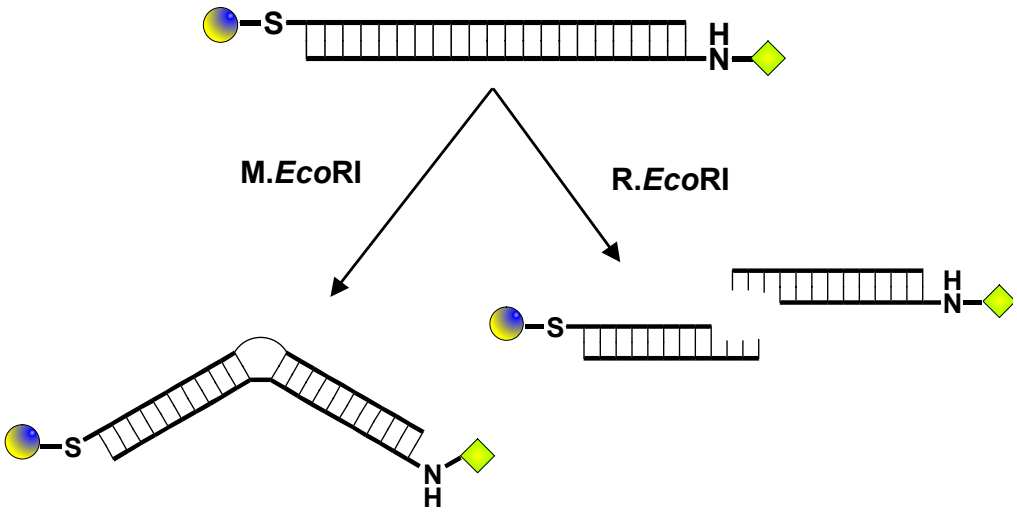

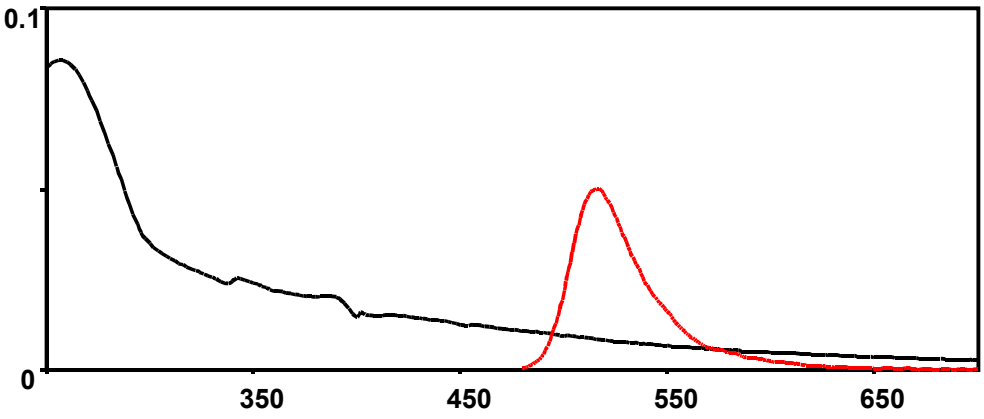

Figure 1. A) Cartoon representing the Au nanocrystal DNA FAM construct and the topological and structural changes induced upon binding by M.*Eco*RI and R.*Eco*RI. B) is the absorption spectra of 1.4nm Au nanocrystals and the emission spectra of Fluorescein.

(FAM) as the donor moiety on the complementary strand (Figure 1). The longer measurable distances arise from a R^{-4} separation dependence on quenching efficiency for the Nano-FRET mechanism, which results in an measurable R_0 value of 92 Å or an experimentally useable distance measurement range between 53 and 160 Å based on a 10-90% quenching efficiency curve for the 1.4 nm Au. The R_o value for Nano-FRET is significantly larger than observed for a Förster energy transfer pair such as TAMRA / FAM donor – acceptor pair with a R_0 of 56 Å.[3-10] The distance dependence of the Au-nanomaterial based Nano-FRET process is described in terms of a CPS type energy transfer mechanism.[15,16] We demonstrate the biological suitability of the Nano-FRET approach with a well-characterized sequence-specific DNA binding protein. In addition, these studies provide critical proof that energy transfer between a molecular donor and a nanoscale metal particle is more appropriately described in terms of an array of dipoles mechanism,[15,16] rather than a simple local dipole interaction, as suggested in earlier studies.[17-19]

The energy transfer behavior for three separation lengths of Au-DNA-FAM structures between 15 and 60 base pairs was analyzed (Figure 2). In all cases the gold nanocrystal-appended DNA exhibited length-dependent photoluminescence quenching. Gold attachment to the DNA via a monomaleimido functional group was carried out according to literature procedures.[20, 21] The 15-mer (6.2nm) displays a 68.2% quenching of the emission of the appended fluorescein relative to the DNA with the fluorophore alone. The 30-mer (10.1nm) and 60-mer (18.1nm) show 16.7%

Figure 3-2. Columns 1-3 present the photoluminescence data (λ_{ex} = 472 nm, 298K) for energy transfer in the Nano-FRET pair FAM – DNA- Au (1.4 nm) at 100 nM, where column 1 is for the 15 bp, column 2 is for the 30 bp and column 3 is for the 60 bp conjugate. The first row of spectra shows the photoluminescence of DNA-FAM without an appended acceptor (–), and with an appended acceptor (–), where Au and TAMRA are the respective acceptors in columns 1-4. The second row of spectra is the FRET conjugate in the presence (–) and absence (–) of 300 nM M.*Eco*RI, a 55-60° DNA bending and methylating enzyme. The third row presents the data for the FRET conjugates without the acceptor (–), with the acceptor (–), and following treatment with R.*Eco*RI endonuclease, a cutting enzyme (–).

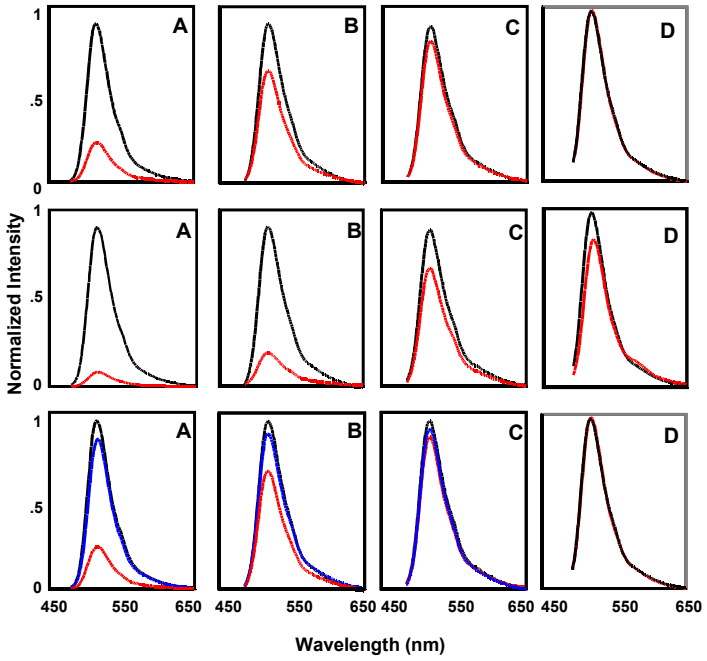

and 2.6% quenching respectively (Figure 2).[22-24] For comparison, energy transfer from FAM to TAMRA in a 30-mer assembly accounts for an energy transfer efficiency of less than 1%, which fits to the normal expected values for this FRET pair (Figure 2). As a control to ensure quenching does not arise from intermolecular interactions, the DNA was cut with R.*EcoR*I endonuclease, thereby releasing the FAM and Au nanocrystal. In analogy to molecular beacons[25-27] the FAM fluorescence intensity is increased, consistent with a characteristic loss of contact distance between the FAM and Au nanoparticle acceptor in the Nano-FRET conjugate structure.

A graphical representation of the distance-dependent behavior for Nano-FRET is shown in Figure 3. The energy transfer efficiency ($\Phi_{eff}=1-I/I_0$) can be calculated from the relative fluorescence intensity of FAM (I/I_0), where I is the intensity of Au-DNA-FAM and I_0 represents the intensity of FAM-DNA without the acceptor attached. Rewriting Φ_{eff} to represent the separation distance of the donor and acceptor (R) allows the Φ_{eff} to be related to the quenching radius R_0, where 50% of the emission intensity is quenched.

$$\Phi eff = \frac{1}{1+\left(R/R_0\right)^n} \qquad (1)$$

The quenching radius R_0, and the distance-scaling factor, *n*, were allowed to float during the fitting. In all replicated experiments, the value of *n* minimized to ~4.0. The minimization of *n*=4 strongly indicates that the distance scaling law is inconsistent with a classical Förster type mechanism typically invoked for a FRET

pair.[2,12] From the quantum efficiency plot, the value of R_0 can be determined when the quenching efficiency is 50%, yielding a surprising value of 92 Å. As a comparison, a theoretical plot indicating the predicted energy transfer efficiency un a purely Förster process between FAM and the 1.4nm Au nanocrystal is shown in Figure 3, which produces a calculated value of R_0 of 59Å in poor agreement with the experimentally observed data for Nano-FRET. From Figure 3, it is obvious that the quenching mechanism cannot be of the Förster-type.

The observation of enhanced long-range energy transfer following a R^{-4} distance dependence for Nano-FRET can be readily understood by inspection of the mathematical relationship for energy transfer from a local donor (FAM) to a nanoscale metallic acceptor ($Au_{1.4}$). The nanoscale metal particle can be described as an array of dipoles arising from the array of electrons with a metallic Fermi gas-like nature at the particle surface.[28] The theory for energy transfer between a molecular local dipole with an array of dipoles on a metallic surface was described by Chance, Prock, and Silbey (CPS) to follow an R^{-4} distance dependence for energy transfer.[15, 16, 29] The change in the scaling law for the distance dependence arises from the nature of the dipole interactions and the selection rules for dipole-dipole coupling. In the classical Förster energy transfer mechanism with a R^{-6} distance dependence, the electrons are assumed to be non-interacting, and therefore the distance-dependence tracks the interaction of two discrete electronic dipoles.[12] In energy transfer by CPS theory, the selection rule for the acceptor is no longer its oscillator strength, as found in Förster's theory, but rather the mean free path of the

Figure 3-3. Energy transfer efficiency plot of experimental quenching data for various DNA lengths of the FAM-DNA-Au conjugate. The red line (—) represents the best fit of the data using CPS theory, while the blue line (—)is the theoretical plot for Förster energy transfer in the FAM-DNA-Au conjugate. Circles (●) represent linear DNA, while triangles (▲) represent DNA treated with the enzyme, M.*Eco*RI. Data for a 30-bp FAM-DNA-TAMRA structure in the absence (○) and presence of M.*Eco*RI (△) are shown for comparison.

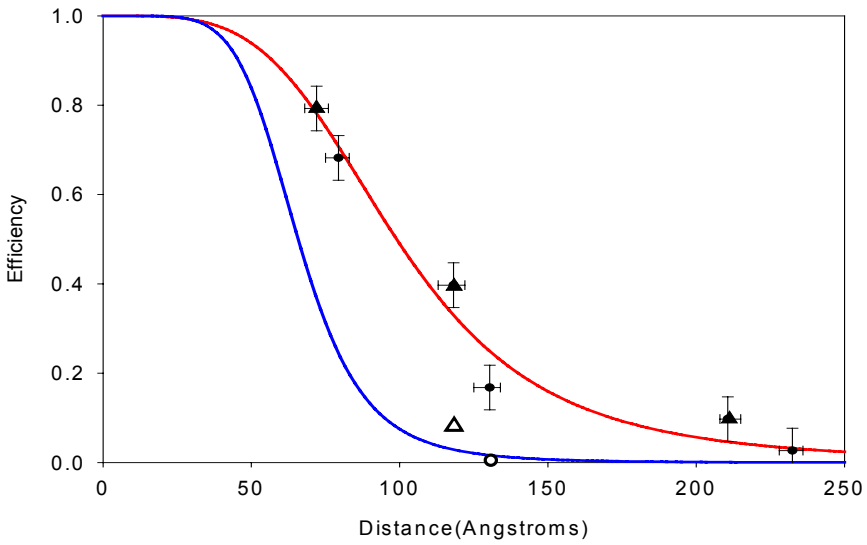

electron (l_e), which is an intrinsic property of the metal.[15,16,29] In the metal nanomaterial – organic dye conjugate the donor dipole oscillations interact with the multiple dipoles on the metal surface, which are parallel with the donor dipole vector. This vectorial selection rule is similar to the single dipole-dipole interaction described in Förster theory by the orientation factor, κ.

The R^{-4} drop in the observed efficiency (Φ_{CPS}) in CPS theory is described mathematically as a product of its rate (k_{CPS}) and the observed lifetime (τ), and depends on the interaction of the electronic transition moment of the electron in the molecule (μ) and the electron array velocities of the metal (l_e). (15)

$$\Phi_{CPS} = k_{CPS}\tau \sim \frac{|\mu|^2}{(l/l_e)}\frac{\tau}{R^4} \qquad (2)$$

This expression can be simplified by expanding the observed lifetime, and incorporating many of the constants, such as the lifetime (τ_0), into the cofactor R_0.

$$\Phi_{CPS} \sim \frac{1}{1+(R/R_o)^4}; \text{ where } R_o \sim \sqrt[4]{\frac{(l/l_e)}{\tau_0|\mu|^2}} \qquad (3)$$

There will also be a dependence on the diameter of the metal, l, such that this effect is enhanced when $l<l_e$; however, this does not suggest that smaller clusters always transfer more efficiently since the number of electrons in the array is correspondingly decreased. Since a "bulk-like" value for the conduction electron

population has been assumed, there will be a global maximum in the efficiency as a function of metal cluster size, as the competing effects of the number of conduction electrons (n_e) and the mean free path of those electrons (l_e) balance out. The experimentally measured distance dependent energy transfer efficiencies and the value of R_0 (Figure 3) in this study is consistent with the values found in CPS previous studies (50-300 Å) on bulk metal surfaces, confirming a metal surface mediated energy transfer mechanism is involved for these Nano-FRET conjugates.[16,29]

Further support for a CPS mechanism in the Nano-FRET process was sought by modulating the separation distance between the molecular donor and nanomaterial acceptor by treatment with a protein that induces a well-known topological change in the DNA structure. M.*Eco*RI, an enzyme known to bind a *GAATTC* sequence in duplex DNA, induces a 50-60^o bend in the DNA, as determined by gel-shifting and AFM methods.[30] This discretely closes the distance between the 5' end of each strand, thereby decreasing the FAM donor and $Au_{1.4}$ quencher separation distance by a predetermined length using a simple geometrical approximation. The DNA bending and subsequent stabilization of the target adenine in an extrahelical position, are critical for the AdoMet-dependent methylation reaction catalyzed by the enzyme.[30] These large-scale conformational transitions occur in the presence of the inactive AdoMet analog, sinefungin.[31,32] Unique to this approach, the enzyme allows discrete distance changes to be induced, thereby providing an internal standard for measurement of the distant-dependent energy transfer in Nano-FRET. Upon combining M.*Eco*RI methyltransferase (300nM), sinefungin 1 μM, and Au-DNA-

fluorescein (100nM), the fluorescein emission is decreased relative to the sample in the absence of protein (Figure 2). The introduction of M.*Eco*RI to the Au-DNA-FAM solutions required the use of protocols to exclude thiol-based reductants. Thiol based reductants were removed from the protein sample by dialysis at 4^0C for 36 h against buffer previously sparged with Argon.

The magnitude of the observed FAM emission quenching upon addition of the site-specific enzyme is increased by 79% for the 15-mer, 40% for the 30-mer, and 10% for the 60-mer (Figure 2) due to the shortened separation distance arising from the induced 55^o bend in the DNA backbone. Comparison to TAMRA and FAM on a 30-mer ds DNA yielded only an 8% change in energy transfer efficiency as predicted for the change in separation distances due to the M.*Eco*RI binding the DNA duplex. The efficiency of energy transfer for these materials follows an R^{-4} distance-dependence, providing further evidence of the participation of a CPS energy transfer mechanism for the Nano-FRET conjugates (Figures 2 and 3).

Measuring the stability of protein-ligand interactions is a hallmark of many bio-assays, and we sought to demonstrate the applicability of the Nano-FRET method to determine the disassociation constant (K_d) for the DNA-M.*Eco*RI complex. The experimentally measured donor fluorescence intensity at a given enzyme concentration (*I(Enz)*) is related to the fractional sum of the intensities without enzyme (*I(0)*) (emitting) and in the presence of a large excess of enzyme (*I(∞)*) (quenched emission). Thus, K_d can be extracted from the signal change of the donor

Figure 3-4: K_d calculations by Nano-FRET analysis of FAM intensity changes for the titration of 5 nM DNA with M.*Eco*RI in the presence of 1*u*M sinefungin for A) 15-mer, B) 30-mer, C) 60-mer.

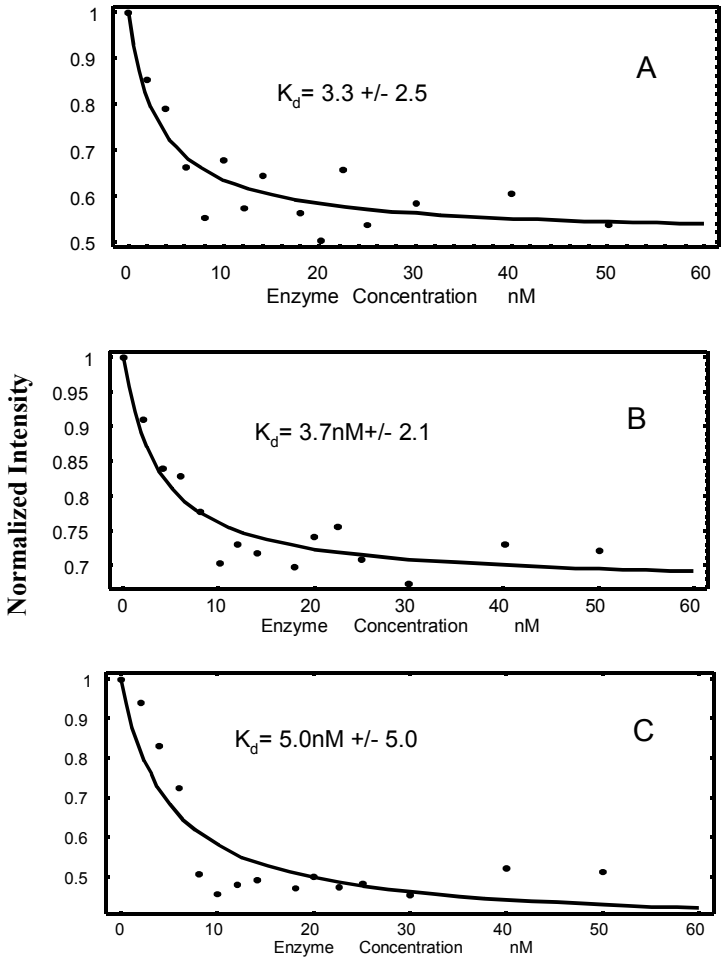

Figure 4: K_d calculations by Nano-FRET analysis of FAM intensity changes for the titration of 5 nM DNA with M.*Eco*RI in the presence of 1*u*M sinefungin for A) 15-mer, B) 30-mer, C) 60-mer.

molecule with increased enzyme concentration. Where E(∞) is the quenching efficiency with excess enzyme, and is a function of the distance-dependent energy transfer efficiencies in both bound ($\Phi_{EnT}(r_b)$) and unbound (Φ^{rb}_{EnT}) species, and

$$E(\infty) = 1 - \frac{I(\infty)}{I(0)} = 1 - \frac{1 - \Phi(r_b)_{EnT}}{1 - \Phi(r_u)_{EnT}} \quad (4)$$

Figure 4 shows the results of fitting Eq. 6, which gives rise to a K_d value between 3.3nM (15 mer) and 5.0nM (60 mer) for the DNA lengths. The measured K_d value is experimentally within the range found in similar experiments of native DNA duplexes (K_d value of 5nM) (32), providing evidence that the Nano-FRET system can be applied in bio-assay applications.

In addition to the studies conducted on the 1.4nm gold nanocrystals, further studies where done in the line of varying sizes of small gold nanocrystals. In this study we add a new dimension by measuring the effect to R_0 by varying the gold nanocrystal sizes in similar energy transfer experiments done with the 1.4nm. The sizes where chosen to flank the 1.4nm; one the smaller side undecagold, a cluster containing 11 gold atoms with a diameter of 0.7nm,[33] and on the larger side the 1.5nm gold nanocrystal[34] that are made up of 101 gold atoms.

B. 0.7nm Gold nanocrystal-DNA-FAM

In the case of the 0.7nm Au (Au_{11} or undecagold), the Au-DNA-FAM conjugates where assembled using the same methodology as that of the 1.4nm nanocrystal hybrids. The treatment of the construct with the M.*Eco*RI enzyme gave a reduction

Figure 3-5. Photoluminescence analysis (λ_{ex}= 472 nm, 298K) of Nano-FRET behavior for the donor-acceptor FRET pair FAM(D) - 0.7 nm Au nanocrystals (A) appended to the 5'-end of A) 10 bp (150nM) , B) 15 bp (150nM), C) 30 bp (150nM) duplex DNA, and D) 60 bp (50nM in buffer, pH = 7). The four spectra in each image represent the photolumonescence of DNA-Fluorescein without appended Au (—), Au-DNA-FAM (—), and Au-DNA-FAM treated with 300nM M.*Eco*RI, a 55° DNA bending and methylating enzyme (—) in the presence of 5*u*M Sinefungin.

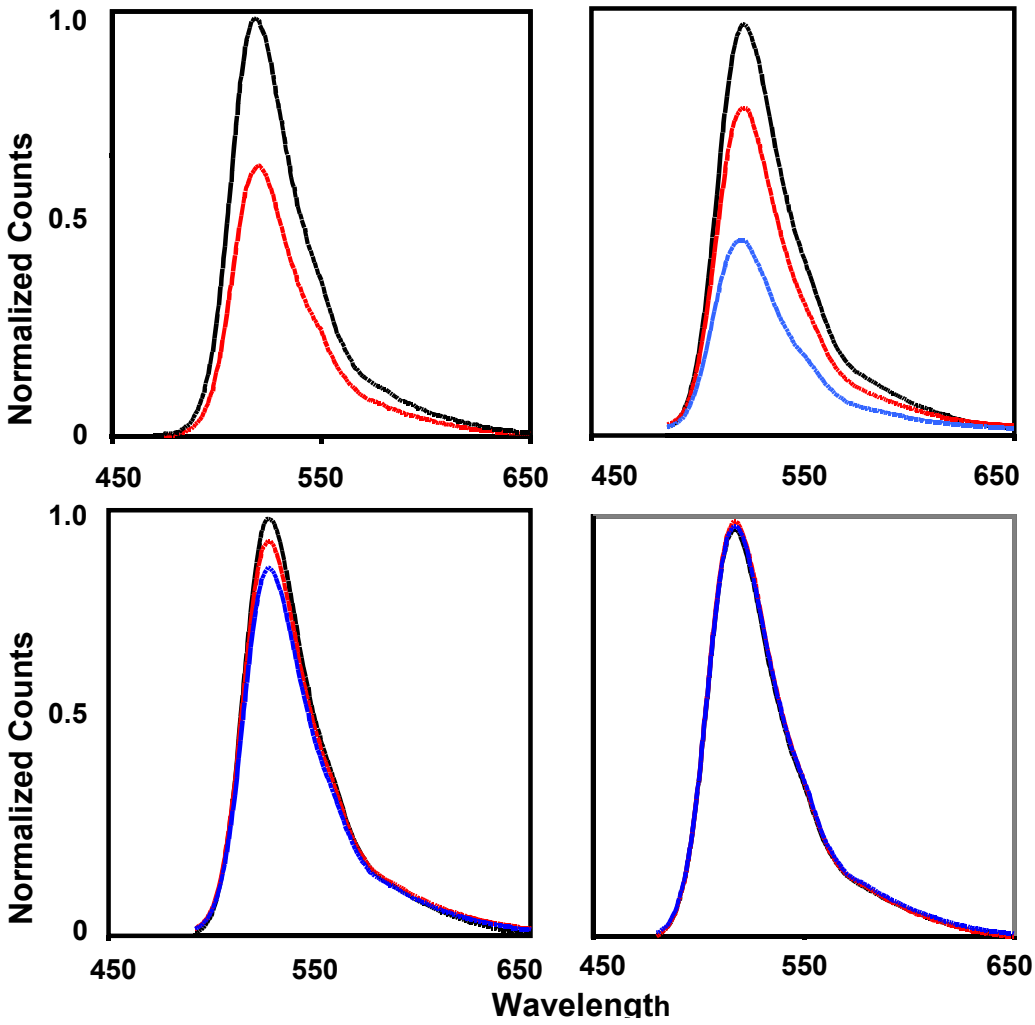

in the photoluminescence of the FAM as the topology of the DNA is bent by 55^{o}. The same experiments where done on the varying lengths of DNA, 15 bp, 30 bp, 60 bp, and an additional length of 10 bp. The results of the quenching experiments of the fluorophore by the nanocrystal are shown in figure 5. Once again there is an exhibition of length dependent quenching in all cases except the 60mer. Here the length of the DNA seems to have reached or exceeded the maxium distance of the nanomaterial to quench the fluorophore. As for the rest of the DNA strands, the gold nanomaterial quenches the FAM with an efficiency of 38%, 21%, and 2% for the 10mer, 15mer, and 30mer. With the treatment of the M.*Eco*RI methyltransferase, the energy transfer from the FAM to the gold nanocrystal is increased. The efficiency of energy transfer increases as the distance decreases between the donor and acceptor. The 15 bp and 30 bp DNA strands showed an increase of energy transfer of 45% and 9% respectively. For reasons of thermal stability the 10 bp DNA oligomer was designed without a recognition site for the methyltransferase thus did not participate in the enzyme bending experiment.

The efficiency of energy transfer between the undecagold and the FAM of various DNA lengths were plotted and fitted to an appropriate energy transfer theory. (Figure 6) The top plot shows the energy transfer efficiencies plotted to an R^{-4} based upon CPS theory while the bottom shows the efficiencies based upon an R^{-6} system. The curve fits are close to both theories, with the CPS theory with an R_0 of 58 Å while the Förster energy transfer yields a value of 62Å. This suggests that the

Figure 3-6. Energy transfer efficiency plot of experimental quenching data for various DNA lengths of the FAM-DNA-Undecagold conjugate. The top graph represents the best fit using CPS theory, while the bottom graph is the theoretical plot for Förster energy transfer in the FAM-DNA-Au conjugate. Circles (●) represent linear DNA, while triangles (▲) represent DNA treated with the enzyme, M.*Eco*RI.

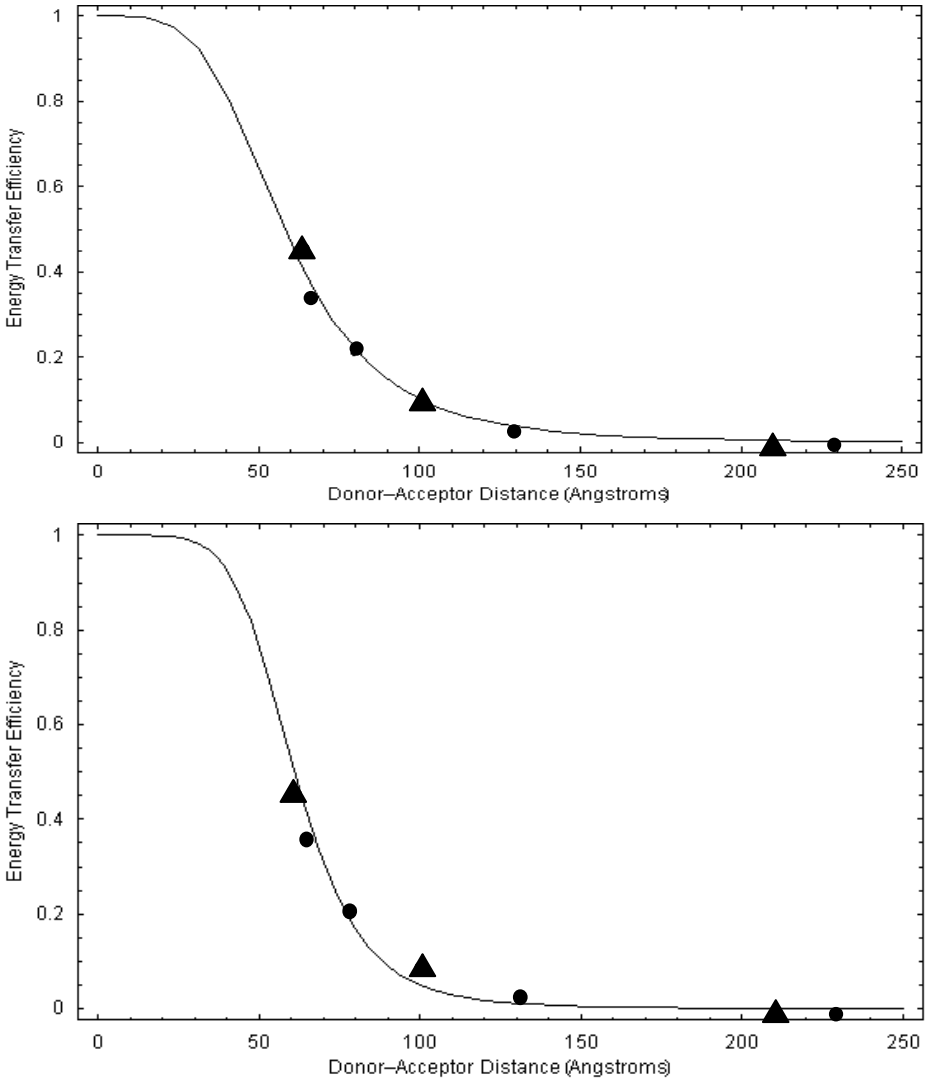

0.7nm gold nanomaterial behaves like a single dipole approximation, suggesting a nanomaterial with 11 gold atoms is molecular like.

C. 1.5nm Gold nanocrystal-DNA-FAM

The 1.5nm Au nanocrystal was used in conjunction with the DNA-FAM conjugate to examine the rates of energy transfer. Unlike the undeacagold and the 1.4nm gold nanocrystal, which bound the DNA through an indirect linkage, a functionalized arylphosphine of the surface that reacted with thiols, the 1.5nm Au nanocrystal was attached to the DNA-FAM complex via a direct linkage from the DNA to the gold surface. The DNA was synthesized with a 5' hexane thiol that can bind to the gold atoms on the surface of the nanomaterial. The attachment of the hexane thiol modified DNA to the nanomaterial is done by ligand exchange of one of the surface ligands.

All four lengths of DNA where employed in the experiment to determine the degree of energy transfer. Under the same conditions the 1.5nm gold nanocrystals appended with duplex DNA with FAM, showed DNA length dependence that is indicative of CPS theory. Figure 7 presents the photoluminescence data for the $Au_{1.5nm}$-DNA-FAM system. When the DNA-FAM system was attached to the surface of the nanomaterial through via the thiol linkage, the fluorphore intensity decreased by 81.6%, 61.1%, 21.7%, and 12% with respect to the 10mer, 15mer, 30mer, and the 60mer. Similarly the introduction of the M.*Eco*RI methyltransferase afforded increase

Figure 3-6. Photoluminescence analysis (λ_{ex}= 472 nm, 298K) of Nano-FRET behavior for the donor-acceptor FRET pair FAM(D) - 1.5 nm Au nanocrystals capped with (A) appended to the 5'-end of 10bp (150nM) B) 15 bp (150nM), C) 30 bp (150nM), and D) 60 bp (150nM) duplex DNA (20nM in buffer, pH = 7). The four spectra in each image represent the photolumonescence of DNA-Fluorescein without appended Au (—), Au-DNA-FAM (—), and Au-DNA-FAM treated with 300nM M.*Eco*RI, a 55 ◦ DNA bending and methylating enzyme (—) in the presence of 5*u*M Sinefungin.

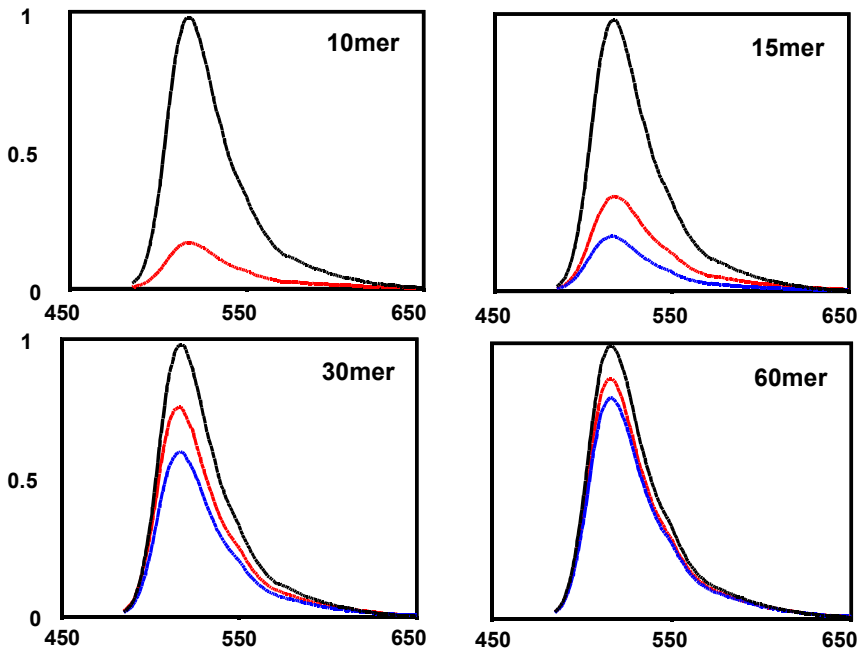

Figure 7. Photoluminescence analysis (λ_{ex}= 472 nm, 298K) of Nano-FRET behavior for the donor-acceptor FRET pair FAM(D) - 1.5 nm Au nanocrystals capped with (A) appended to the 5'-end of 10bp (150nM) B) 15 bp (150nM), C) 30 bp (150nM), and D) 60 bp (150nM) duplex DNA (20nM in buffer, pH = 7). The four spectra in each image represent the photolumonescence of DNA-Fluorescein without appended Au (—), Au-DNA-FAM (—), and Au-DNA-FAM treated with 300nM M.*Eco*RI, a 55 ◦ DNA bending and methylating enzyme (—) in the presence of 5*u*M Sinefungin.

in energy transfer to give a 78%, 31.6%, and 18% with respect to the 15 bp, 30 bp, and 60 bp DNA.

Ploting the energy transfer efficiencies as a function of distance gives a plot that presents a trend that follows the CPS-type of energy transfer. The R_0 that is derived from the plot gives a value of 86Å +/- 9Å compared to the theoretical Förster theory gives an R_0 value of 58Å. (Figure 8) This value is good agreement with the 1.4nm gold nanocrystal suggesting that they are similar materials that the 1.5nm Au nanocrystal follows the same trends as the both the undecagold and the 1.4nm Au nanocrystal. Traditionally the 1.4nm gold nanocrystal were synthesized and classified by Gunther Schmid *et al*. as gold cluster made up of 55 gold atoms and are uniformly monodisperse,[35] though marketed as a similar species of nanomaterial, nanogold is synthesized using a methodology developed by Schlog et al.[36] which has been known to be disperse with an average size at 1.4nm +/- 0.4nm in diameter. The 1.5nm gold nanocrystals are synthesized in a manner that gives them an average core diameter of 1.5nm +/- 0.4nm. It is possible that 1.4nm gold nanocrystals are similar in size to the Hutchison synthesis of gold nanocrystal. This could explain the similarities between the two species of nanomaterials as energy transfer acceptors.

D. Conclusion

Applying CPS-type energy transfer to a biological problem using Nano-FRET methodology allows enhanced energy transfer efficiency over long distances to be realized. Although the efficiency plots are consistent with the participation of a CPS energy transfer process, the absence of a true extended surface in a nanomaterial

Figure 3-7. Energy transfer efficiency plot of experimental quenching data for various DNA lengths of the FAM-DNA-Au 1.5nm conjugate. The plot is a best fit using CPS theory which gives the R_0 of 86Å +/- 9Å while Förster theory gives an R_0 value of 58Å. Circles ( ) represent linear DNA, while triangles ( ) represent DNA treated with the enzyme, M.*Eco*RI.

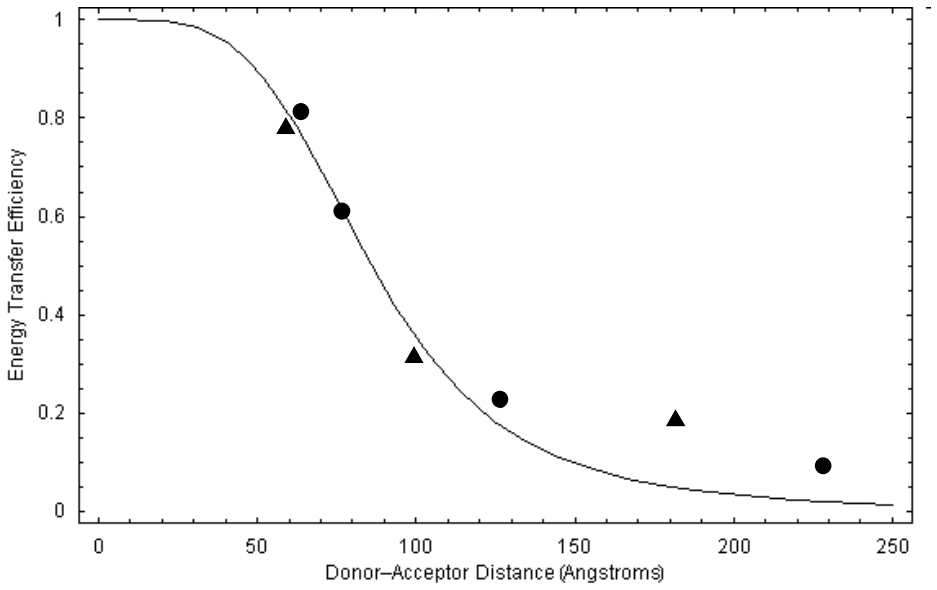

Figure 6. Energy transfer efficiency plot of experimental quenching data for various DNA lengths of the FAM-DNA-Au 1.5nm conjugate. The plot is a best fit using CPS theory which gives the R_0 of 86Å +/- 9Å while Förster theory gives an R_0 value of 58Å . Circles (●) represent linear DNA, while triangles (▲) represent DNA treated with the enzyme, M.*Eco*RI.

cannot be denied. It is therefore not entirely correct to describe this mechanism exclusively as a surface energy transfer process. However, within experimental error the data is consistent with a virtual plane of dipoles, which interact with the donor dipole; thus, although other interactions and mechanisms may be involved, the CPS process is clearly dominant. The Nano-FRET paradigm based on CPS theory extends the experimentally useable distances in biological systems by roughly a factor of two, without influencing the viability of the molecular interactions involved in protein binding on duplex DNA. Preliminary results on larger gold nanomaterials (diameter > 2nm) indicate the distance can be extended by an order of magnitude, consistent with CPS predictions.[14] These results will have a significant impact on the development of long-range optical assay technologies in biochemistry and biosensing.

Reference:

1. D. M.J. Lilly, T. J, Wilson, *Curr. Op. Chem. Bio.* **2000**, 4, 507-517.
2. S. Weiss, *Nat. Struc. Bio.* **2000**, 7, 724.
3. L. Stryer and R. P. Haugland, *Proc. Nat. Acad. Sci. U.S.A.* **1967**, 58, 719.
4. J. Li, R. Geyer. W. Tan, *Nuc. Acid Res.* **2000**, 28 E52.
5. T. Heyduk, E. Heyduk, *Nat. Biotech.* **2000**, 20, 171.
6. M. J. David, W. Lilley, J. Timothy, *Curr. Op. Chem Bio.* **2000**, 4, 507.
7. P. R. Selvin, *Nat. Struc. Bio.* **2000**, 7, 730-734.

8. A. Hillisch, M. Lorenz, S. Diekmann, *Curr. Op. Chem Bio.* **2000**, 11, 201-207.

9. B. Dubertret, M. Calame, A. J. Libchaber, *Nat. Biotech.* **2001**, 19, 365-70.

10. P.G. Shultz, *Proc. Nat. Acad. Sci. U.S.A*. **1999**, 96, 3670.

11. A.N. Kapanidis, Y.W. Ebright, R.D. Ludescher, S. Chan, R.H. Ebright*., J. Mol. Biol.* **312**, 453 (2001).
12. T.H. Förster, *Disc. Faraday Soc*. **1959**, 27.

13. J. R. Lakowicz, *Principles of fluorescence spectroscopy*, (Kluwer Academic/Plenum: New York, ed.2, 1999). [Second edition]

14. C.S. Yun, N.O. Reich, G.F. Strouse, unpublished results.

15. R. R. Chance, A. Prock, R. Silbey, *Adv. Chem. Phys.* **1978**, 37, 1-65.

16. A. P. Alivisatos, D. H. Waldeck, C. B. Harris, *J. Chem. Phys.* **1985**, 82, 541.

17. Artemyev, M. *Nanolett*, **2002**, 2, 1449.

18. Aguila, A.; Murray, R. W. *Langmuir***, 2000,** *16,* 5949.

19. El-Sayed, M. A. *Photochem. and Photobio.*, **2002**, 75, 591–597.

20. C.S. Yun, G.A. Khitrov, D.E. Vegona, N.O. Reich, G.F. Strouse, *J. Am. Chem.* **2002**, 124, 7644.

21. A.P. Alivisatos *et al. Nature,* **1996**, 382, 609.

22. DNA Sequence (15mer): 5'FAM CGA CGA ATT CCG AGC; 5' HS GCT CGG AAT TCG TCG.

23. DNA Sequence (30mer): 5'FAM CGC CTA CTA CCG AAT TCG ATA GTC ATC AGC; 5' HS GCT GAT GAC TAT CGA ATT CGG TAG TAG GCG.

24. DNA Sequence (60mer): 5' FAM CAC TGA TGC TAT ACG GCT GAT GAC TAT CGA ATT CGG TAG TAG GCG AGC TCC TTC ATA GGC; 5' HS GCC TAT GAA GGA GCT CGC CTA CTA CCG AAT TCG ATA GTC ATC AGC CGT ATA GCA TCA GTG.

25. N. E. Broude, *Trends in Biotech.* **2002**, 20, 249.

26. X. Fang, J. J, Li, J. Perlette, W. Tan, K. Wang, *Anal. Chem.* **2000**, 72, 747A.

27. A centered *GAATTC* sequence recognized by M.*Eco*RI methyltransferase[1] and R.*Eco*RI endonuclease was included to enable studies involving protein-DNA interactions.

28. M. Quinten, *Zeitschrift fur Phys. B-Cond. Mat.* **1996**, 101, 211.

29. K. Kuhnke *et al. Phys. Rev. Lett.* **1997**, 79, 3246.

30. R.A. Garcia, C.J. Bustamante, N.O.Reich, *Proc. Natl. Acad. Sci. U.S.A.* 1996, 93, 7618.

31. N. O. Reich, J. Mashhoon, *J. Bio. Chem.* **1990**, 265**,** 8966.

32. N. O. Reich, N. Mashhoon, *Biochem*, **1991**, 30, 2933.

33. Jahn, W. *Journal of Structural Biology* **1999**, 127, 106-112.

34. Weare, W. W.; Reed, S. M.; Warner, M. G.; Hutchison, J. E. J. Am. Chem Soc. **2000**, 122, 12890-12891.

35. Schmid, G.; Pfeil, R.; Boses, R.; Banderman, F.; Meyer, S.; Calis, G. H. M.; van der Velden, J. W. A. Chem Ber. **1981**, 114, 3634.

36. Rapoport, D. H.; Vogel, W.; Colfen, H.; Schlogl, R. *J. Phys. Chem. B.* **1997**, *101*, 4175.

Chapter 5. Oligophenylethylene Assembly of Quantum Dots:

Javier, A.; Yun, C.S.; Strouse, G.F. *Mat. Res. Soc. Symp. Proc*, **2003**, Vol. 776, Q2.1.1. Javier, A.; Yun, C.S.; Sorena, J.; Strouse, G.F. *J. Phys. Chem. B*, **2003**, 107, 435-442.

A. Introduction

Multifunctional organic ligands provide the bases of architectonic assembly of nanomaterials through the rigidity and/or topology of the linking molecule. In addition to the organizational properties of the assembly ligands, an enhancing or benevolent effect to the nanomaterial and its construct are important for the bottom up strategy to designing systems to be used in nanoelectronics and sensors.[1,2] Such benefits can be imparted with the modification of the linkers by varying the ligand length and constituents that allow changes in the electronic structure of the organic molecule to induce changes in the electronic or optical properties of the nanomaterials. The goal of engineering inorganic-organic hybrid nanomaterials is the culmination of the properties of both materials is to not only overcome the inadequacies of both materials but rather the augment the properties of both materials. In this chapter is the assembly and characterization of the CdSe nanocrystals assembled by oligo-phenyleneethylene.

In the assembly strategy for constructing inorganic and organic assemblies we employed oligomeric and polymeric phenyleneethylene (OPE and PPE, respectively) units equipped with varying length for the assembly of semi-conducting nanocrystals

Figure 5-1. Pictorial of the assembly strategies of CdSe with the OPE system

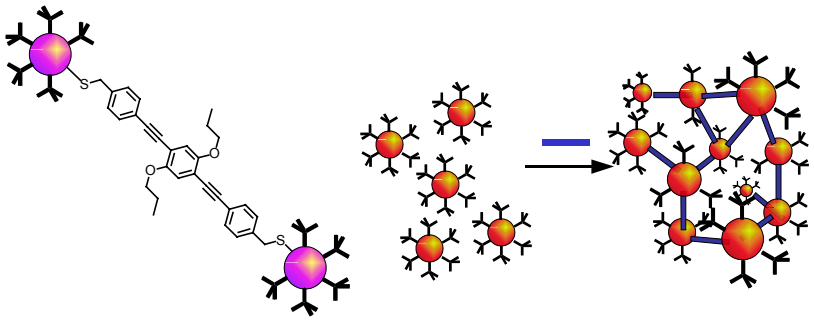

(CdSe) of varying size. (Figure 5-1) Ligand synthesis is accomplished with governing factors such as length of the overall linker, the number of repeat units, the substituents on the phenyl system to aid the solubility and the electronic properties of the of the oligomers, and the types of head groups that can be synthesized into the linker, for instance homofunctional groups will afford homogenous assemblies.

The assembly of the CdSe was performed with various linker lengths and nanocrystal sizes. In addition the assemblies where formed under a variation of time and concentrations of the nanocrystal and the organic molecules. Controlling the reaction time afforded control over the size of the inorganic-organic assemblies. The dimensions of the construct can be controlled from dimeric structures to monolithic structures that are several centimeters in diameter. Varying the concentration of the nanomaterial and the organic ligands produced different types of constructs and different levels of photoluminescence intensities. All of these factors governed the overall pathway to the synthesis of the materials. This section presents the synthesis and limited optical for the CdSe-OPE assemblies. A full description of the energy transfer procees and read-write technology in the thesis of A. Javier, 2005.

B. Discussion

The synthetic strategy for the preparation of the monodisperse oligo (1,4-phenyleneethynylene)'s is accomplished through a series of Hagihara-Sonogashira reactions. The type of reaction is a palladium - copper catalyzed cross coupling reaction between an arylhalide and a monoprotected or functionalized terminal

Figure 5-2. Synthetic scheme for OPE-1

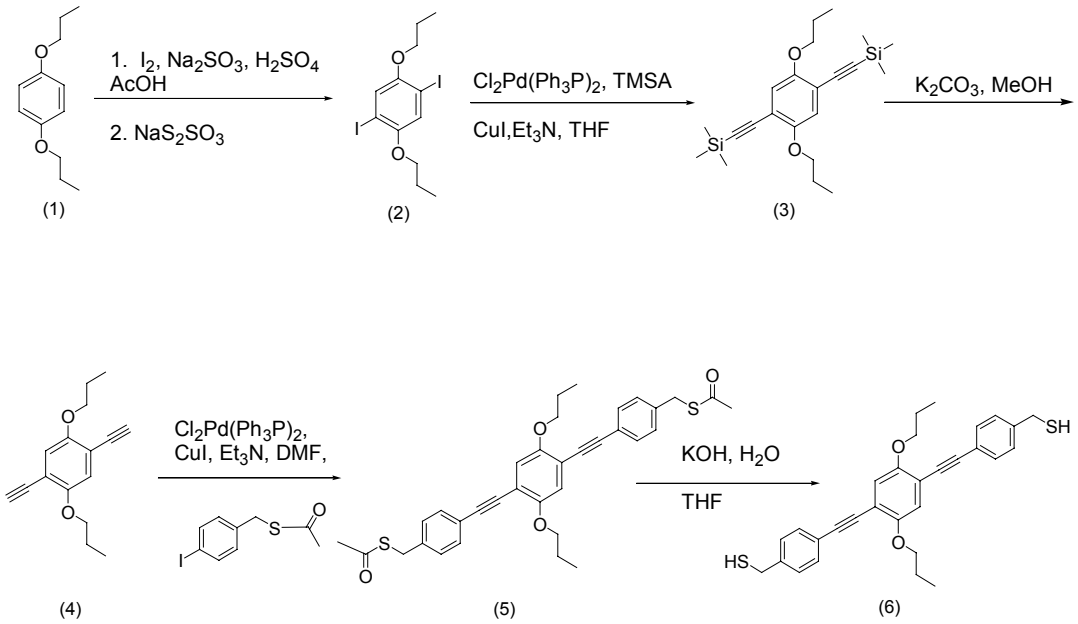

acetylene.[3] The strategy that was employed was based upon Tours *et al.*[4] synthesis of creating longer phenylethynylene repeat units *via* coupling of protected acetylene and aryliodies, deprotecting the acetylenic unit and coupling again another phenyl unit. Addition of alkoxy units to the phenyl moiety was done to enhance the solubility of the oligomeric and polymeric materials. The choice of benzylic thiols as binding groups was chosen for the strong metal thiol bound that is known to form between surface cadmium atoms. Another reason for the choice of the benzylic thiols rather than aryl thiols typically used by other researchers interested in the use of OPE's as molecular wires or to assemble gold nanocrystals, is that the homologation of the thiol by one carbon significantly raises the oxidation potential of the sulfhydryl group preventing photo-oxidation. This observation was made by Pietro et al.[5] when the CdS nanocrystals capped with thiophenol was photoexcited and the researchers saw the removal of the thiophenol capping group and formation of phenyldisulfide. In addition to loosing the capping group off the surface of the nanocrystal, the photoluminence of the CdS was completely quenched and eventually lead to the decomposition of the nanocrystal.

For the synthesis of the OPE-1, (Figure 5-2) an electrophyllic substitution ortho to the ether functionalities on compound (1) was done with iodine and potassium iodate gave the para-substituted aryl iodides (2) in 84% yield. The introduction of the ethynl groups to the benzene unit was done via a Hagihara-Sonogashira reaction with trimethylsilylethyne to give compound (3) in 98% yield. Deprotection of the trimethylsilyl group was done under basic methanolic solution to yield compound (4) in quantitative yield. The placement of the binding head groups was done with an

Figure 5-3. Synthetic scheme for OPE-0

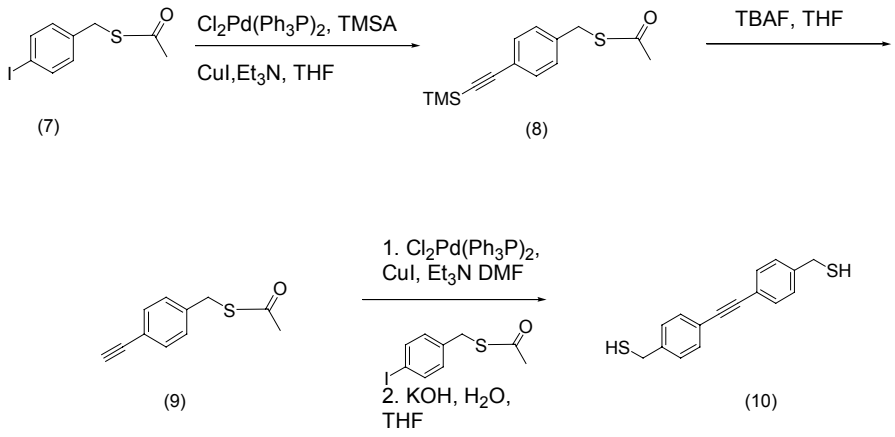

Figure 5-4. Synthetic scheme for OPE-3

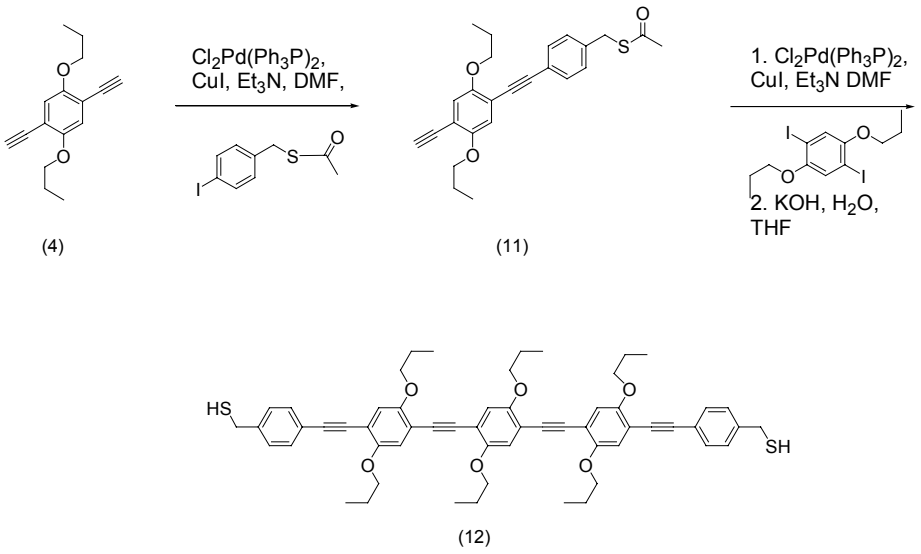

additional Hagihara-Sonogashira 4-iodobenzylthiol acetate (7) yielded compound (6) in 93% yield. Deprotection of the acetate protection groups was done with potassium hydroxide in a THF and water mixture to give in 89% yield compound (7). The total synthetic yield was 68%.

OPE-0 (Figure 5-3) was synthesized starting from the Hagihara-Sonogashira coupling of the protected iodobenzylthiol acetate and TMS-ethyne yielding compound (8) in 90%. The subsequent and quantitative deprotection of the TMS group with tetrabutylammonium fluoride in THF gives compound (9). A second Hagihara-Sonogashira coupling of (9) with 4-iodobenzylthiol acetate (7) gave 1,2 dibenzylthiolacetate-ethyne. The reaction was further carried on to the deprotection of the acetate group in a basic aqueous/THF solution to give 1,2 dibenzylthiolethyne (10) in an 80% yield.

OPE-3 (Figure 5-4) was synthesized similar to OPE-1 but diverged from compound (4). Here the diethynyldipropoxy benzene was reacted under Hagihara-Sonogashira coupling conditions with only one equivalent of 4-iodobenzylthiolacetate (7) to give compound (11) in an 84% yield. To extend the oligomeric section (11) was coupled with 2,5 diiodo 1,4 dipropoxybenzene (2). The reaction mixture was then deprotected using basic aqueous/THF solution to give compound (12) in 74% yield.

Cadmium Selenide synthesis was done using lyothermal methods based upon the use of dimethylcadmium and TOPSe to yield nanocrystals with a TOP/TOPO passivation surface[6,7]; a $Cd_{10}Se_4$ single source precursor providing a nanocrystals

Figure 5-5. TEM of 5nm CdSe assembled with OPE-1. Inset is a SAED of the assembly showing long-range order.

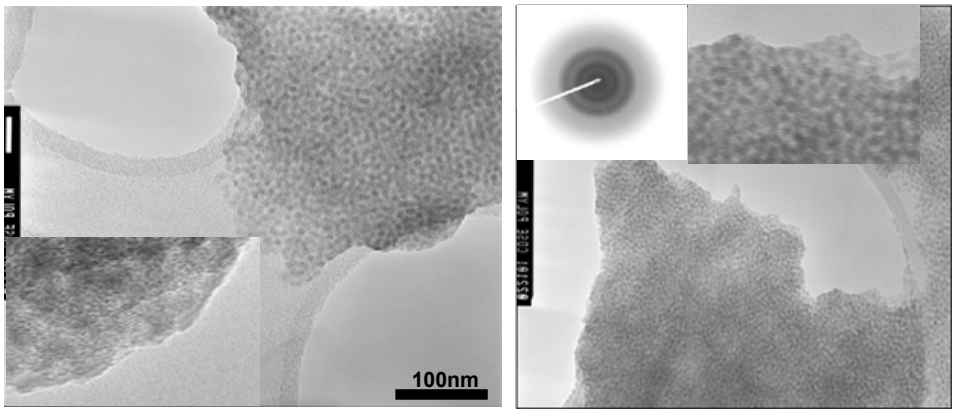

hexadecylamine ligand shell;[8] or aCdSe nanocrystals using CdO and TOPSe providing CdSe nanocrystals strongly passivated by dodecylphosphinate.[9]

Assembly of the nanocrystals was done by the addition of 2ml of 0.1M of OPE in toluene into a solution of 0.5 mg of CdSe in 5ml of toluene over a period of 10minutes. The mixture was allowed to react for 24 hours and slowly assembly from solution. The supernatant containing excess OPE and unreacted CdSe were decanted from the assembly. The precipitate was washed five times with 5ml of toluene and the smaller aggregates placed upon a TEM grid for visualization.

The OPE-1 assemblies (Figure 5-5) under TEM show large formations of free standing nanocrystals tightly packed together spanning large holes in the TEM grid. Small angle electron diffraction (SAED) showed that the constructs have no short-range order. Due to the three-dimensionality of the constructs the distances between the nanocrystals were difficult to resolve. When the OPE-3 was used to assemble the CdSe nanocrystals, the constructs once again showed the same lack of order by SAED, but upon examining the constructs from TEM images the distance between the nanocrystals are noticeably separated. Due to the dimensions of the construct the spacing between nanocrystals cannot be exactly measured. Though not quantitative, the length of the OPE does effect the separation distances of the nanocrystals in the assembly. This provides evidence that the rigid organic linkers can control nanocrystal separation distances. (Figure 5-6)

The constructs formed ranged from sizes of a few millimeters to a centimeter in diameter. The size was dependent upon the length of time that the assembly was

Figure 5-6. TEM of 5nm CdSe assembled with OPE-3. Inset is a SAED of the assembly showing long range order

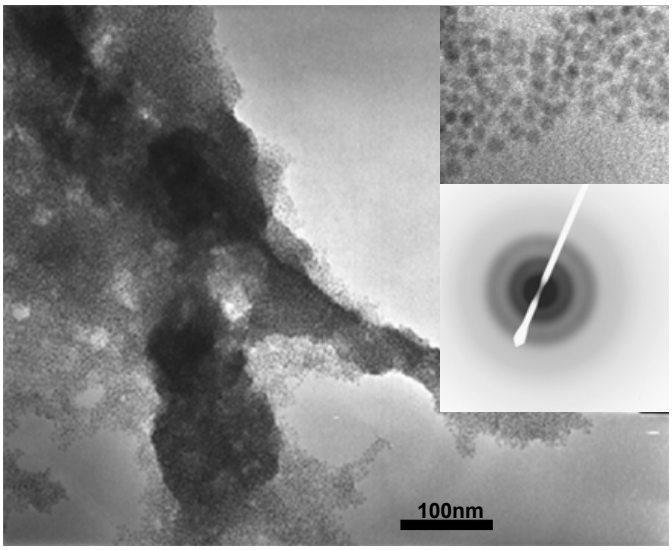

allowed to form. In the assemblies shown in the TEM's above the assembly time where done for extended period of time, however to control the size of the assemblies the reaction times can be shortened to create assemblies that are dimeric assemblies to constructs that are micrometers in size. (Figure 5-7) The assemblies can be stopped by the addition of methanol into the reaction mixture to precipitate the CdSe nanocrystals from the solution of OPE's. This allows the separation of the organic linker by decanting off the OPE solution from the precipitate. Introduction of toluene to the precipitate will solvates the unreacted nanocrystals, which can be decanted from the assemblies. Similar methodology has been used by Novak *et al*.[10] to generate and isolate the dimeric and trimeric gold nanocrystals assembled with a similar oligomers.

Reaction times for the assembly of CdSe nanocrystals with the OPE-0, 1, and 3, is dependent upon the nature of the ligand passivating the surface of the nanomaterial. The above reaction times apply for the CdSe passivated by trioctylphosphine oxide and hexadecylamine. For nanocrystals capped with dodecylphosphonate the assembly times require up to six days. The reason for the slow reaction time is the tight binding affinity of the phosphonate group to the cadmium surface. This reduced the rate at which the OPE ligands exchanged with the ligands on the surface of the nanomaterial and cross-linked the nanocrystals into the assembly. In addition to the longer duration for the assembly to form, the release of the phosphonate ligand from the surface of the nanocrystal interfered with the isolation of the assembly and in some cases remained in the assembly matrix. This

Figure 5-7. 5nm CdSe assembled of varying sizes with OPE-1.

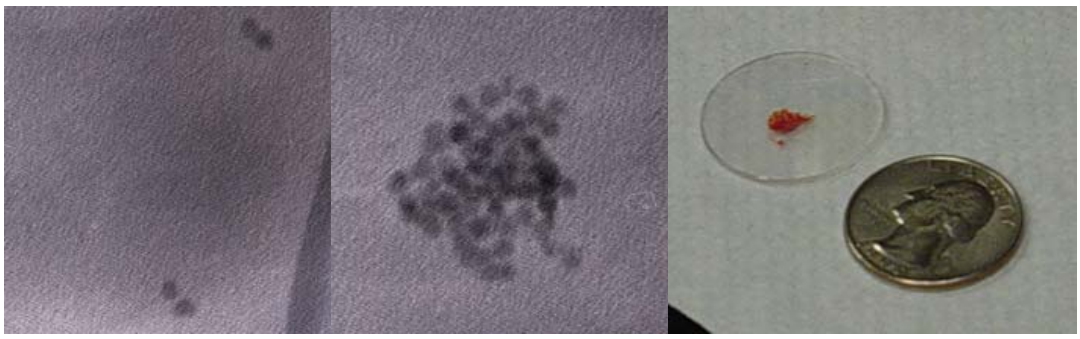

was evident by the formation of crystals of the dodecylphosphonate within the matrix of the assembly.

Upon forming the assembly, the CdSe nanocrystals maintain their photoluminescence and exhibit increased stability under continual excitation for durations of several days in atmospheric conditions. Unorganized CdSe nanocrystals that are exposed to photoexcitation will rapidly deteriorate over time (<6hours).[11] What is more notable about the construct is that the OPE linkers acts as an antennae that transfers electronic energy to the CdSe nanocrystal. In the case of these organic linkers they have been observed to form higher order aggregates in solution[12] as well as highly organized crystalline solids. (Figure 5-8) The formation of these aggregates on the surface of the nanocrystal are theorized to allow sufficient coupling between the nanocrystals and the OPE to facilitate energy transfer from the OPE to the nanocrystal. (Figure 5-9) The efficiency of energy transfer is dependent upon the size of the CdSe nanocrystal and the length of the OPE molecule used. Figure 5-10 shows the efficiency of energy transfer for various CdSe and OPE's 0,1,3. There is a supporting literature that the formation of the ordered aggregates on the surface of the nanomaterial lends to this phenomenon.[13] It is further confirmed by experimental observation during the assembly of CdSe nanocrystals and the OPE's. While determining the concentration and amounts of the OPE solutions to add to the nanocrystals, it was observed that the variations in the concentrations of the OPE solutions (greater than 0.1M) and amounts greater then 5ml of OPE solution added will lead to immediate aggregation of the nanocrystals. However unlike the conjugates formed, the nanocrystals in these aggregates did not maintain their

Figure 5-8. Crystal structure of OPE-1

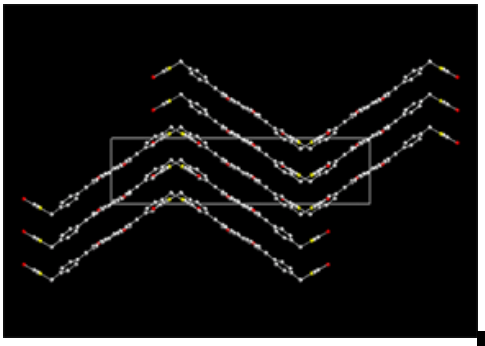

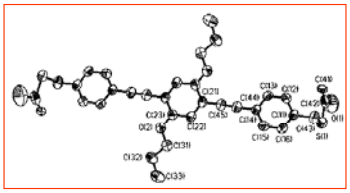

View down (1 0 0)

Orthorhombic
Pbca

a=11.106(2)Å
b=8.503(2)Å
c=33.444(7)Å

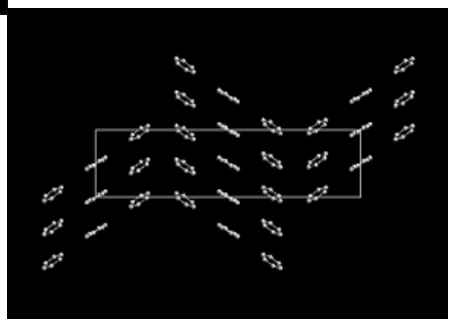

Figure 5-9. Luminescence from OPE is quenched with increasing CdSe NC size.

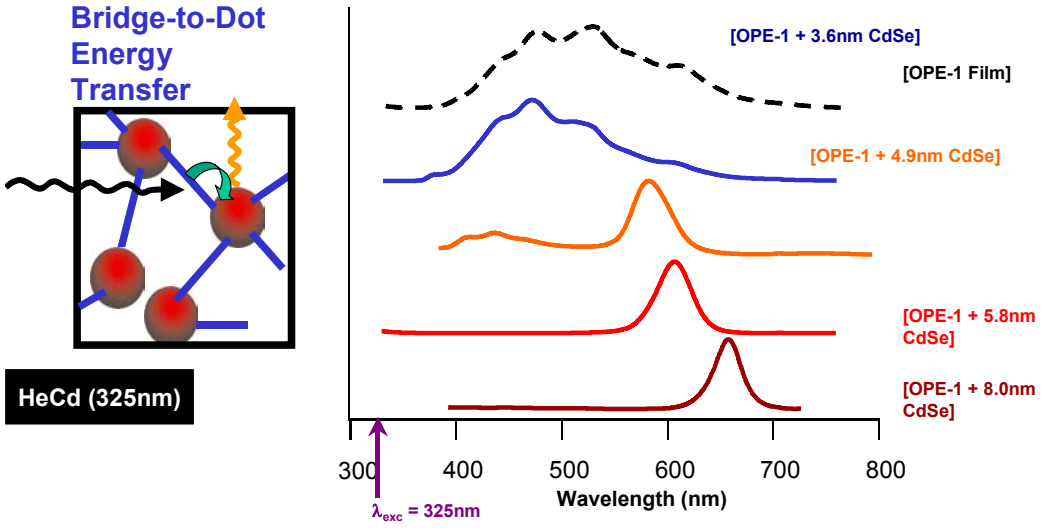

Figure 5-10. Spectra of photoluminescence OPE 0,1,3 and various sizes of CdSe quantum dots.

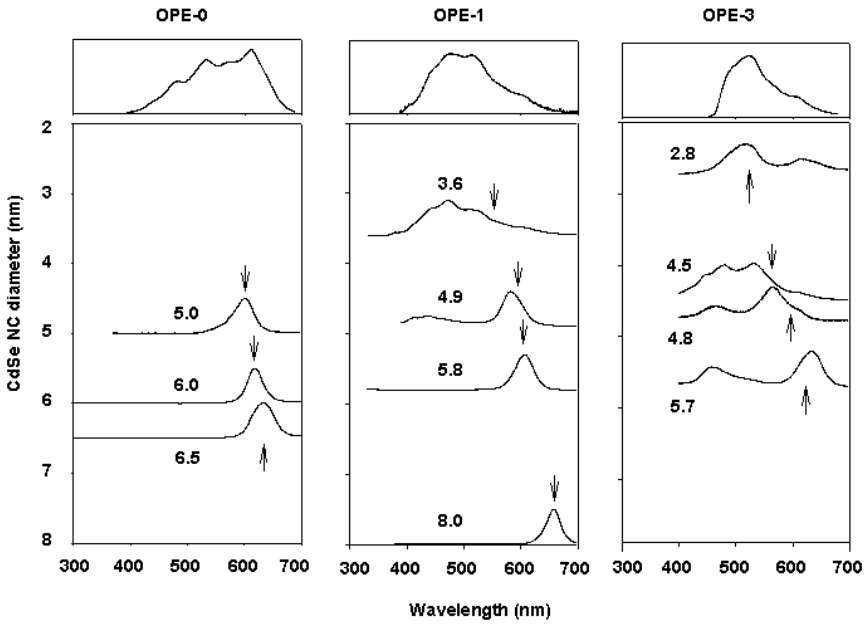

photoluminescence, exhibiting little or no emission. This gives further evidence that the formation of the organic ligands on the surface must organize to provide the necessary conditions to maintain the photoluminescence of the quantum dots and allow energy transfer from the organic ligand to the nanocrystals. More extensive studies of the photo-physical properties of the constructs are still under investigation. There is a preliminary result that indicates that the organic ligands act as a thermo-active liquid crystal. The application of heat to the assembly disorients the stacking of the ligands on the surface of the nanomaterial and thus shutting off the energy transfer mechanism.[14,15]

C. Experimental

Compound (2): Dipropoxybenzene (40.0 g, 0.21mol) was dissolved in acetic acid (120 mL) and Dichloromethane (30 mL). To this solution was added iodine (45.7 g, 0.18 mol), conc. sulfuric acid (14 mL), distilled water (7 mL), and finally potassium iodate (18.4 g, 0.086 mol). The mixture was stirred and refluxed for 24 hrs. Removal of excess iodine was done by the addition of $NaHSO_3$ was added until the violet color of iodine disappeared. The mixture was poured into ice/water (1.5 L) and extracted with chloroform (5 X 300 mL). The organic phases were neutralized with saturated $NaHCO_3$ and dried with anhydrous Na_2SO4. After removal of the solvent, the residue was recrystallized from methanol. Yield: 75.0 g (82%) of colorless crystals. (m/z: 446, 404, 362, 235, 189, 150, 108, 79, 53)

Compound (3): 1,4-Diiodo-2,5-dipropoxybenzene (1) (2.0 g, 4.5 mmol) was dissolved in dry trimethylamine/THF (20 mL) and the system was flushed with

argon. Bis(triphenylphosphine)palladium dichloride (0.24 g, 0.55 mmol), copper(I) iodide (0.12 g, 0.63 mmol), triphenylphosphine (0.24 g, 0.91 mmol), and trimethylsilylacetylene (1.0 g, 9.9 mmol) were added. The reaction was heated to 60^{o}C and stirred for 12 hrs. The solvent was then evaporated, and chloroform was added to the residue and extracted with saturated NH_4Cl and water. After having been washed with saturated $NaHCO_3$, the organic phases were dried with anhydrous Na_2SO_4. The crude product was purified by chromatography (toluene/hexane, 1:1). Yield: 1.7 g. (98%) of colorless crystals. (m/z: 386, 302, 278, 271, 73)

Compound (4): Compound (2) (2.0 g, 5.15 mmol) was dissolved into methanol (20 mL) along with K_2CO_3 (2.86g. 21 mmol). The mixture was stirred for 4 hrs and followed by TLC. With the disappearance of the starting material the reaction was filtered through a medium fritted funnel and the solution evaporated. The product was purified by elution with hexane through a silica plug. Yield: 1.23 g. (99%) of a grayish solid. (m/z: 242, 217,175, 132)

Compund (5): Compund (3) (2.0 g, 8.26 mmol) was dissolved in dry trimethylamine/DMF (40 mL) and the system was flushed with argon. Bis(triphenylphosphine)palladium dichloride (0.48 g, 1.1 mmol), copper(I) iodide (0.24 g, 1.26 mmol), triphenylphosphine (0.5 g, 2 mmol), and 4-iodobenzylthiol acetate (5.25 g, 18 mmol) were added. The reaction was stirred and heated to 60^{o}C for 12 hours. The solvent was then evaporated and the residue re-suspended in dichloromethane. The solution was washed with NH_4Cl and then $NaHCO_3$. The organic phase was then dried over anhydrous $NaSO_4$. The product was purified by column chromatography with (toluene/dichloromethane/hexane, 1:1:48) Yield: 4.14

g. (88%) of a yellow solid. (m/z: 570, 528, 495, 453, 326, 311, 255, 216, 202, 175,151,106)

Compound (6): Compound (4) (1.0 g. 1.75 mmol) was added to a 100ml 50:50 solution of aqueous 3M KOH and THF. The reaction was monitored by TLC. When the reaction was neutralized with HCl and organic phase was separated and dried over sodium sulfate. The organic phase was then removed under vacuum and product purified by column chromatography with (toluene/hexane/Dichloromethane, 1:47:2). Yield: 0.89 g. (95%) of a yellow solid. (m/z: 486, 453, 307, 235, 219, 154)

Compound (8): 4-iodobenzylthiol acetate (7) (2.0 g, 6.84 mmol) was dissolved in dry trimethylamine/DMF (70 mL) and the system was flushed with argon. Bis(triphenylphosphine)palladium dichloride (0.48 g, 0.68 mmol), copper(I) iodide (0.065 g, 0.342 mmol), triphenylphosphine (0.089 g, 0.342 mmol) and TMS-acetylene (0.705 g, 0.718 mmol) were added and the reaction was heated to 60^{o}C for 16 hours. The solvent was then evaporated and the residue re-suspended in dichloromethane. The solution was washed with NH_4Cl and then $NaHCO_3$. The organic phase was then dried over anhydrous $NaSO_4$. The product was purified by column chromatography with (toluene/dichloromethane/hexane, 1:1:48). Yield was 1.61 g. (90%). (m/z: 262, 247, 232, 205, 187, 172, 159, 143, 129, 115, 101, 91, 73, 59)

Compound (9): 4-Trimethylsilylethynylbenzylthiol acetate (8) (2.0g, 7.62mmol) was dissolved in 80 mL of THF and cooled in an ice bath. An equal molar amount tetrabutylammonium fluoride in THF was added dropwise into the reaction and allowed to stir for 15 min. The reaction was then added into 100 ml of diethylether

and then the batch was washed with water. The organic phase was then dried over sodium sulfate and then filtered. The organic phase was then removed and product was purified by column chromatography with (dichloromethane/hexane, 1:9). Yield was 1.3 g. (95%) gray solid. (m/z: 190, 169, 147, 115, 103, 89, 75, 63, 51)

Compound (10): 4-iodobenzylthiol acetate (7) (2.0 g, 6.84 mmol) was dissolved in dry trimethylamine/DMF (70 mL) and the system was flushed with argon. Bis(triphenylphosphine)palladium dichloride (0.48 g, 0.68 mmol), copper(I) iodide (0.065 g, 0.342 mmol), triphenylphosphine (0.089 g, 0.342 mmol) and 4-Ethynylbenzylthiol acetate (9) (1.37 g, 0.718 mmol) were added and the reaction was heated to 60^{o}C for 16 hours. The solvent was then evaporated and the residue re-suspended in dichloromethane. The solution was washed with NH_4Cl and then $NaHCO_3$. The organic phase was then dried over $NaSO_4$. The residue was then passed though a glass frit with silica. The mixture was then added to a 100ml 50:50 solution of aqueous 3M KOH and THF. The reaction was monitored by TLC. When the reaction was neutralized with HCl and organic phase was separated and dried over sodium sulfate. The organic phase was then removed under vacuum and product purified by column chromatography with (toluene/hexane/Dichloromethane, 1:45:4). Yield: 1.48 g. (80%) of an off white color solid. (m/z: 270. 223, 147, 123, 75)

Compound (11): 1,4-Diethynyl-2,5-dipropoxybenzene (4) (1.0 g, 4.13 mmol) was dissolved in dry trimethylamine/DMF (30 mL) and the system was flushed with argon. Bis(triphenylphosphine)palladium dichloride (0.24 g, 0.55 mmol), copper(I) iodide (0.12 g, .063 mmol), triphenylphosphine (0.25 g, 1 mmol), and 1,4-Diiodo-

2,5-dipropoxybenzene (1.84 g, 4.34 mmol) were added. The reaction was stirred and heated to 60^{o}C for 14 hours. The solvent was then evaporated and the residue re-suspended in dichloromethane. The solution was washed with NH_4Cl and then $NaHCO_3$. The organic phase was then dried over Na_2SO_4. The product was purified by column chromatography with (toluene/dichloromethane/hexane, 1:1:48) Yield: 1.76 g. (84%) of a yellow solid. (m/z: 406, 363, 338, 296, 253, 146, 115)

Compound (12): Compound (11) (1.0 g, 1.96 mmol) was dissolved in dry trimethylamine (50 mL) and the system was flushed with argon. Bis(triphenylphosphine)palladium dichloride (0.148 g, 0.2 mmol), copper(I) iodide (0.02 g, 0.1 mmol), triphenylphosphine (0.026 g, 0.1 mmol) and 1,4-Diiodo-2,5-dipropoxybenzene (0.379 g, 0.98mmol) were added and the reaction was heated to 60^{o}C for 16 hours. The solvent was then evaporated and the residue re-suspended in dichloromethane. The solution was washed with NH_4Cl and then $NaHCO_3$. The organic phase was then dried over anhydrous $NaSO_4$. The residue was then passed though a glass frit with silica. The mixture was then added to a 100ml 50:50 solution of aqueous 3M KOH and THF. The reaction was monitored by TLC. When the reaction was neutralized with HCl and organic phase was separated and dried over sodium sulfate. The organic phase was then removed under vacuum and product purified by column chromatography with (toluene/ hexane/Dichloromethane, 1:40:9). Yield: 1.33 g. (74%) of yellow solid. (m/z: 918, 460, 391, 307, 219, 154)

D. Conclusion

The ability to construct new materials by combining both organic and inorganic compounds and derive assemblies that have enhanced or new properties is one of the goals in the nanomaterial field. The interface of different disciplines of chemistry can bring about new materials that have potential in the areas of sensing, and electronics. The conjugate presented is a foundation that incorporation of conjugated organic molecules and their properties can translate to augment as well as to organize nanomaterials. Further investigations into new and varying types of organic ligands that possess both photoluminescent and liquid crystal properties to develop new materials and compounds that can be utilized in LED's and solid-state lighting.

Appendix : NMR Data

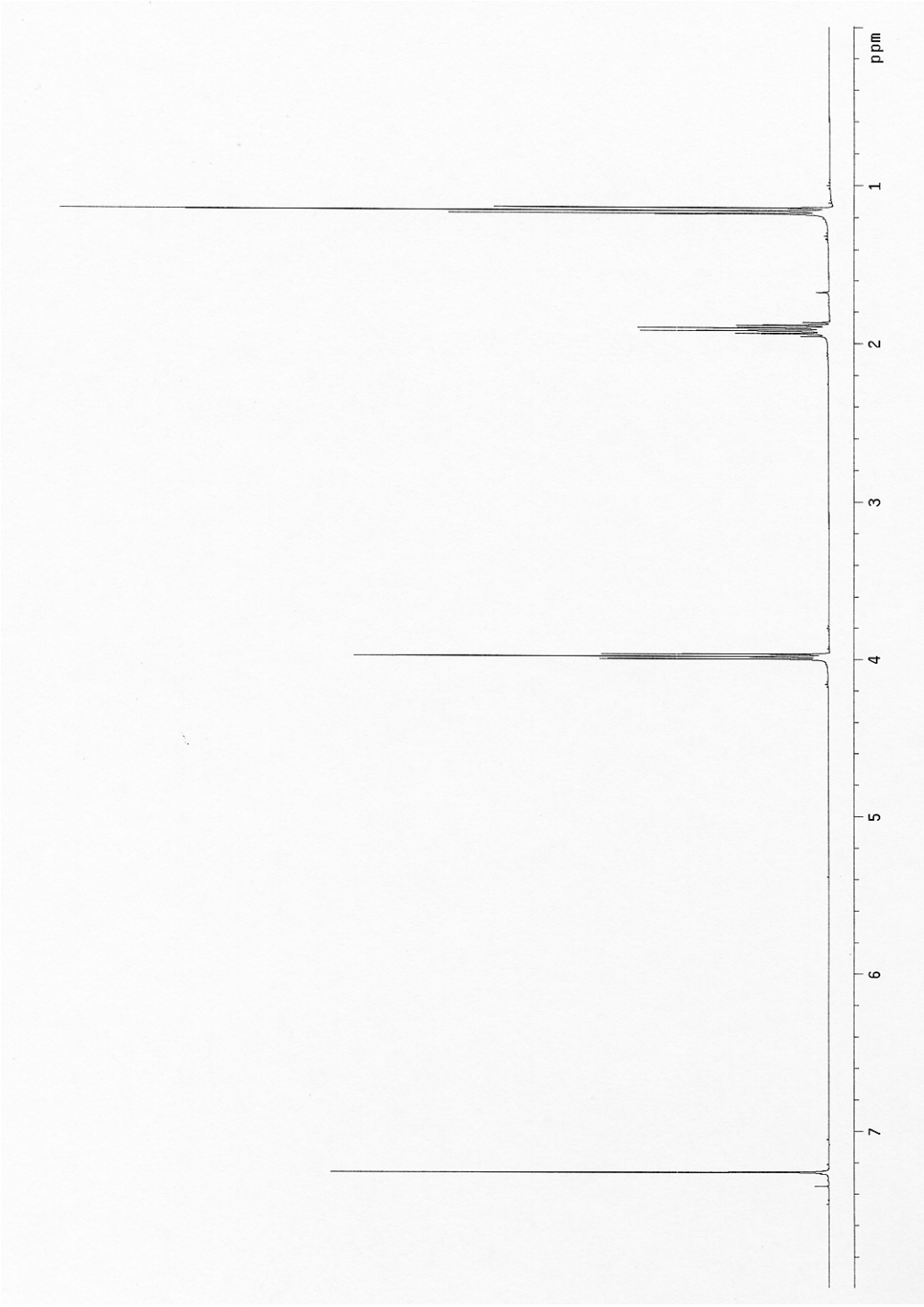
ppm
1
2
3
4
5
6
7

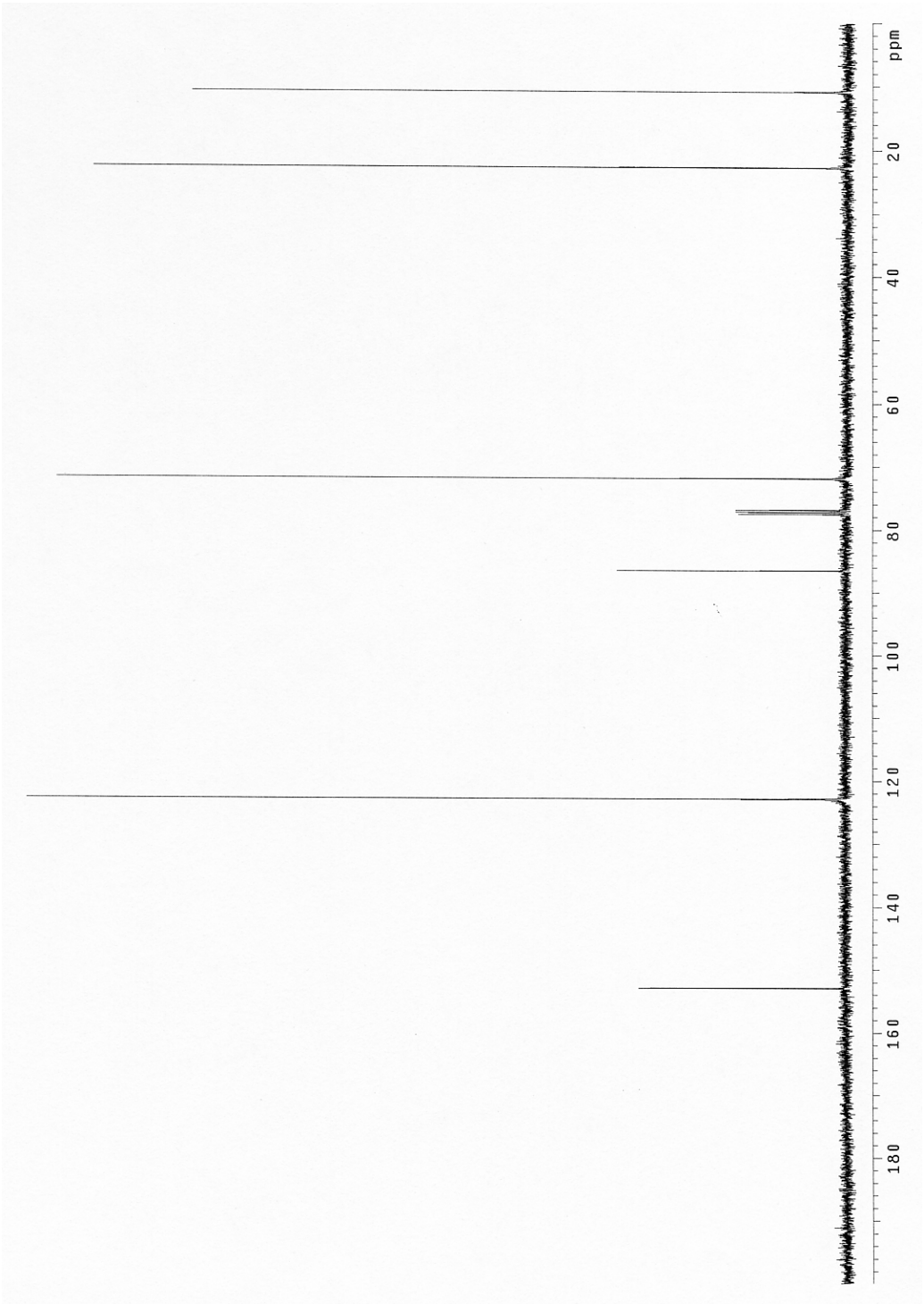
ppm
20
40
60
80
100
120
140
160
180

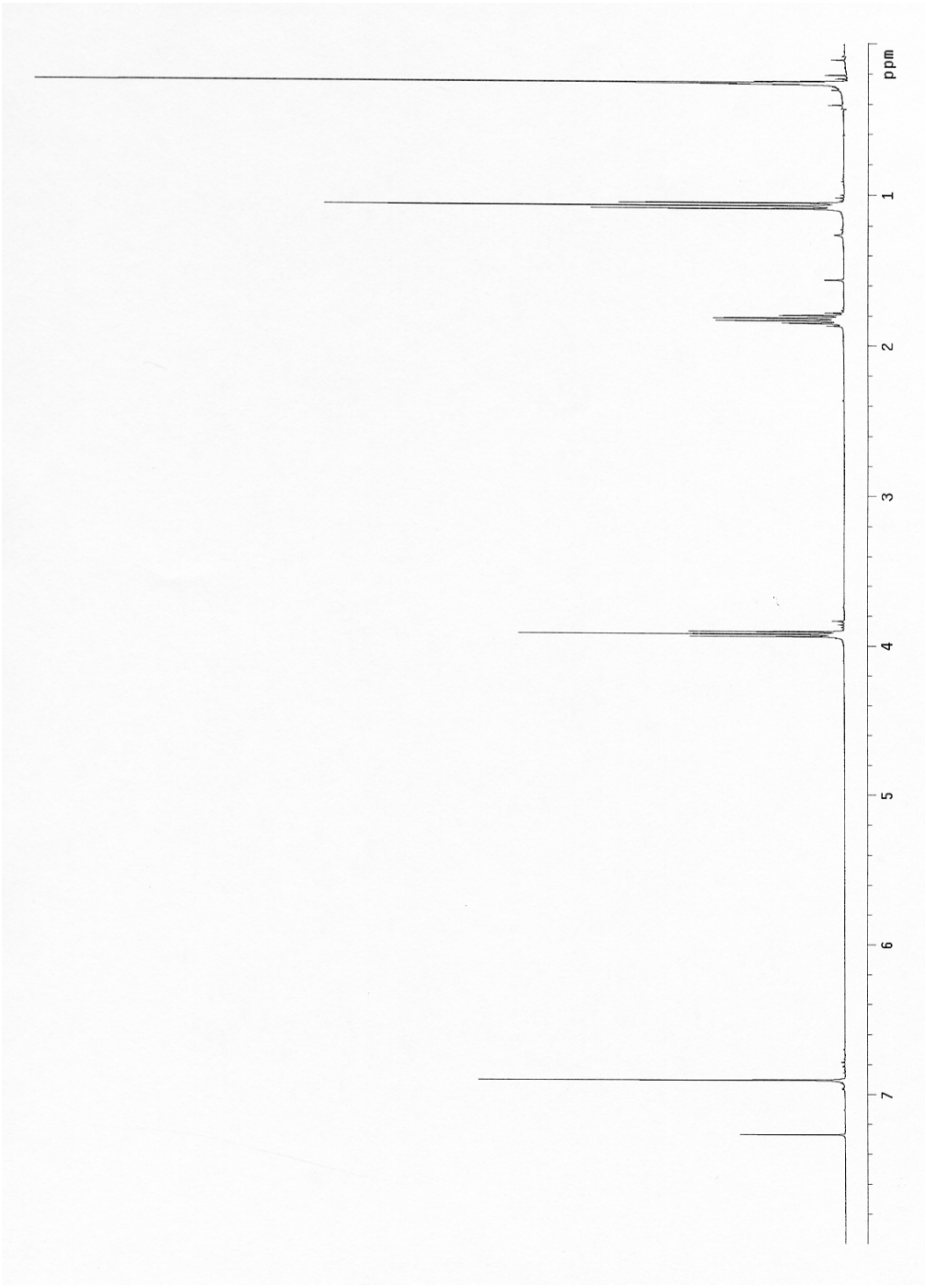
ppm
1
2
3
4
5
6
7

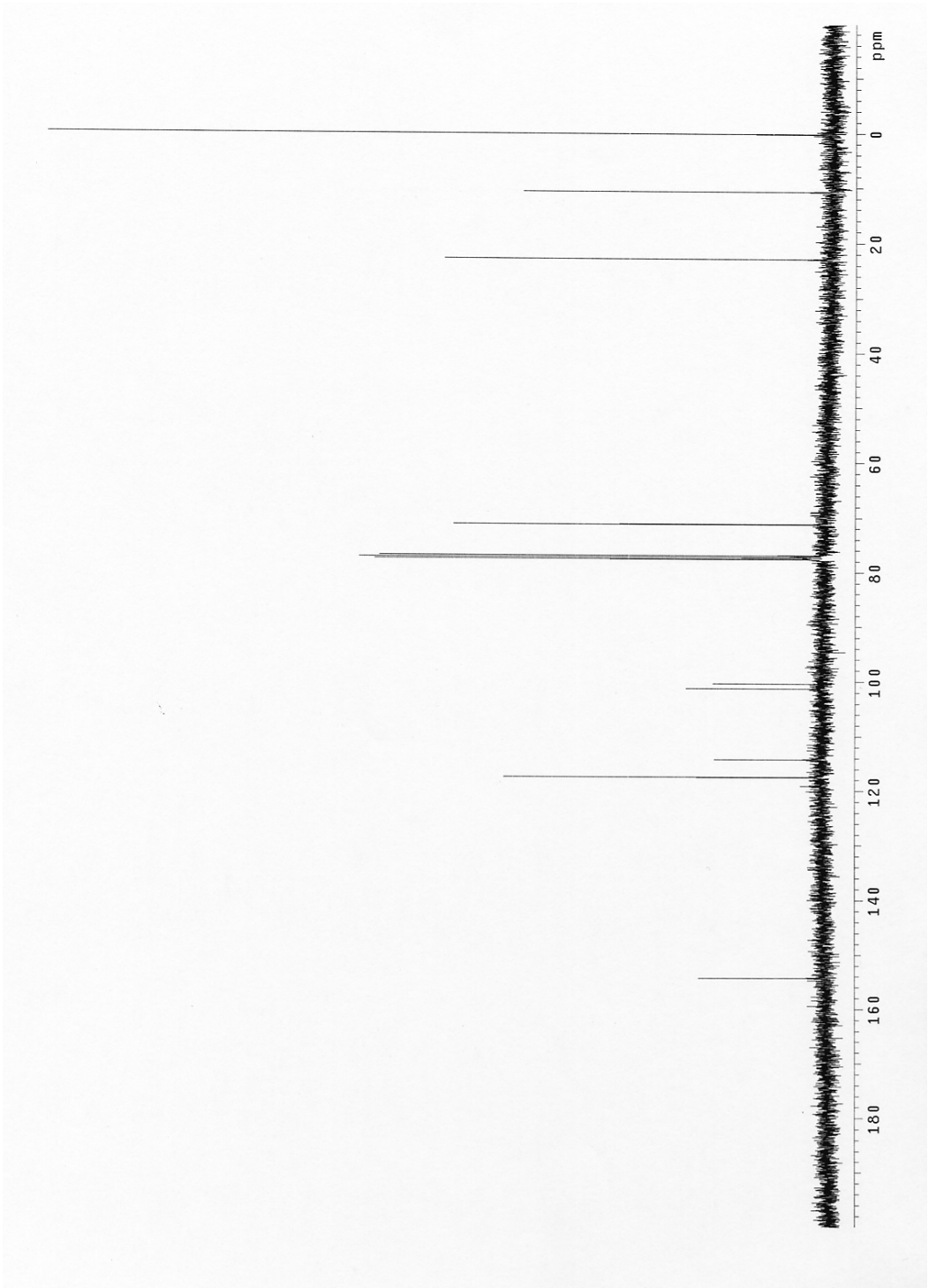
ppm
0
20
40
60
80
100
120
140
160
180

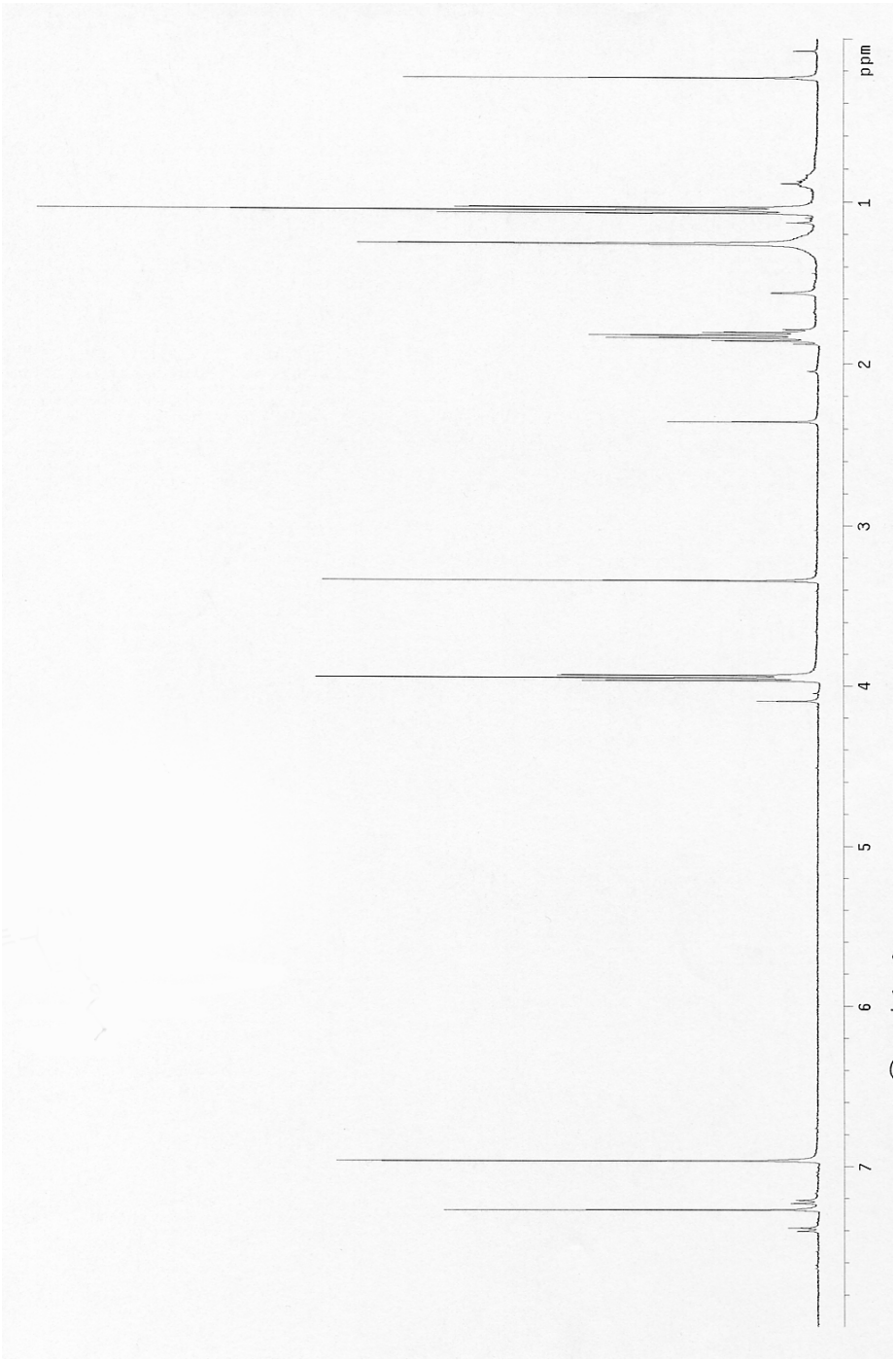
ppm
1
2
3
4
5
6
7


ppm
20
40
60
80
100
120
140
160


ppm
1
2
3
4
5
6
7


ppm
0
20
40
60
80
100
120
140
160
180
200


ppm
1
2
3
4
5
6
7

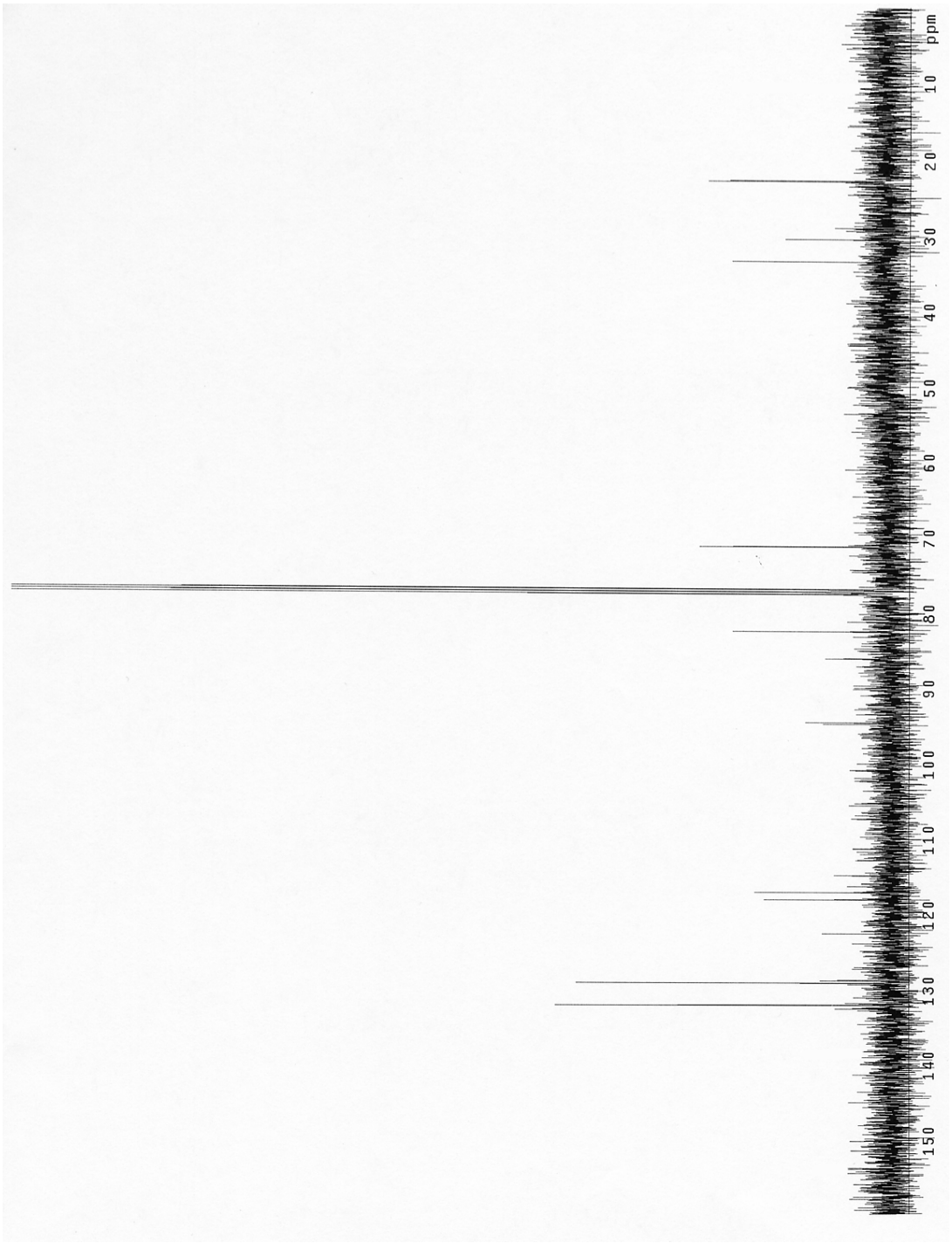
ppm
10
20
30
40
50
60
70
80
90
100
110
120
130
140
150


ppm
1
2
3
4
5
6
7

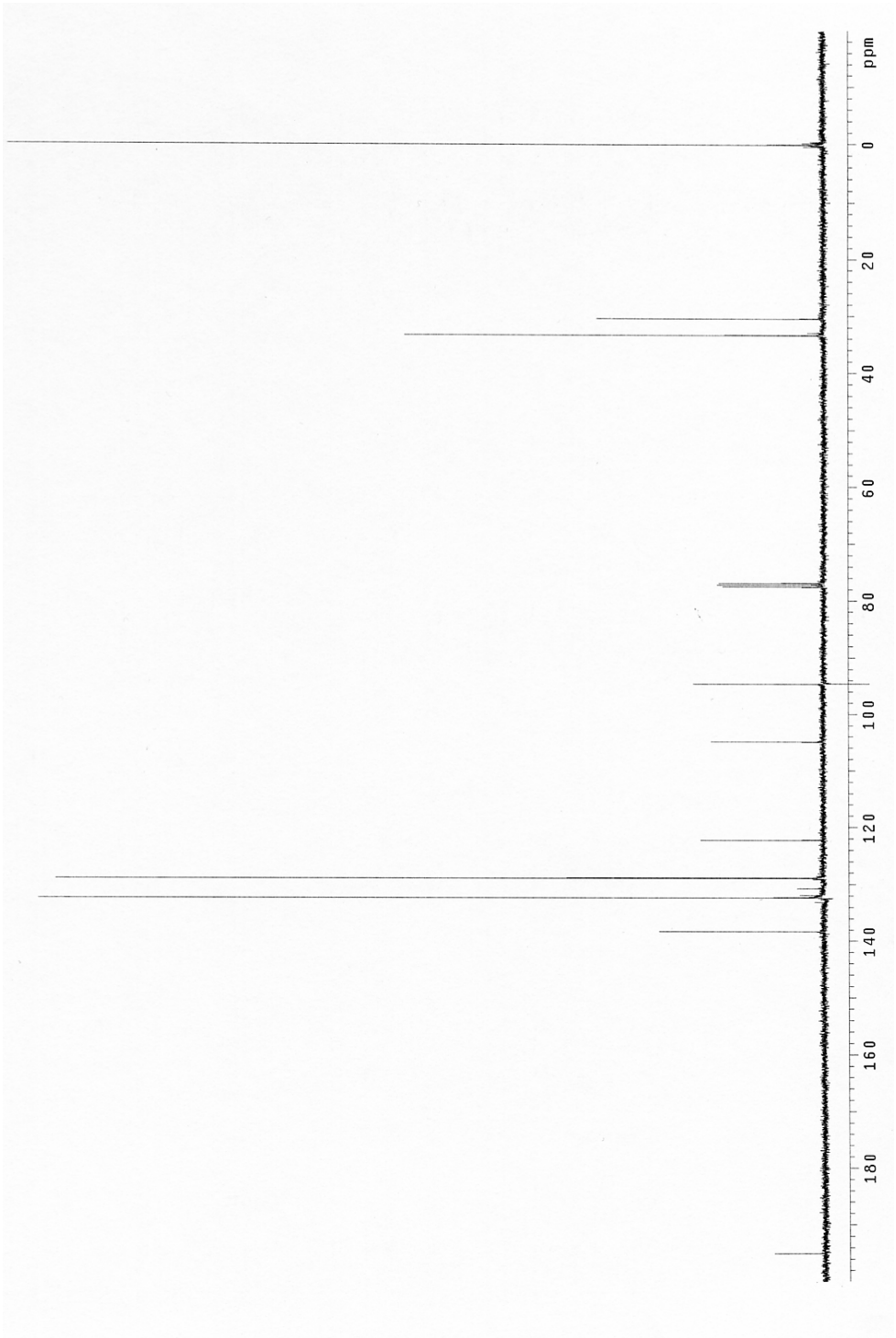
ppm
0
20
40
60
80
100
120
140
160
180

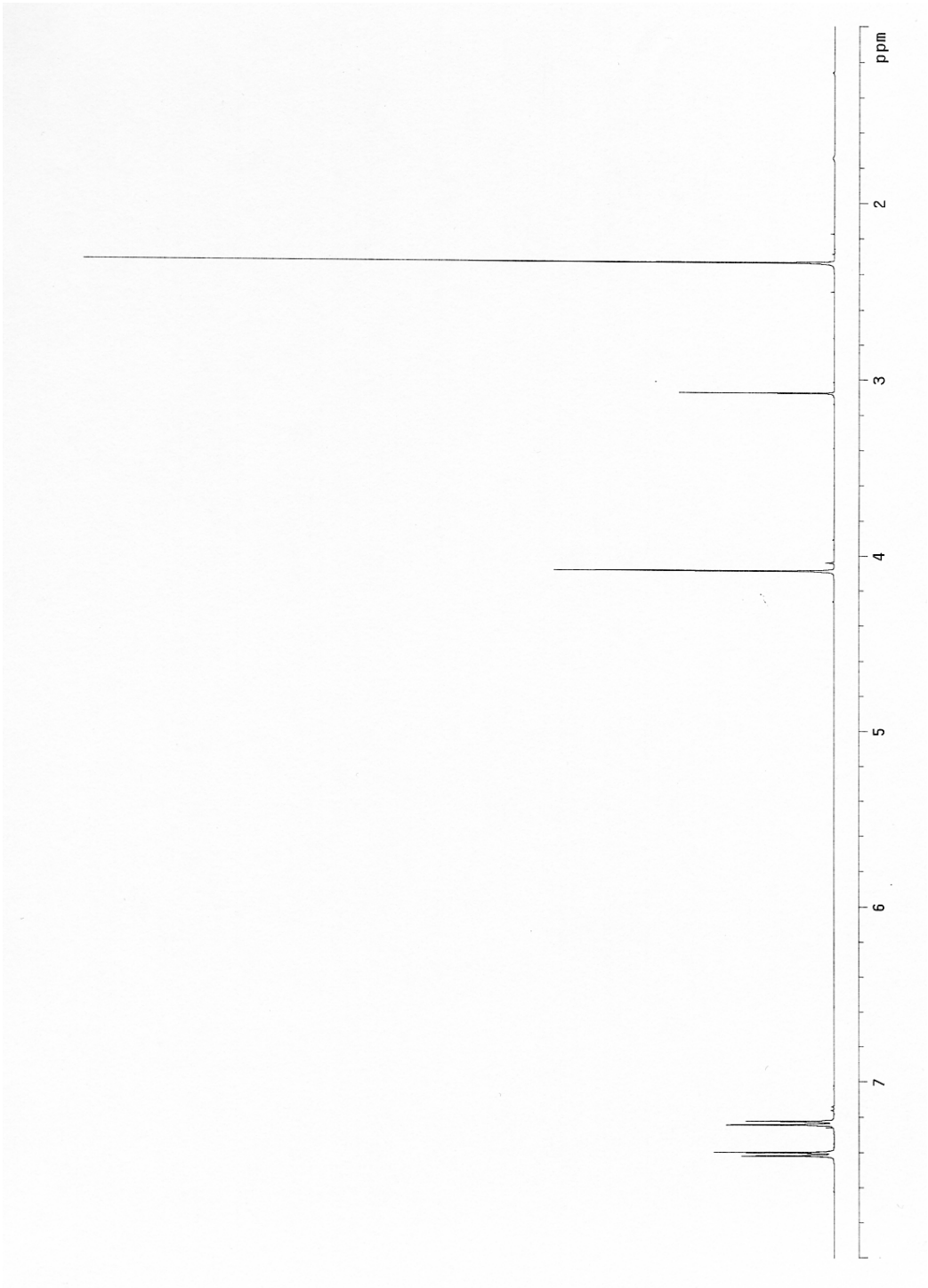
ppm
2
3
4
5
6
7

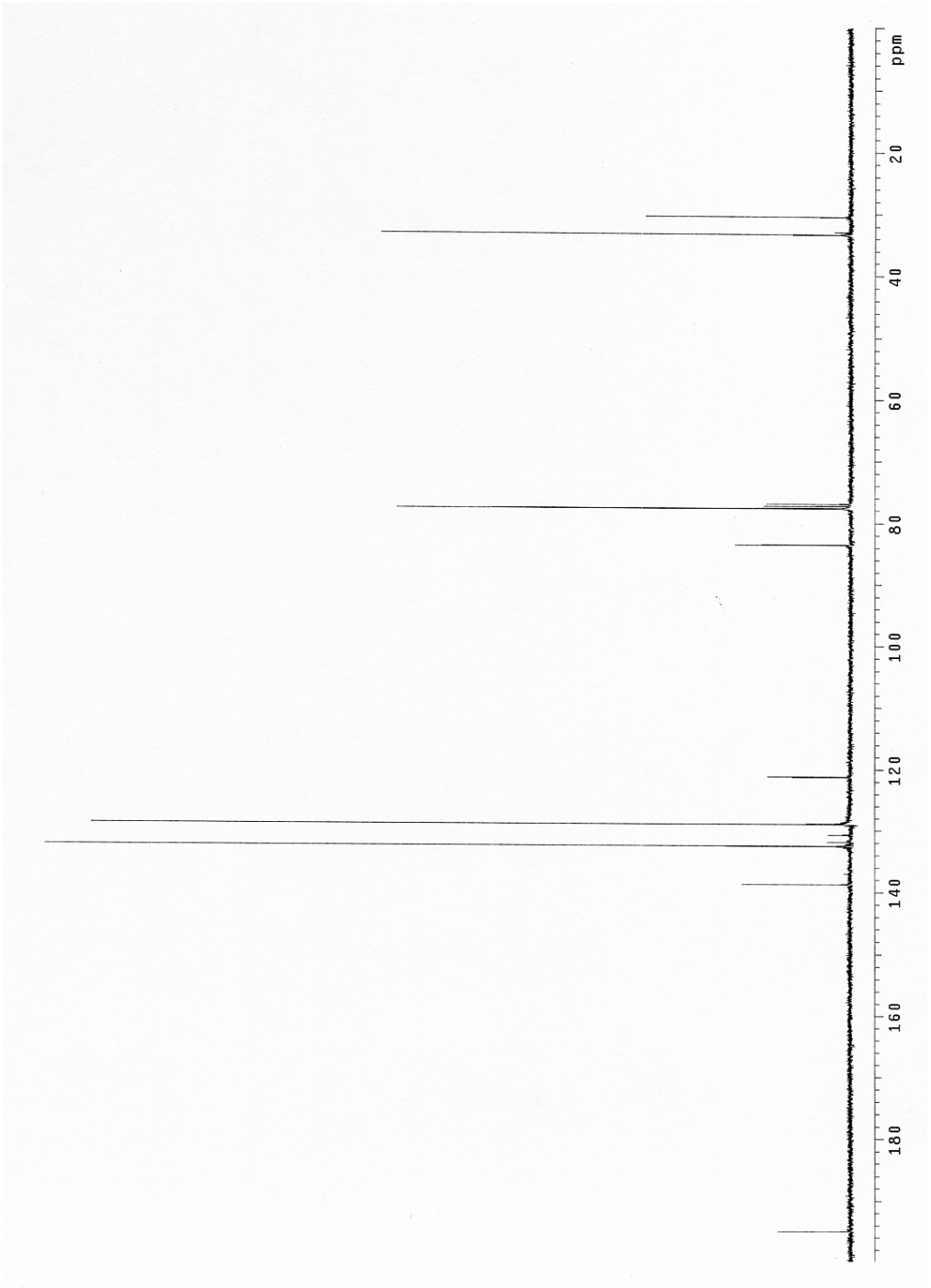
ppm
20
40
60
80
100
120
140
160
180

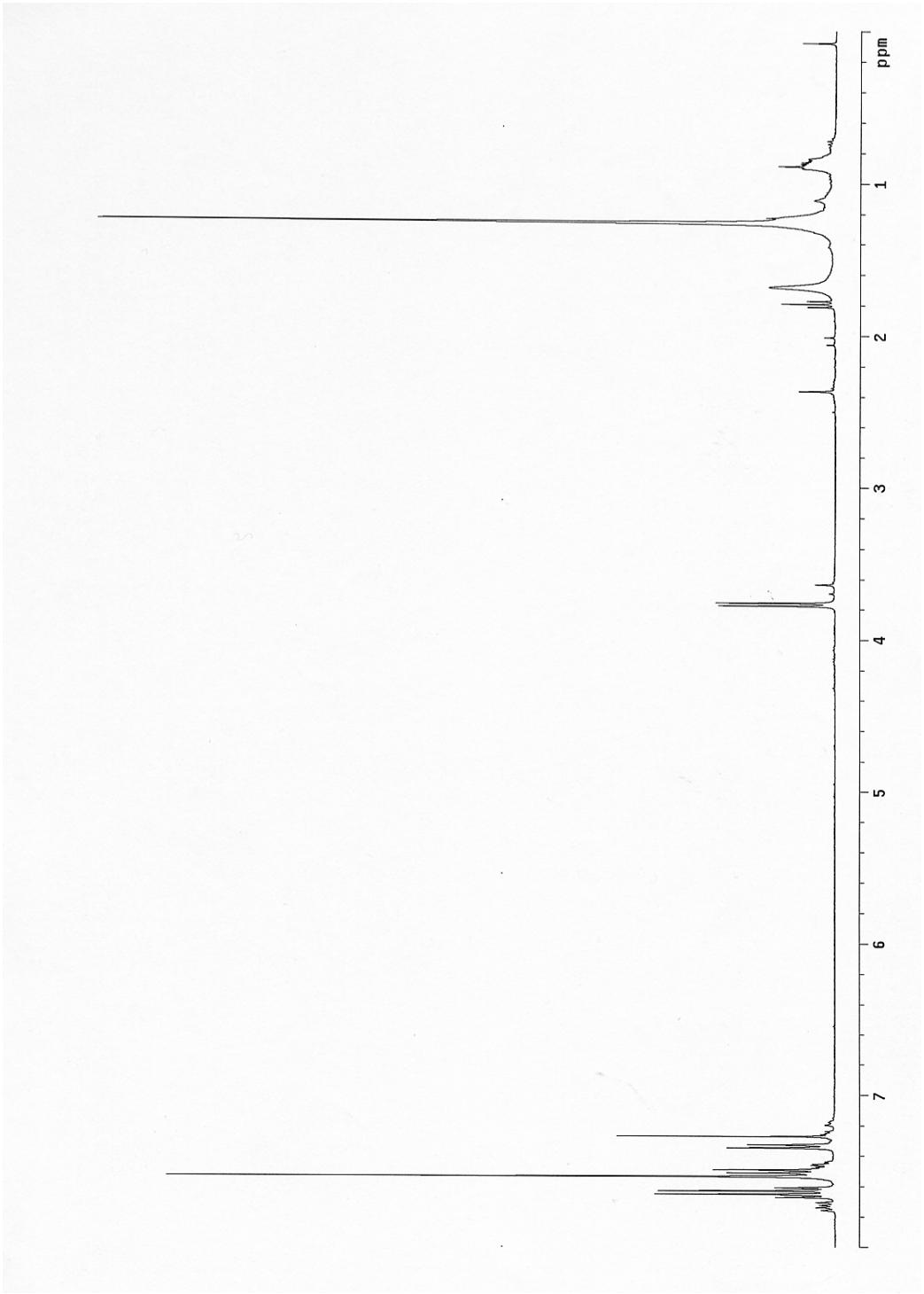
ppm
1
2
3
4
5
6
7

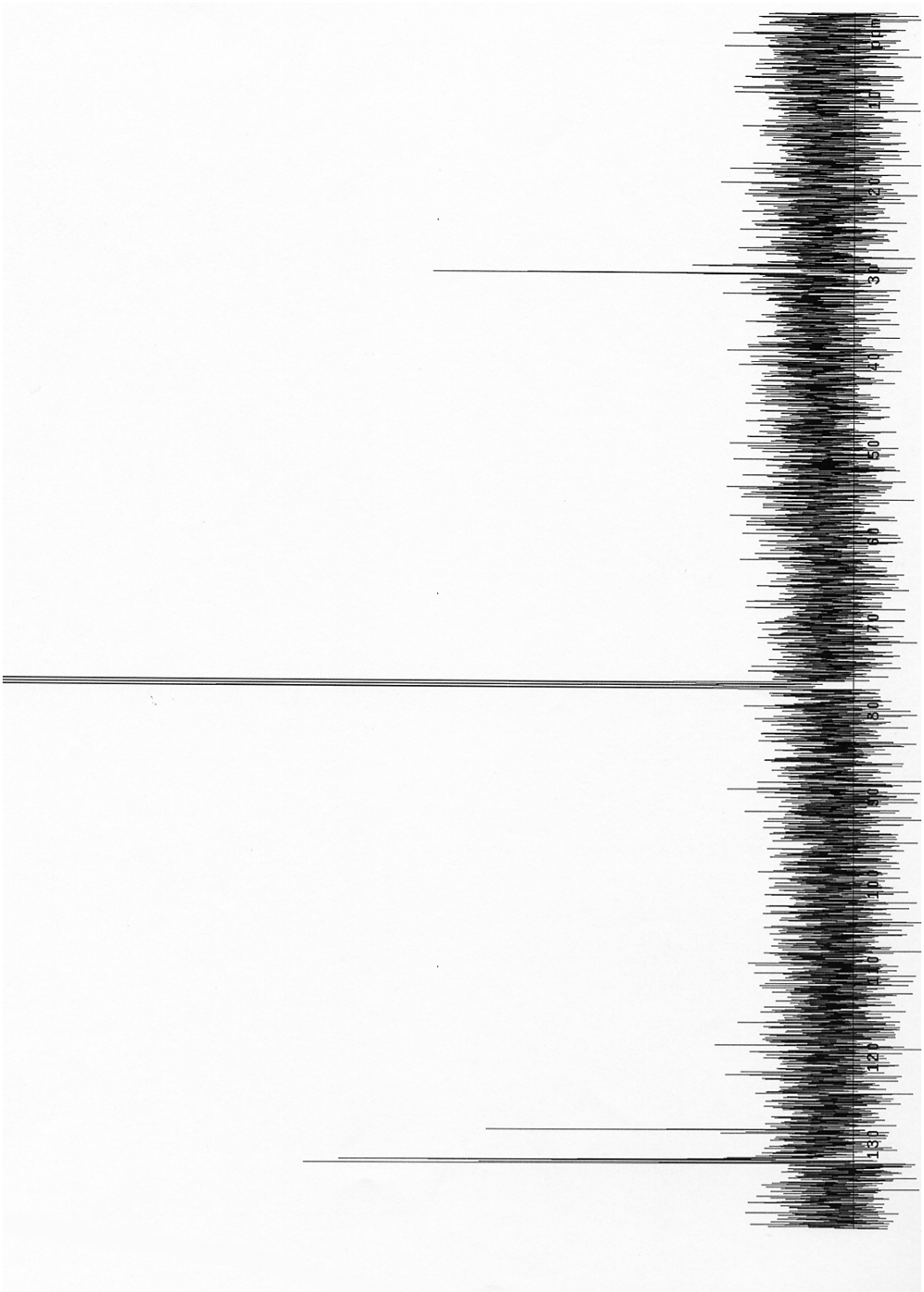

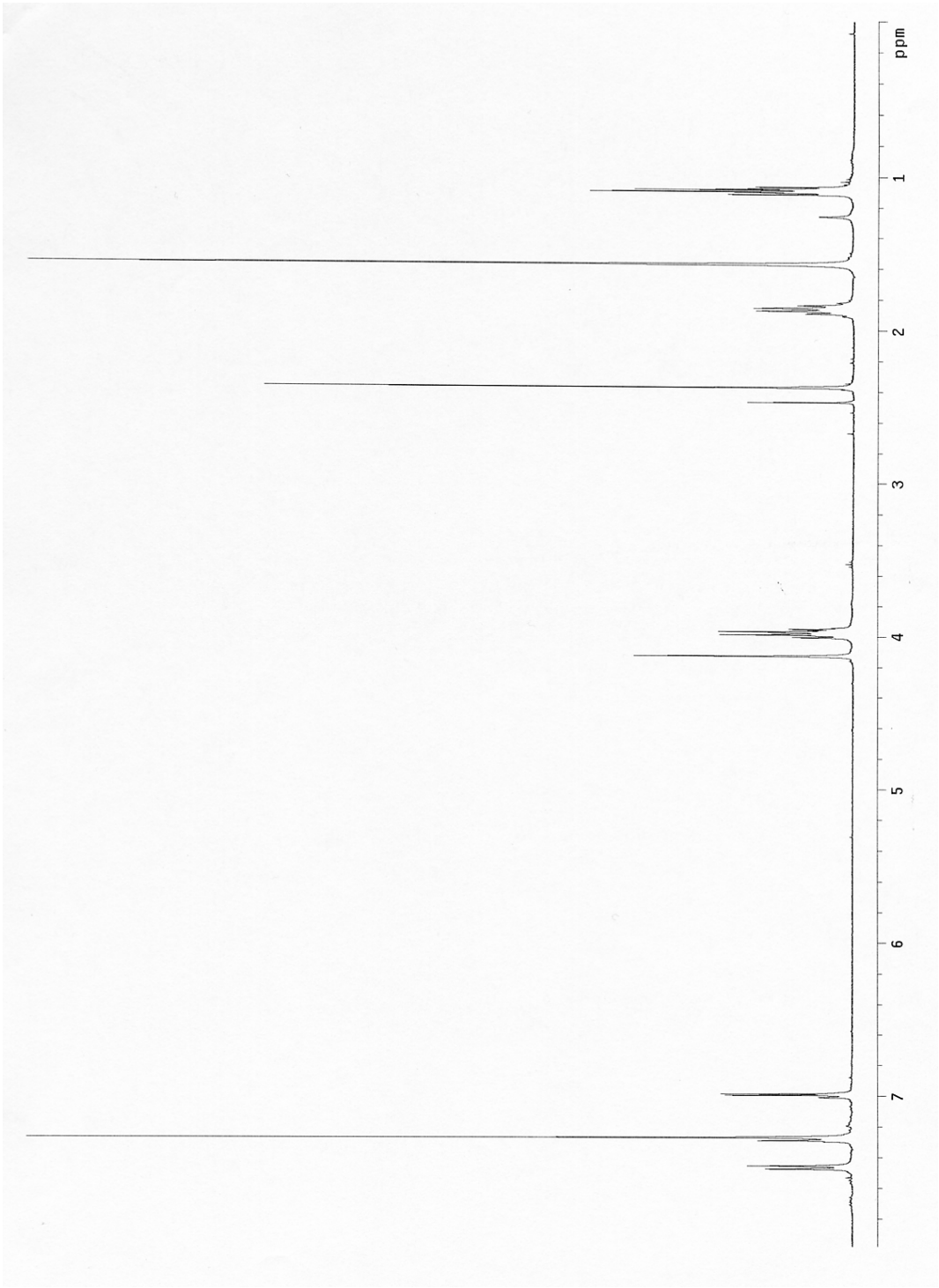
ppm
1
2
3
4
5
6
7

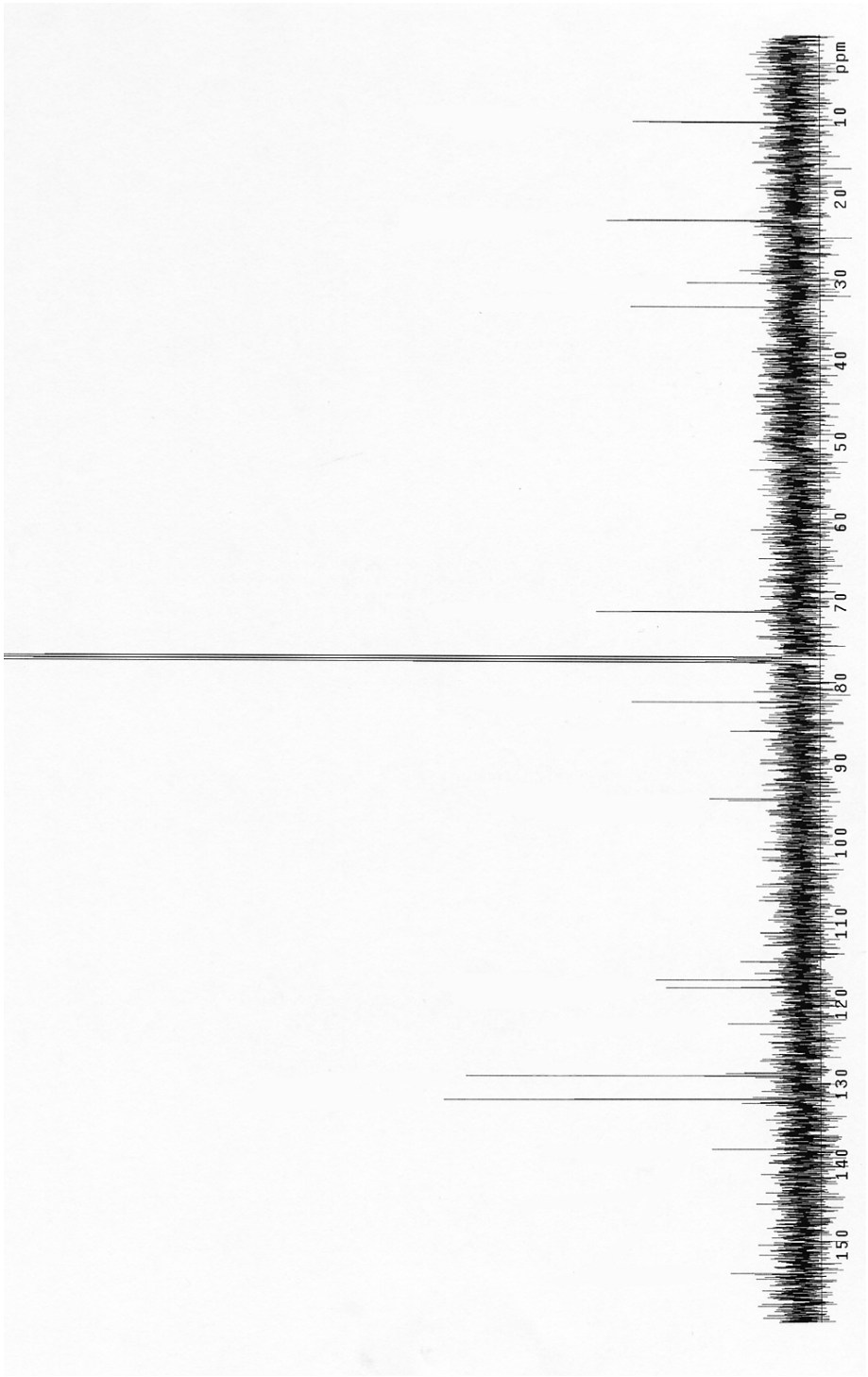
ppm
10
20
30
40
50
60
70
80
90
100
110
120
130
140
150


ppm
1
2
3
4
5
6
7

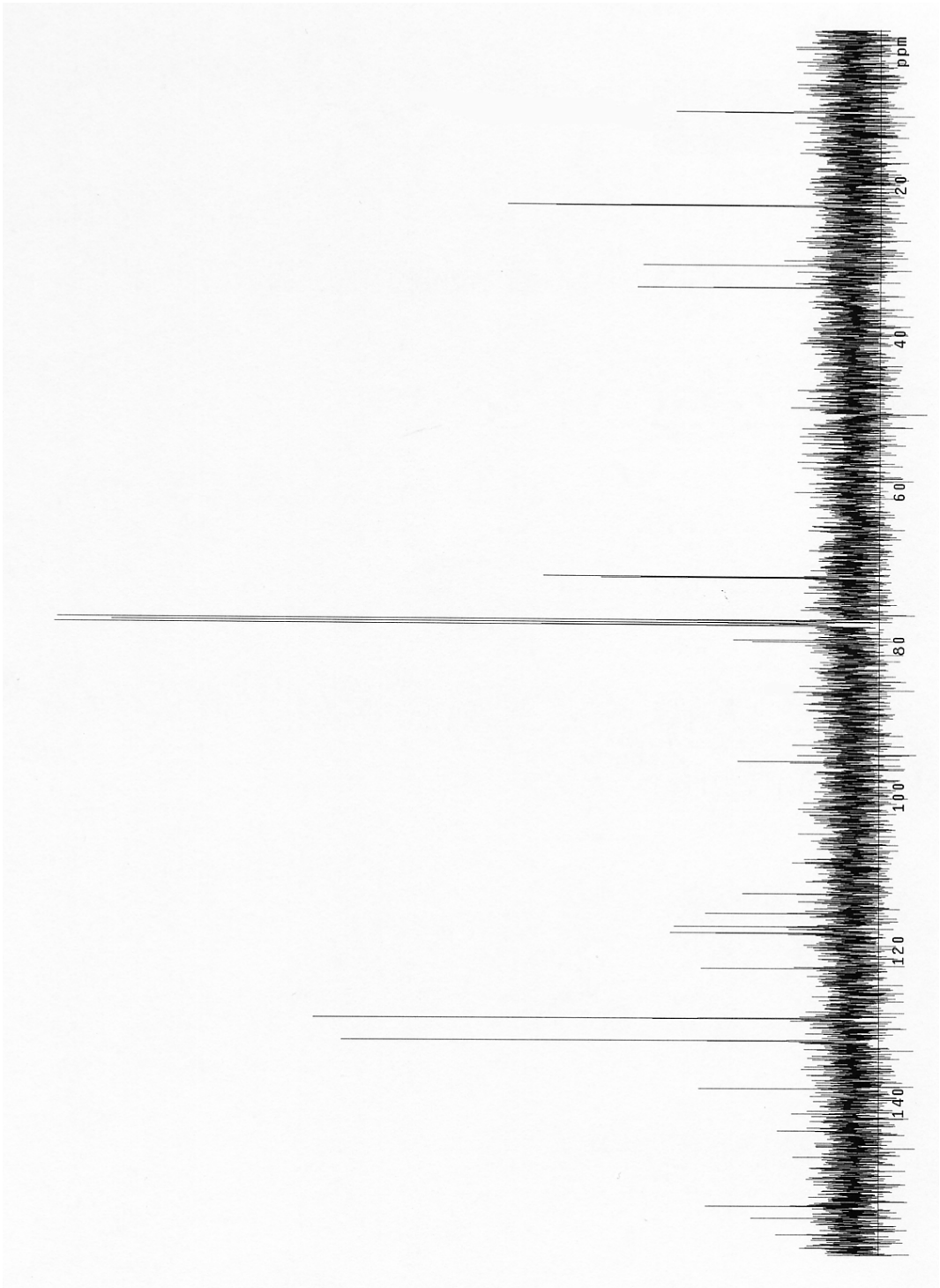
ppm
20
40
60
80
100
120
140

Table 1. Crystal data and structure refinement for 1.

Identification code	10-3-2001
Empirical formula	C34 H34 O4 S2
Formula weight	570.73
Temperature	293(2) K
Wavelength	0.71073 A
Crystal system	Orthorhombic
Space group	Pbca
Unit cell dimensions	a = 11.106(2) A alpha = 90 deg. b = 8.503(2) A beta = 90 deg. c = 33.444(7) A gamma = 90 deg.
Volume, Z	3158.5(11) A^3, 4
Density (calculated)	1.200 Mg/m^3
Absorption coefficient	0.203 mm^-1
F(000)	1208
Crystal size	0.40 x 0.40 x 0.10
Theta range for data collection	1.22 to 24.99 deg.
Limiting indices	-14<=h<=13, -11<=k<=10, -44<=l<=44
Reflections collected	23956
Independent reflections	2778 [R(int) = 0.0839]
Refinement method	Full-matrix least-squares on F^2
Data / restraints / parameters	2775 / 0 / 183
Goodness-of-fit on F^2	1.134
Final R indices [I>2sigma(I)]	R1 = 0.0651, wR2 = 0.1820
R indices (all data)	R1 = 0.1113, wR2 = 0.2067
Largest diff. peak and hole	0.333 and -0.302 e.A^-3

Table 2. Atomic coordinates (x 10^4) and equivalent isotropic displacement parameters (A^2 x 10^3) for 1. U(eq) is defined as one third of the trace of the orthogonalized Uij tensor.

	x	y	z	U(eq)
S(1)	7167(1)	646(1)	7251(1)	97(1)
O(1)	6024(5)	-737(6)	6620(1)	209(2)
O(2)	6839(2)	-6029(3)	10491(1)	85(1)
C(11)	6393(3)	549(4)	8039(1)	71(1)
C(12)	5272(3)	-135(4)	8088(1)	82(1)
C(13)	5045(3)	-1106(4)	8410(1)	76(1)
C(14)	5930(3)	-1433(4)	8682(1)	64(1)
C(15)	7045(3)	-770(4)	8630(1)	80(1)
C(16)	7260(3)	218(4)	8306(1)	76(1)
C(21)	5228(3)	-4157(3)	9651(1)	68(1)
C(22)	6173(3)	-4660(4)	9893(1)	71(1)
C(23)	5967(3)	-5495(4)	10240(1)	70(1)
C(31)	8062(3)	-5768(4)	10391(1)	81(1)
C(32)	8850(4)	-6519(5)	10696(1)	96(1)
C(33)	10163(4)	-6458(5)	10585(1)	113(2)
C(41)	4856(3)	451(5)	7146(1)	86(1)
C(42)	5773(5)	140(5)	7014(1)	98(1)
C(43)	6632(4)	1633(5)	7689(1)	97(1)
C(44)	5694(3)	-2453(4)	9016(1)	75(1)
C(45)	5467(3)	-3248(4)	9302(1)	74(1)

Table 3. Bond lengths [A] and angles [deg] for 1.

S(1)-C(43)	1.787(4)
S(1)-C(42)	1.791(5)
O(1)-C(42)	1.541(6)
O(2)-C(23)	1.361(4)
O(2)-C(31)	1.417(4)
C(11)-C(16)	1.343(5)
C(11)-C(12)	1.385(5)
C(11)-C(43)	1.514(5)
C(12)-C(13)	1.380(5)
C(12)-H(12)	0.93
C(13)-C(14)	1.369(4)
C(13)-H(13)	0.93
C(14)-C(15)	1.373(4)
C(14)-C(44)	1.438(5)
C(15)-C(16)	1.392(5)
C(15)-H(15)	0.93
C(16)-H(16)	0.93
C(21)-C(22)	1.393(5)
C(21)-C(23)#1	1.408(5)
C(21)-C(45)	1.425(5)
C(22)-C(23)	1.380(5)
C(22)-H(22)	0.93
C(23)-C(21)#1	1.408(5)
C(31)-C(32)	1.489(5)
C(31)-H(31A)	0.97
C(31)-H(31B)	0.97
C(32)-C(33)	1.505(6)
C(32)-H(32A)	0.97
C(32)-H(32B)	0.97
C(33)-H(33A)	0.96
C(33)-H(33B)	0.96
C(33)-H(33C)	0.96
C(41)-C(42)	1.141(5)
C(41)-H(41A)	0.96
C(41)-H(41B)	0.96
C(41)-H(41C)	0.96
C(43)-H(43A)	0.97
C(43)-H(43B)	0.97
C(44)-C(45)	1.196(4)
C(43)-S(1)-C(42)	100.8(2)
C(23)-O(2)-C(31)	118.9(3)
C(16)-C(11)-C(12)	118.6(3)
C(16)-C(11)-C(43)	121.1(3)
C(12)-C(11)-C(43)	120.3(3)
C(13)-C(12)-C(11)	120.5(3)
C(13)-C(12)-H(12)	119.7(2)
C(11)-C(12)-H(12)	119.8(2)
C(14)-C(13)-C(12)	120.7(3)
C(14)-C(13)-H(13)	119.7(2)
C(12)-C(13)-H(13)	119.7(2)
C(13)-C(14)-C(15)	118.7(3)
C(13)-C(14)-C(44)	120.6(3)

C(15)-C(14)-C(44)	120.7(3)
C(14)-C(15)-C(16)	120.1(3)
C(14)-C(15)-H(15)	119.9(2)
C(16)-C(15)-H(15)	119.9(2)
C(11)-C(16)-C(15)	121.4(3)
C(11)-C(16)-H(16)	119.3(2)
C(15)-C(16)-H(16)	119.3(2)
C(22)-C(21)-C(23)#1	119.7(3)
C(22)-C(21)-C(45)	120.1(3)
C(23)#1-C(21)-C(45)	120.2(3)
C(23)-C(22)-C(21)	121.4(3)
C(23)-C(22)-H(22)	119.3(2)
C(21)-C(22)-H(22)	119.3(2)
O(2)-C(23)-C(22)	125.0(3)
O(2)-C(23)-C(21)#1	116.1(3)
C(22)-C(23)-C(21)#1	118.9(3)
O(2)-C(31)-C(32)	109.4(3)
O(2)-C(31)-H(31A)	109.8(2)
C(32)-C(31)-H(31A)	109.8(2)
O(2)-C(31)-H(31B)	109.8(2)
C(32)-C(31)-H(31B)	109.8(2)
H(31A)-C(31)-H(31B)	108.2
C(31)-C(32)-C(33)	112.7(4)
C(31)-C(32)-H(32A)	109.1(2)
C(33)-C(32)-H(32A)	109.0(2)
C(31)-C(32)-H(32B)	109.1(2)
C(33)-C(32)-H(32B)	109.1(2)
H(32A)-C(32)-H(32B)	107.8
C(32)-C(33)-H(33A)	109.5(2)
C(32)-C(33)-H(33B)	109.5(2)
H(33A)-C(33)-H(33B)	109.5
C(32)-C(33)-H(33C)	109.5(2)
H(33A)-C(33)-H(33C)	109.5
H(33B)-C(33)-H(33C)	109.5
C(42)-C(41)-H(41A)	109.5(3)
C(42)-C(41)-H(41B)	109.5(3)
H(41A)-C(41)-H(41B)	109.5
C(42)-C(41)-H(41C)	109.5(3)
H(41A)-C(41)-H(41C)	109.5
H(41B)-C(41)-H(41C)	109.5
C(41)-C(42)-O(1)	127.1(5)
C(41)-C(42)-S(1)	123.0(4)
O(1)-C(42)-S(1)	109.8(4)
C(11)-C(43)-S(1)	114.0(3)
C(11)-C(43)-H(43A)	108.8(2)
S(1)-C(43)-H(43A)	108.77(14)
C(11)-C(43)-H(43B)	108.8(2)
S(1)-C(43)-H(43B)	108.8(2)
H(43A)-C(43)-H(43B)	107.7
C(45)-C(44)-C(14)	177.0(3)
C(44)-C(45)-C(21)	177.7(3)

Symmetry transformations used to generate equivalent atoms:
#1 -x+1,-y-1,-z+2

Table 4. Anisotropic displacement parameters (A^2 x 10^3) for 1.
The anisotropic displacement factor exponent takes the form:
-2 pi^2 [h^2 a*^2 U11 + ... + 2 h k a* b* U12]

	U11	U22	U33	U23	U13	U12
S(1)	89(1)	125(1)	76(1)	11(1)	10(1)	-2(1)
O(1)	285(6)	202(5)	140(4)	-7(3)	-8(3)	-2(4)
O(2)	89(2)	87(2)	79(2)	10(1)	-2(1)	-2(1)
C(11)	84(3)	60(2)	68(2)	-2(2)	16(2)	-3(2)
C(12)	74(2)	100(3)	72(2)	13(2)	-4(2)	1(2)
C(13)	67(2)	87(2)	75(2)	7(2)	5(2)	-13(2)
C(14)	74(2)	58(2)	59(2)	-2(2)	13(2)	-1(2)
C(15)	75(3)	86(2)	78(2)	2(2)	-2(2)	-3(2)
C(16)	72(2)	81(2)	73(2)	-2(2)	12(2)	-12(2)
C(21)	87(3)	55(2)	60(2)	0(2)	8(2)	-4(2)
C(22)	82(2)	62(2)	70(2)	-2(2)	9(2)	-4(2)
C(23)	89(3)	59(2)	62(2)	0(2)	-3(2)	0(2)
C(31)	93(3)	71(2)	78(2)	-7(2)	-2(2)	4(2)
C(32)	108(3)	92(3)	88(3)	-13(2)	-21(2)	5(2)
C(33)	109(4)	102(3)	129(4)	-34(3)	-31(3)	14(3)
C(41)	43(2)	141(4)	73(2)	18(2)	-5(2)	6(2)
C(42)	139(4)	84(3)	70(3)	22(2)	-22(3)	-5(3)
C(43)	128(3)	76(2)	87(2)	12(2)	14(2)	-16(2)
C(44)	89(3)	69(2)	67(2)	-7(2)	11(2)	0(2)
C(45)	90(2)	63(2)	68(2)	-7(2)	8(2)	-3(2)

Table 5. Hydrogen coordinates (x 10^4) and isotropic displacement parameters (A^2 x 10^3) for 1.

	x	y	z	U(eq)
H(12)	4667(3)	62(4)	7902(1)	99
H(13)	4283(3)	-1542(4)	8442(1)	92
H(15)	7659(3)	-981(4)	8812(1)	95
H(16)	8020(3)	659(4)	8274(1)	91
H(22)	6960(3)	-4428(4)	9819(1)	86
H(31A)	8223(3)	-4647(4)	10380(1)	97
H(31B)	8231(3)	-6210(4)	10129(1)	97
H(32A)	8610(4)	-7608(5)	10729(1)	115
H(32B)	8736(4)	-5991(5)	10950(1)	115
H(33A)	10635(5)	-6898(34)	10798(4)	170
H(33B)	10398(8)	-5385(6)	10542(9)	170
H(33C)	10293(6)	-7052(32)	10345(5)	170
H(41A)	4756(10)	1573(5)	7146(7)	128
H(41B)	4806(9)	64(27)	7415(3)	128
H(41C)	4233(3)	-21(26)	6987(5)	128
H(43A)	7223(4)	2413(5)	7768(1)	116
H(43B)	5894(4)	2184(5)	7623(1)	116

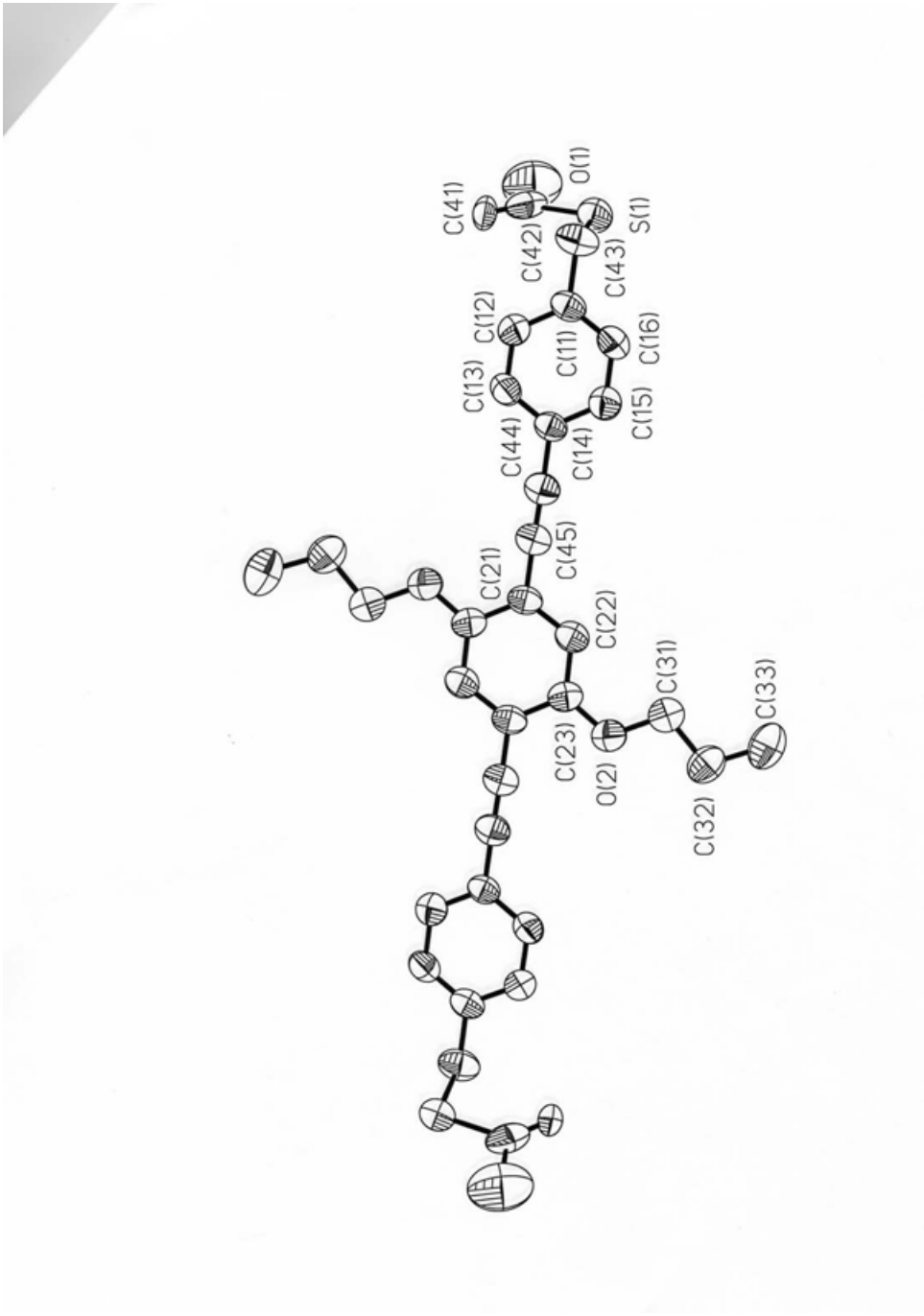
C(41)
O(1)
C(42)
S(1)
C(43)
C(12)
C(11)
C(16)
C(13)
C(15)
C(44)
C(14)
C(45)
C(21)
C(22)
C(31)
C(33)
C(23)
O(2)
C(32)

References

1. Heath, J. R. *Acc. of Chem. Res.* **1999**, 32, 388.
2. Cao, G. *Adv. Mat.* **2004**, 16, 1864-1865.
3. Sonogashira, K.; Tohda, Y.; Hagihara, N. *Tet. Lett.* **1975**, 4467-4470
4. Fan, F. F.; Yang, J.; Cai, L.; Price, D. W.; Dirk, S. M.; Kosynkin, D. V.; Yao, Y.; Rawlett, A. M.; Tour, J. M.; Bard, A. J. *J. Am.Chem. Soc.* **2002**, 124, 5550-5560.
5. Veinot, J. G. C.; Ginzburg, M.; Pietro, W. J. *Chem. of Mat*. **1997**, 9, 2117-2122.
6. Hines, M. A.; Guyot-Sionnest, P. *J. of Phys. Chem.* **1996**, 100, 468-71.
7. Murray, C. B.; Norris, D. J.; Bawendi, M. G. *J. Am.Chem. Soc.* **1993**, 115, 8706-15.
8. Cumberland, S. L.; Hanif, K. M.; Javier, A.; Khitrov, G. A.; Strouse, G. F.; Woessner, S. M.; Yun, C. S. *Chem. Mat.* **2002**, 14, 1576-1584.
9. Peng, Z. Adam; Peng, Xiaogang. *J. Am.Chem. Soc.* 2001, 123, 183-184.
10. Novak, J. P.; Feldheim, D. L. *J. Am.Chem. Soc.* **2000**, 122, 3979-3980
11. Ota, T.; Maehashi, K.; Nakashima, H.; Oto, K.; Murase, K. *Phys. Stat. Sol. B: Basic Research*, **2001**, 224, 169-172.
12. Collison C.; Treemaneekarn, V.; Oldham, W. J.; Hsu, J. H.; Rothberg, L. J.; *Synth. Mat.* **2001**, 119, 1-6

13. Javier, A.; Yun, C. S.; Sorena, J.; Strouse, G. F. *J. Phys Chem B.* **2003**, 107, 435-442.

14. Javier, Artjay; Yun, C. Steven; Strouse, Geoffrey F. *Mat. Res. Soc. Symp. Proc.,* **2003**, 776, 17-22.

15. Javier, A; Yun, C. S.; Meulenber, R. *J. Phys. Chem. B.* Submitted 2004

Chapter 6. Synthetic Appendix

13nm citrate stabilized gold nanocrystals[1]: 13 nm diameter Au nanocrystals were prepared by the citrate reduction of auric acid. All glassware was cleaned in aqua regia (3 parts HCl, 1 part HNO_3), rinsed with Millipure H_2O, and then oven dried. All solutions were freshly prepared. An aqueous (Millipure) solution of $HAuCl_4$ (1 mM, 500 mL) was stirred and heated to reflux. 50 mL of a 38.8 mM trisodium citrate solution was added quickly, which resulted in the solution color to change from yellow to red. After the color change, the solution was heated for an additional 15 min, allowed to cool to room temperature and subsequently filtered through 0.45 *u*m nylon filter. (Figure 6-1)

5.7nm citrate/tannic acid stabilized gold nanocrystals[2]: Gold nanocrystals were prepared by the sodium citrate and tannic acid reduction of auric acid. All glassware was prepared as above. To a stirred and refluxing 100mL of 0.001% (w/v) solution of freshly prepared tetrachloroauric acid, a solution containing 2 mL of a 1% (w/v) solution of sodium citrate and 0.45 mL of a 1% (w/v) tannic acid solution was rapidly added. The solution was stirred at reflux for an additional 5 min followed by cooling. This reaction produces a pH of 4.5 colloidal gold solution that is stable for an indefinite period of time at room temperature. The gold nanoparticles exhibit a mean diameter of 5.7 nm. (Figure 6-2) 1.5nm phosphine capped gold nanocrystals[3]: Reaction is done with glassware prepared as above. Auric acid (1.00 g, 2.54 mmol)

Figure 6-1. TEM of 13 nm gold nanocrystals.

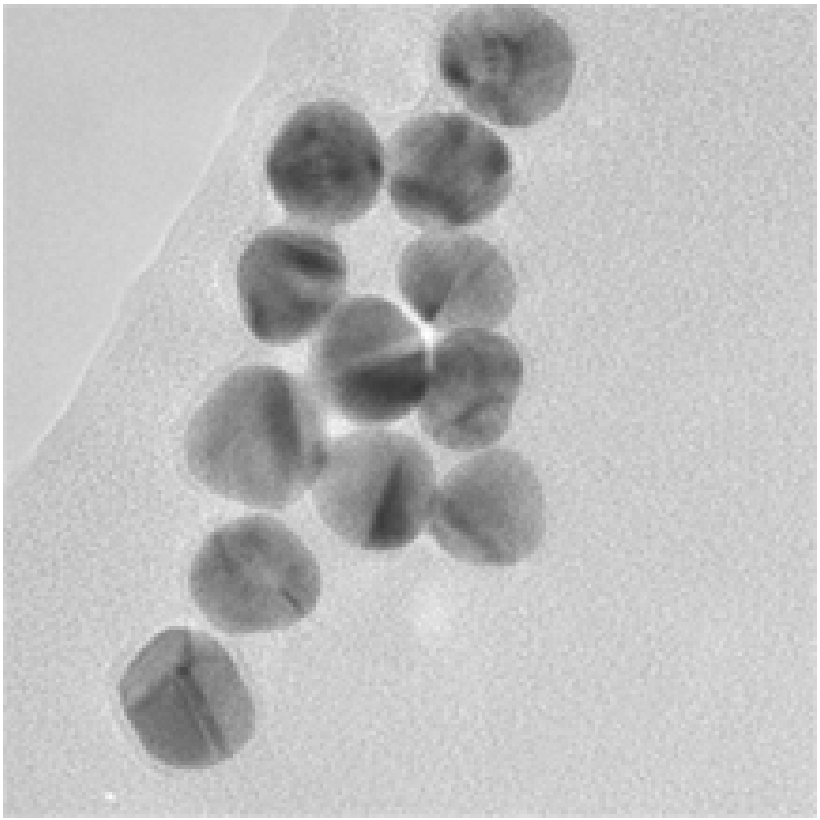

Figure 6-2. TEM of 5.7 nm gold nanocrystals

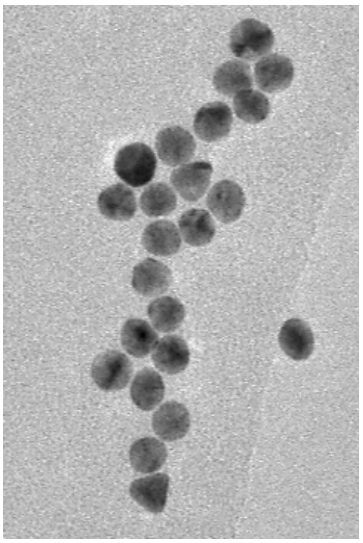

and tetraoctylammonium bromide (TOABr) (1.60 g, 2.93 mmol) were dissolved in nitrogen or argon sparged water/toluene mixture (50 mL/65 mL). The biphasic solution was stirred until the organic phase turned yellow and the aqueous phase was colorless. Triphenylphosphine (2.32 g, 8.85 mmol) was then added under a flow of inert gas and the solution was stirred vigorously until the organic phase was white and cloudy. A freshly prepared aqueous solution of sodium borohydride (1.41 g, 37.3 mmol, dissolved in 10 mL of water) was rapidly added. (Note a 500 ml round bottom flask was used to the vigorous evolution of gases.) The organic phase immediately turned dark purple after which it was stirred for an additional 3 hours under inert atmosphere. The organic layer was separated using a separatory funnel and washed with water (2X100 mL). The solvent was removed by rotovap at room temperature to yield a black solid. The solid was then washed with hexane (2x100 mL), saturated aqueous sodium nitrite (2x100 mL), and a 2:3 methanol:water mixture (2x100 mL) to remove any byproducts. Additional purification can be done by taking up the product in chloroform and precipitating with a slow addition of pentane (2-3 precipitations). (Figure 6-3)

Recapping of citrate stabilized Gold nanocrystals[4]: To a solution of freshly prepared citrate stabilized gold nanocrystals 25-30 mg of tris(3-sulfatophenyl)phosphine (purchased from Strem) was added and stirred under inert atmosphere for 24 hour (for the citrate/tannic acid stabilized gold nanocrystals the reaction time was took from 48-72 hours). After addition of phosphine, there is no

visible change to the color of the solution of nanomaterial however the completion of

Figure 6-3. TEM of 1.5 nm gold nanocrystals.

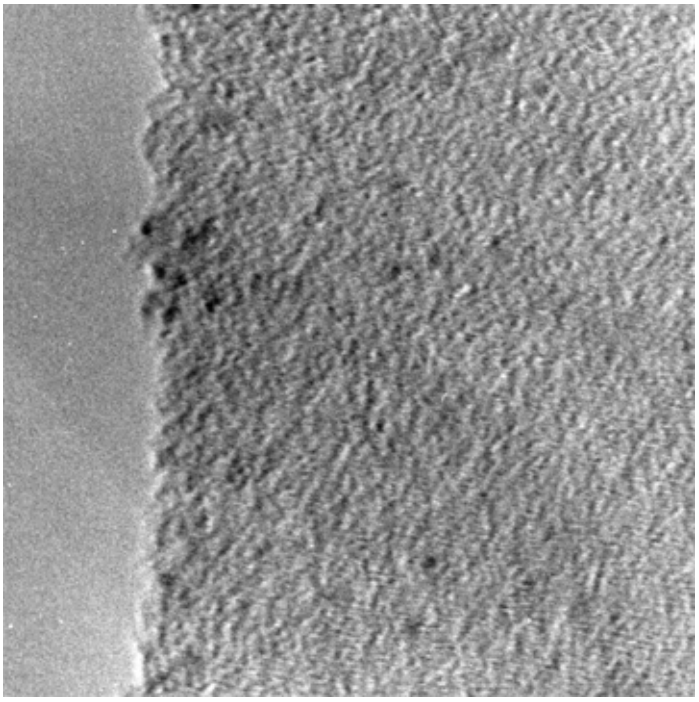

recapping can be determined by taking aliquots of solution and precipitating the nanocrystals with 1M NaCl solution. Centrifugation and decanting of the supernatant will leave a ppt of gold nanocrystals. If the nanomaterial is completely passivated, the addition of DI water will resuspend the gold nanocrystals. An alternative is to run the nanomaterial through a 3-3.5% agarose electrophoresis gel. A tight band of red moving through the gel shows complete surface recapping. If the surface of the nanocrystal is not recapped the nanomaterial will crash out in the well. Incomplete capping will present it self as bad streaking through the gel. (Figure 6-4)

Upon completion of phosphine re-capping of the gold nanocrystal, a saturated solution of NaCl was added slowly to a stirring solution of the gold colloids until the solution turned blue. The reaction was then centrifuged and the solids collected. A second purification was done by precipitating the phosphine stabilized nanocrystals with ethanol from aqueous solution, centrifuging off the precipitate, and drying it under vacuum.

Water-soluble phosphine capping of 1.5nm gold nanocrystals[5]: 1.5 nm gold nanocrystals (50 mg) synthesized above were suspended in dichloromethane and sparged water (1:1 100 mL). 50mg of tris(3-sulfatophenyl)phosphine was added and the reaction was stirred vigorously for 24 hours. The recapping was considered complete when the mixed phases of the reaction were allowed to sit and the purple color was transferred to the aqueous phase. The aqueous phase was separated and the gold nanocrystals were precipitated with the addition of ethanol. The solids were collected and dried under vacuum.

Figure 6-4. 3.5 % Agarose Gel of 13 nm tris(3-sulfatophenyl)phosphine capped gold nancrystals (left lane) and 4.5nm mercaptopropanesulfonate capped CdSe (right lane)

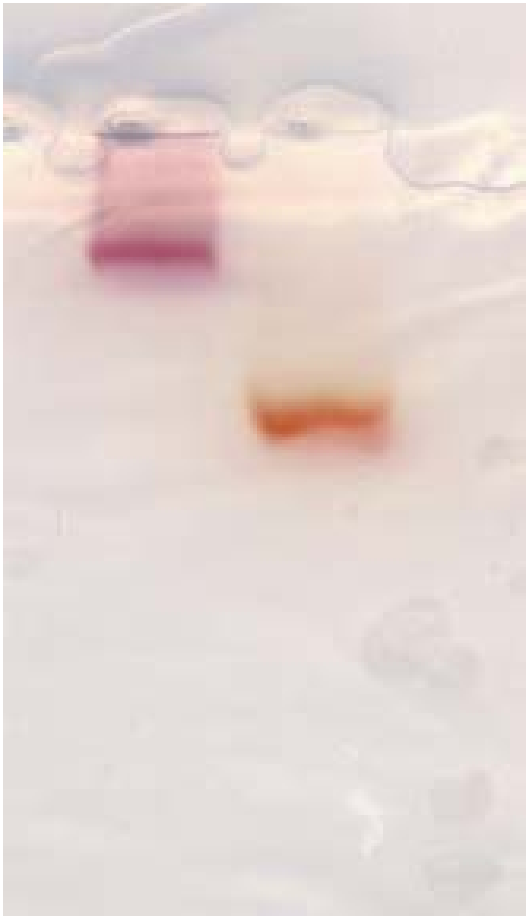

.

Deprotection of 5'C-6 Thiol-DNA Oligomers[6]: 200 nmol of DNA was suspended in 200 μL of 50 μM phosphate buffer pH 7.2 and added 50 μL of 50mM of Dithiothreitol (DTT) for 2-3 hours. Excess DDT was removed by extracting with ethylacetate and then passing the DNA solution through a spin column filled with P-5 size exclusion column. Concentration of recovered DNA was measured by UV-absorption at 260nm (1 OD is equal to 33 μg/mL for single stranded (ss) DNA and 50 μg/mL for double stranded (ds) DNA).[7] After the deprotection DNA was aliquoted into 50 μL portions, quickly frozen in liquid nitrogen and placed into the freezer for further use.

Annealing of DNA: Annealing of single stranded DNA to double stranded DNA was done by placing a ratio of complimentary strands of DNA into 50 μM phosphate buffered saline (PBS) pH 7.2 and heating to 90^{o}C for 10 min and then allowing the DNA solution to cool slowly to room temperature.

DNA conjugation to water-soluble phosphine capped gold nanocrystals: To a freshly prepared 50 μM phosphate buffer 100 mM saline pH 7.2 solution of phosphine capped gold nanocrystals (1 μM, 100 μL) a solution of deprotected 5' C-6 thiol ds DNA (50 μM, 500 μL) was added and gently mixed. The reaction was allowed to sit undisturbed for 48-72 hours. Binding of the thiol of the DNA to the gold surface was monitored by 3.5% agarose gel electrophoresis. The addition of NaCl to the solution will precipitate out the gold nanocrystal-DNA conjugates and is used to remove out any unbound DNA. The precipitated material can then be re-suspended with PBS buffer.

Electrophoresis of gold nanocrystals: 3.5% agarose was repaired by heating 3.5 g of agarose in a total volume of 100ml of tris-borate EDTA (TBEx1) until all solids have dissolved. The solvated agarose was allowed to cool to 45^{o}C and then poured into a gel mold and fitted with 20 μL well comb. The gel was allowed to harden for 30 min and then the comb was removed. The gel was placed into an electrophoresis chamber filled with TBEx1 and run at 100 milliamps for 10 minutes. 15 μL of the gold nanocrystal solution was mixed with 2 μL of 30% glycerol and placed into the well. The gel was allowed to run for 30 min. Gold nanocrystals appear as red bands migrating through the gel media while incomplete capping of the gold nanocrystal leads to broad bands in the gel. This technique will work for gold nanocrystals conjugated to DNA and proteins. 1.5 nm gold nanocrystals will run on electrophoresis gels along with their bio-conjugates. The same technique can be applied to acrylamide gels and 1.4 nm and 1.5 nm gold nanocrystals. Using 20% cross-linked gels and 20 milliwatts will allow for good resolution of such materials. (Figure 6-5)

DNA conjugation to 1.4 nm gold nanocrystals: To a dry sample of maleimido-modified gold nanocrystals (5 nmoles) were added 50 μL of isopropanol and 450 μL of water. The solution was gently mixed by pipetteman and 4.8 nmoles of deprotected thiol ds DNA in PBS buffer pH 7.2 was added again gently mixed. The reaction was placed into a refrigerator and left undisturbed. Reaction was observed, for the fluorescein labeled DNA, by taking aliquots and measuring the fluorescence quenching of the dye the gold nanomaterial. When there were no further changes to

Figure 6-5. Image is of a 20% acrylamide gel of 1.4 nm gold nanocrystals. Left lane contains single stranded 5' C-6 thiol terminated DNA (30 mer) and 5' C-6 thiol terminated duplex DNA reacted with 1.4 nm maleimido-functionalized gold nanoparticle. Right (b) lane is of ss DNA reacted with 1.4 nm maleimido-functionalized gold nanoparticle. The gold nanoparticles were visually enchanced by silver staining.[8]

Figure 6-6. 20% acrylamide gel of 1.4 nm gold nanocrystals conjugated to duplex DNA (30mers). The gold nanocrystals are silver enchanced which increase the size of the nanoparticle by placing a silver shell over the nanomaterial. Silver Enhancement was purchased and enhancement was done following procedures from Nanoprobes.

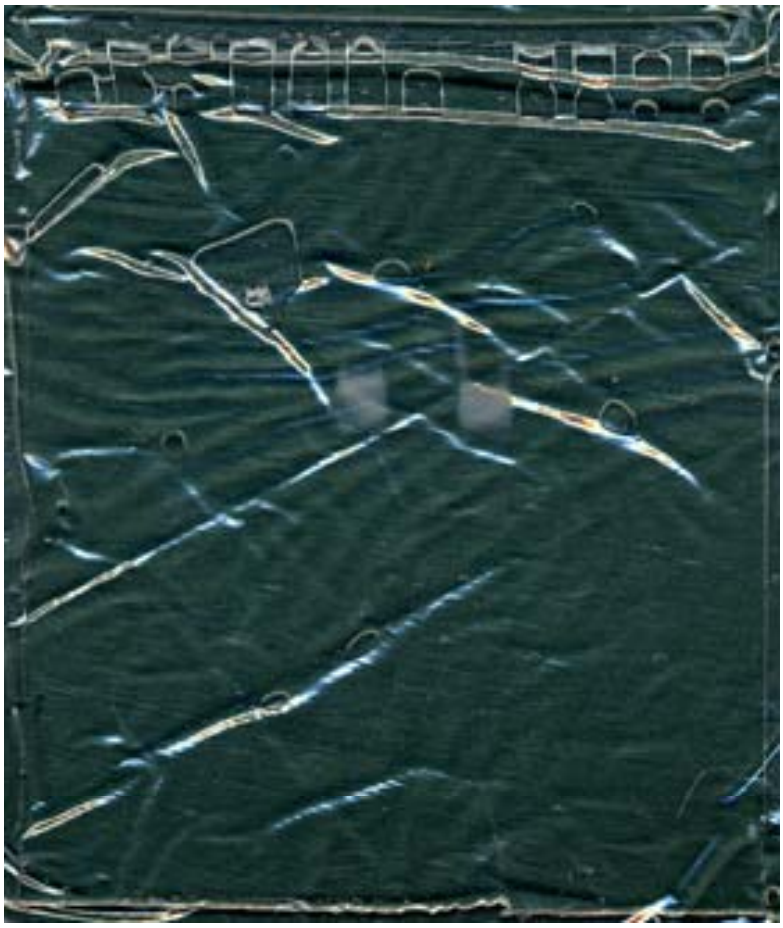

the fluorescence, the reaction was taken a passed through spin columns filled with size exclusion gel. Coupling was visualized by acrylamide gel electrophoresis; uncoupled 1.4 nm gold nanoparticles do not migrate through the gel. (Figure 6-6)

CdSe nanocrystal synthesis from CdO[9]: A synthesis for CdSe nanocrystals starts with 0.0514 g of CdO, 0.2232 g of tetradecylphosphinc acid (TDPA) and 3.7768 g of TOPO were loaded into a 25 mL three-necked flask. The mixture was heated to 300-320 °C under inert atmosphere till the CdO was dissolved. The temperature of the solution was cooled to 270 °C by removing the heating element and then selenium stock solution (0.0441 g of selenium powder dissolved in 2 g of TOP) was quickly injected into a rapidly stirred solution. After injection, reaction was quickly broughtto 250 °C and maintained at that temperature to reach the desired size of nanocrystals. (Figure 6-7)

CdSe nanocrystal synthesis from $Cd_{10}Se_4$ thiolate cluster: CdSe nanocrystals were synthesized using a modification[10] of the single source precursor developed at Cumberland et al.[11] The cluster was synthesized by placing $Cd(NO_3)_2{\cdot}4H_2O$ (1.534 g) in 30 mL of MeOH. This solution was added to a solution of 1.48 g of thiophenol and 2.29 mL of triethylamine in 30 mL of MeOH. This was followed by 0.958 g of tetraethylammonium iodide in 30 mL of MeOH. Once the precipitates were dissolved, the solvent was removed by vacuum and replaced with 70 mL of acetonitrile. Once the solution became clear, 0.192 g of selenium powder and stirred till the selenium was incorporated. The white solids were collected and dried by vacuum. To a solution of heated and degassed hexadecylamine, the inorganic

clusters were added at 120^{o}C. The reaction was slowly ramped to 200^{o}C and maintained till the desired size of nanomaterial is formed.

Figure 6-7. Absorption and Emission Spectra of CdSe made via CdO precursor route.

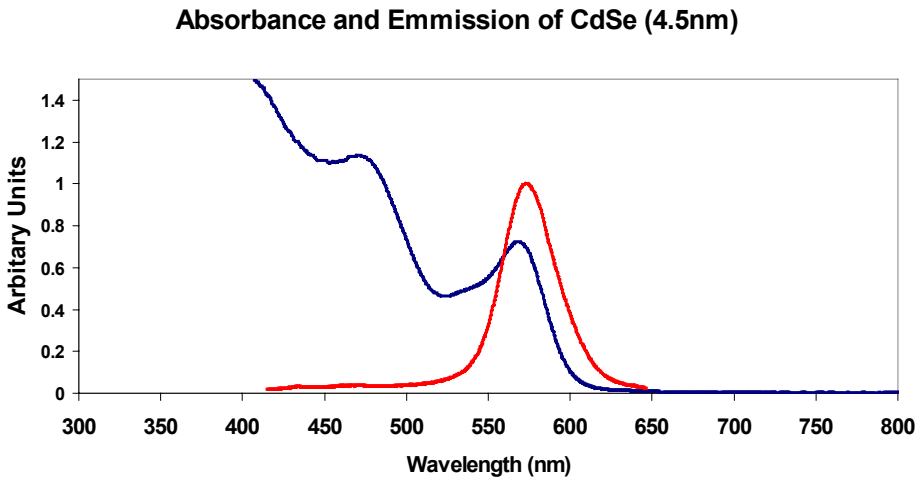

References

1. Storhoff, J. J.; Elghanian, R.T; Mucic, R. C.; Mirkin, C. A.; Letsinger, R. L. *J. Amer. Chem. Soc.* **1998**, 120, 1959-1964.

2. Cumberland, S. L.; Strouse, G. F. *Langmuir,* 2002, 18, 269-276.

3. Weare, W. W.; Reed, S. M.; Warner, M. G.; Hutchison, James E. *J. Amer. Chem. Soc.***2000**, 122, 12890-12891.

4. Schmid,G.; Lehnert, A. *Angew. Chem. Int. Ed. Engl*. **1989**, 28, 780-781.
5. Warner, M. G.; Reed, S. M.; Hutchison, J. E. *Chem. of Mat.* **2000**, 12, 3316-3320.

6. http://www.glenres.com/ProductFiles/10-1936.html

7. Freifelder, D., *Physical Biochemistry: Applications to Biochemistry & Molecular Biology*, W.H. Freeman and Company, CA, 1982, p. 494-536.

8. Gersten, D. M.; Rodriguez, L. V.; George, D. G.; Johnston, D. A.; Zapolski, E. J. *Electrophoresis*, **1991**, 12, 409.

9. Peng, A.; Peng, X. *J. Amer. Chem. Soc.* **2002**, 123, 183-184.

10. Adams, R. D.; Zhang, B.; Murphy, C. J.; and Yeung, L. K. *Chem. Comm.* **1999**, 383-384.

11. Cumberland, S. L.; Hanif, K. M.; Javier, A.; Khitrov, G. A.; Strouse, G. F.; Woessner, S. M.; Yun, C. S. *Chem. Mat.* **2002**, 14, 1576-1584.